**D_GRG_2.5 & 2.8**
# Evaluation report

## Case study validation of stratospheric ozone

**Karolien Lefever (BIRA-IASB)**

Co-investigators
S. Chabrillat, Q. Errera, S. Viscardy, Y. Christophe (BIRA-IASB)
A. Wagner, H. Flentje, W. Thomas (DWD)
J. Flemming, A. Inness (ECMWF)
O. Stein (FZJ)

**Version 1**[*] (15/06/2011)

---

# Table of contents

# 1 Introduction

One of the major objectives of the GRG subproject in MACC is to consolidate, operate and improve the integrated global reactive gases forecasting system for stratospheric ozone and ozone related gases developed in the GEMS project. Validation of the model system based on global in-situ data sets, independent satellite retrievals, and independent model output is an essential part of this. This report describes the non-operational validation activities performed within the GEMS GRG subproject w.r.t. stratospheric ozone, i.e. the validation of the GRG model and assimilation system for particular case studies defined at the start of MACC. The general concept was outlined in the "Work plan for the validation of stratospheric trace gas services". While Task G-RG_1.5 covers the intercomparison of the different assimilation models BASCOE, SACADA and TM3DAM (see D_G-RG_1.5 "Validation report on stratospheric ozone services"), Task G-RG_2.5 focuses on the verification of the coupled system IFS-MOZART (this document).

# 2 Short description case studies

The stratospheric validation activities aim at highlighting any model limitations. Studies focus on stratospheric chemical ozone depletion and its relation to transport processes (PSC formation, chlorine activation, and denitrification). Special attention is given to extraordinary events, including the Antarctic ozone hole and ozone loss in Arctic polar winters. In this respect, the following two case studies will be investigated:

- *Antarctic ozone hole winter/spring 2003*

Extensive ozone depletion was observed over Antarctica during the Southern Hemisphere winter/spring of 2003, with widespread total ozone anomalies of 30 percent or more below the 1979-1986 base period. The Antarctic "ozone hole" area was large than in any of the previous years, with a maximum of more than 27 million square kilometers, with an absolute record in the September-average ozone hole size of 25.8 million square km. Fortunately, meteorological conditions of warming over Antarctica in early October limited further severe ozone destruction as well as the extent and duration of the ozone hole in 2003.

Moreover, ozone analyses by the BASCOE system, which assimilates MIPAS data, cover both the Arctic and Antarctic winter of 2003, starting in July 2002 and ending at the end of March 2004 when MIPAS died. This dataset constituted the ideal reference dataset.

- *Arctic ozone depletion event winter/spring 2011*

Depletion of the ozone layer has reached an unprecedented level over the Arctic this spring due to very cold winter conditions in the stratosphere and the continuing presence of ozone-depleting substances in the atmosphere. The resulting area of low-ozone air reached Scandinavia and North-West Russia by the end of March, leaving them protected from harmful UV radiation by less than 240 Dobson Units.

Besides these two specific case studies, we additionally show the results for:

- ***NRT evaluation 2010***

NRT evaluation of the IFS-MOZART runs with (f93i) and without (f7kn) assimilation, and the IFS-TM5 run f9nd for 2010, using ozone soundings.

- *Long-term continuous data sets to aim at a multi-annual/decadal time series (currently not included yet)*

Besides these two specific episodes, it is very interesting to get a broader view and look at multi-annual/decadal time series. In this respect, the MACC reanalysis, starting in 2003 and aimed at running up to 2010, constitutes a valuable dataset. PROMOTE provides historic records of multi-year assimilated 3D stratospheric ozone analyses combining satellite observations (GOME/NNORSY and UARS/MLS), meteorological data and chemical-transport modeling for the preceding period, from 1996 till 2003. Since this report focuses on the verification of IFS-MOZART, we restrict ourselves to the post-2003 period.

# 3 Case study 1: The Antarctic ozone hole winter/spring 2003

## 3.1 General introduction

The 2003 Antarctic ozone hole was the second largest ozone hole area (i.e. the area covered by extremely low total ozone values of less than 220 Dobson Units) ever recorded so far, with a maximum size of more than 27 million square kilometers on September, 24th, a huge contrast with the previous year, 2002 (Figure 1, Figure 3). The average ozone hole area for September 2003 was 25.8 million square km, which constituted an absolute record for the month September compared to any previous year (Figure 2). On the other hand, minimum ozone values were not as low as seen during other years. (Source: NOAA). Figure 4 shows the monthly mean total ozone for the month October from 1997-2003. This near-record ozone loss was made possible by calm winds and persistent cold temperatures in the lower stratosphere.
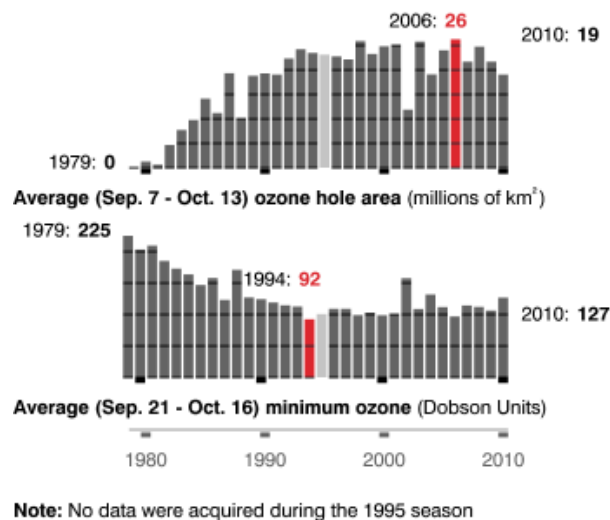


**Figure 1: Average ozone hole area and minimum ozone for the period 1980-2010 (Source: Ozone Hole Watch)**
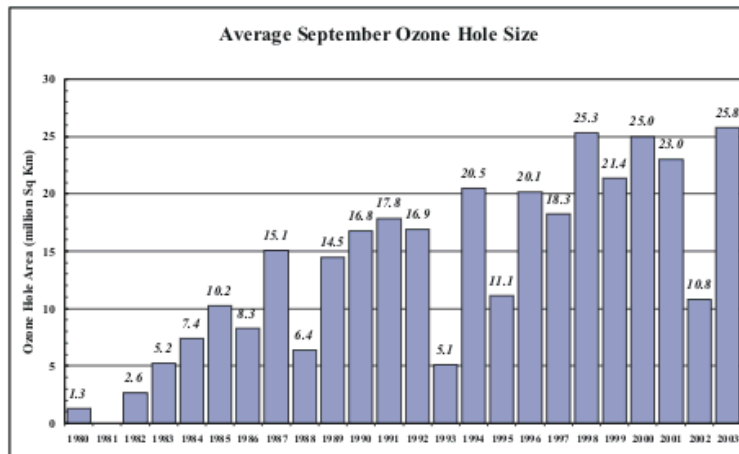
**Figure 2: Average September ozone hole size for the period 1980-2003 (Source: NOAA)**
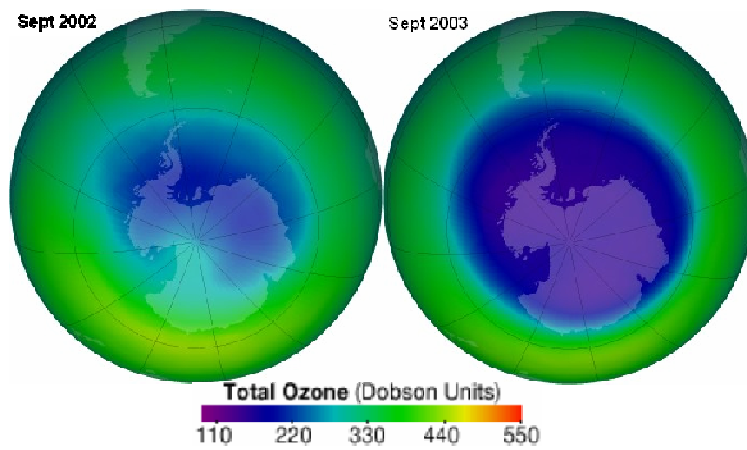


**Figure 3: Monthly mean total ozone for September 2002-2003**
**(Source: http://ozonewatch.gsfc.nasa.gov/).**
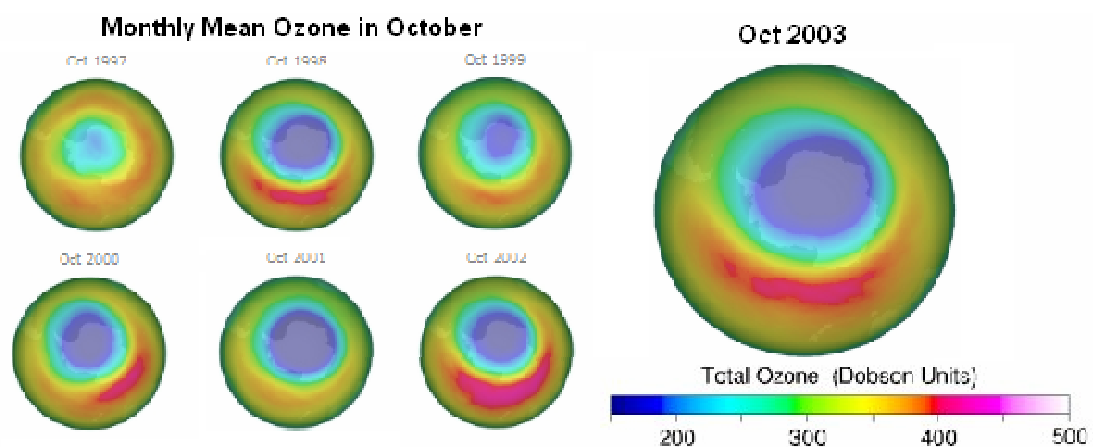


**Figure 4: Monthly mean total ozone for October 1997-2003 from the 30-year Multi Sensor Reanalysis (MSR, 1978-2008, http://www.temis.nl/protocols/o3hole/o3_history.php?lang=0).**

## 3.2    Meteorological context Antarctic Winter/Spring 2003

Figure 5 shows the zonally-averaged (i.e. averaged over the longitudes) time series for latitudes south of 30°S at the 475K potential temperature level, the latter being the approximate location of the ozone layer, where the depletion can be observed most prominently. Using a isentropic level allows us to follow the adiabatic movement of the air. The two potential temperature contours at 188K and 196K shown in Figure 5 indicate the approximate temperatures below which different types of polar stratospheric clouds (PSC) can form. Once temperatures decrease below approximately 196K, solid Nitric Acid Trihydrate (NAT, consisting of a combination of HNO3 and H2O) or liquid Supercooled Ternary Solution (STS, consisting of a combination of HNO3, H2O, and H2SO4) can form (PSC type I). When temperatures decrease below 188K in the stratosphere, ice (frozen H2O) PSC can form (PSC type II). PSCs influence ozone loss through two main processes:
1)    Chlorine activation on PSC particles leading to ozone losses
2)    Sedimentation of PSCs causing denitrification and exacerbating ozone loss

Figure 6 shows the minimum temperature that was reached at the 50 hPa level for latitudes south of 50°S. Temperatures in the lower stratosphere reached values below the 196K level early May, allowing the formation of PSC type I. From end of May till end of September 2003, temperatures were low enough to form ice PSCs. Both the area covered by NAT and by ICE PSCs attained higher values than the average of 1979-2007 (Figure 7). The final stratospheric warming event (coinciding with a high pressure region with descending air, see Figure 8) in early October limited further severe ozone destruction and also limited the extent and duration of the ozone hole in 2003. All NAT and Ice PSCs have disappeared by that time.
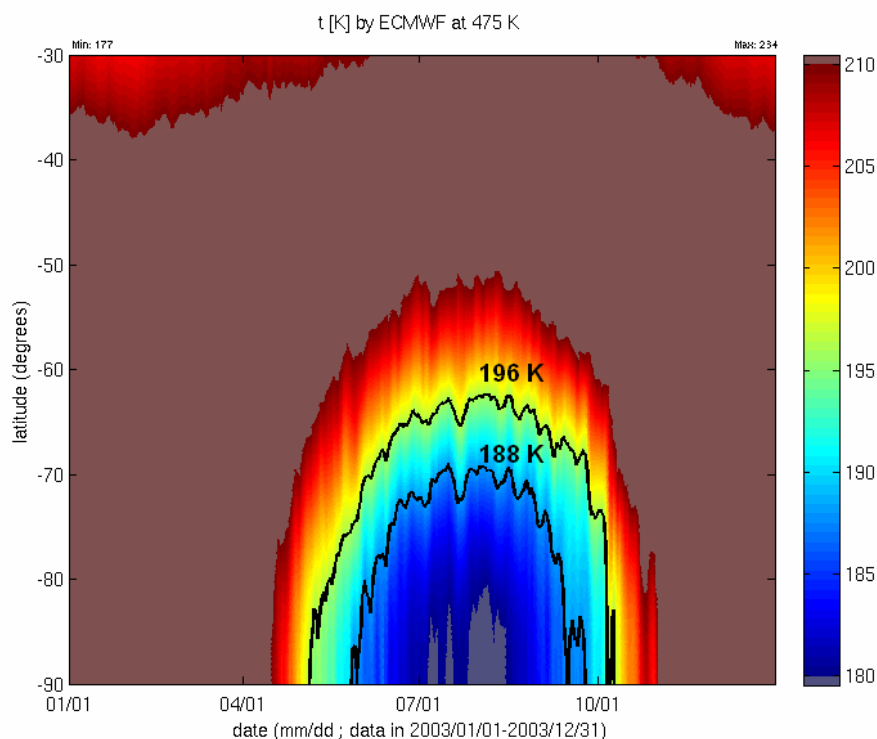


**Figure 5: ECMWF temperature evolution at the 475K isentropic level for 2003, with the isocontours for T=188K and T=196K indicated by the black lines.**
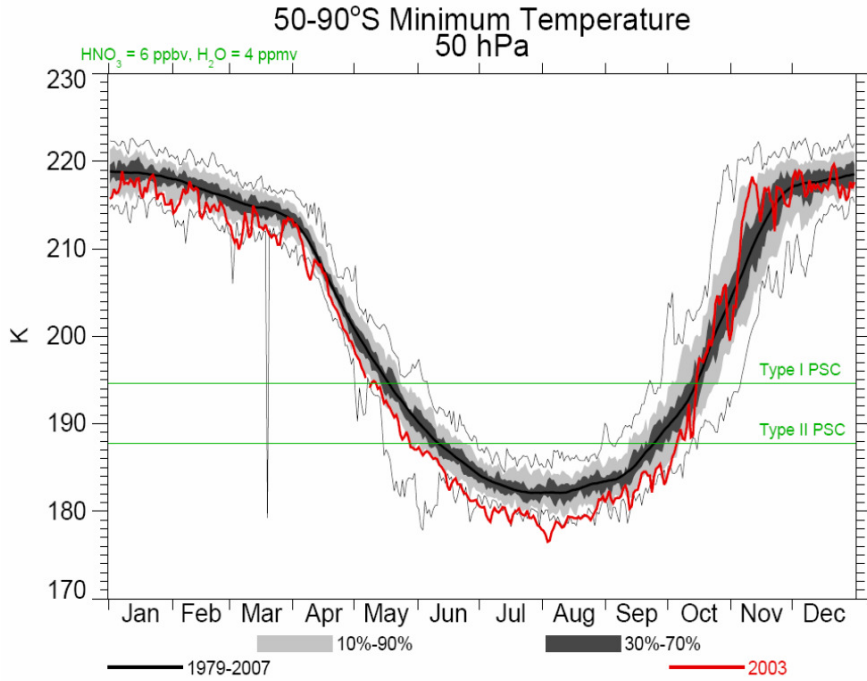
**Figure 6: The 50-hPa minimum Antarctic temperature for latitudes south of 50°S (Source: http://ozonewatch.gsfc.nasa.gov/meteorology/)**
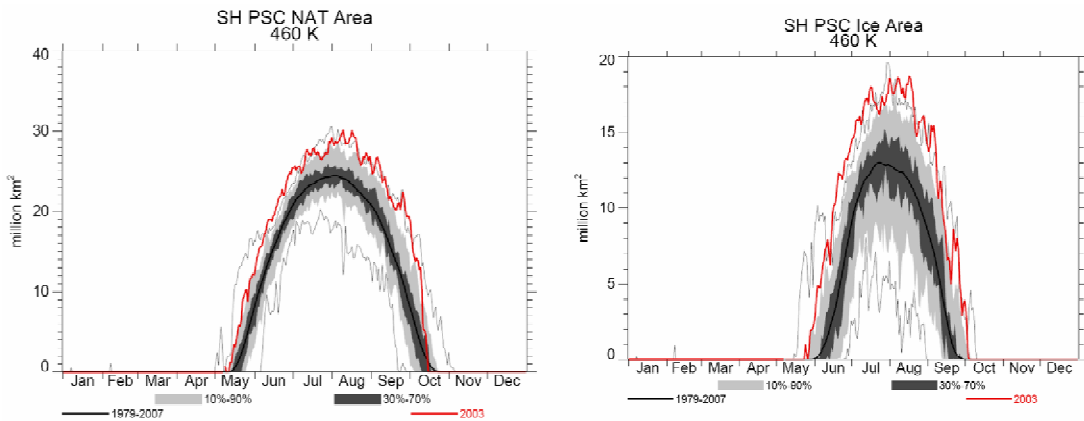


**Figure 7: Area of PSC formed from Nitric Acid Trihydrate (left) and Ice (right) for 2003, compared to the average of 1979-2007 (Source: http://ozonewatch.gsfc.nasa.gov/meteorology/)**
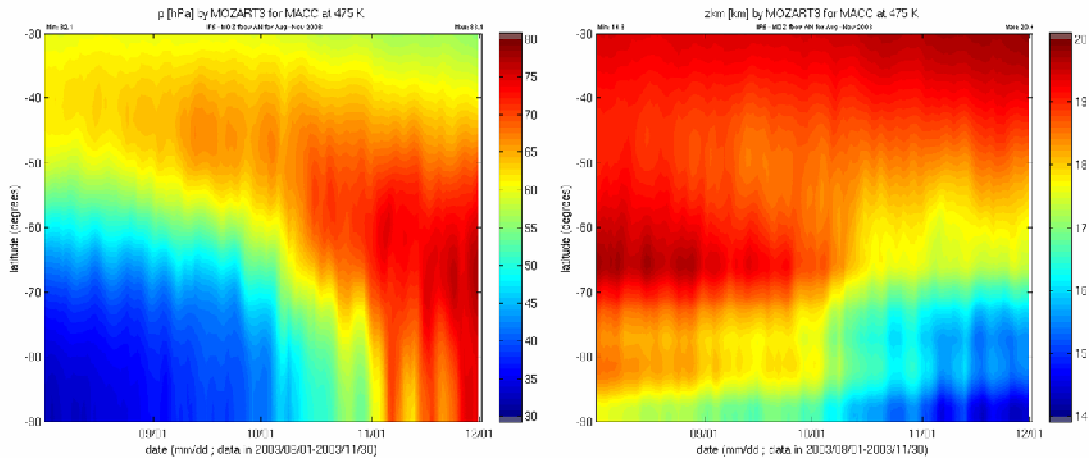


**Figure 8: Height and pressure at the 475K isentropic level for Aug-Nov 2003.**

### 3.3 Total Ozone Columns: IFS-MOZART versus observations

Figure 9 shows the total ozone column for the reanalyses produced by three different systems: IFS (i.e. Cariolle ozone in *fbov* experiment), IFS-MOZART (*fbov*), and BASCOE (v4q30), compared with the total ozone column measured by the Dobson spectrophotometer at Halley Bay (at 75.58° S, British Antarctic Survey BAS) for the ozone hole period 1 July 2003 – 1 Nov 2003.

Both the IFS and coupled system IFS-MOZART show a very good agreement with the groundbased observation. BASCOE is not designed to treat the troposphere and does not assimilate total columns, therefore it shows worse performance.
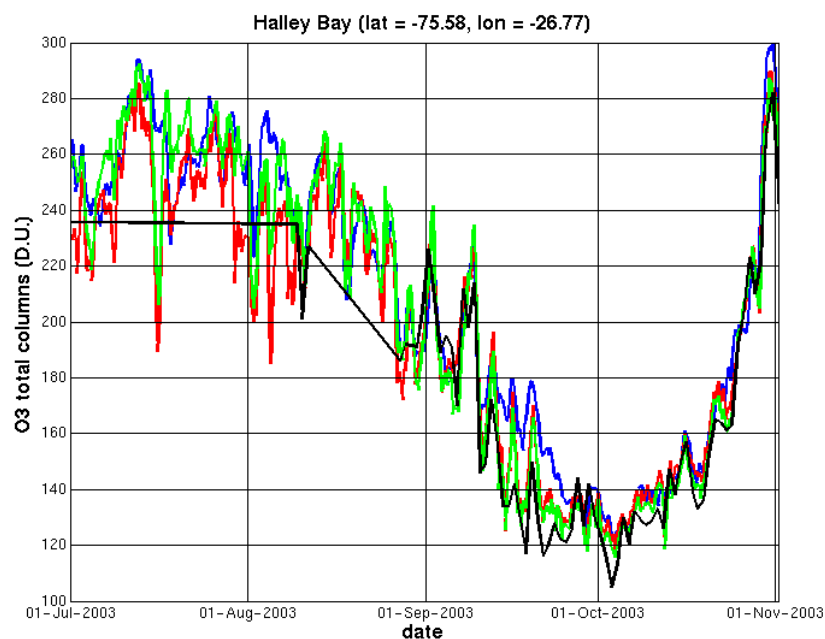


**Figure 9: Comparison of the assimilated and observed total ozone column at Halley Bay (75.58° S, 26.77° W): IFS (green), IFS-MOZART (*fbov*, red), and BASCOE/MIPAS (blue) reanalyses and Dobson observations (black).**

### 3.4 Ozone Profiles

Figure 10 shows a time series of the vertical ozone distribution above the South Pole for the period Aug-Nov 2003. The time series illustrates the near complete ozone destruction between approximately 100 and 50 hPa from late September till the first week of October.
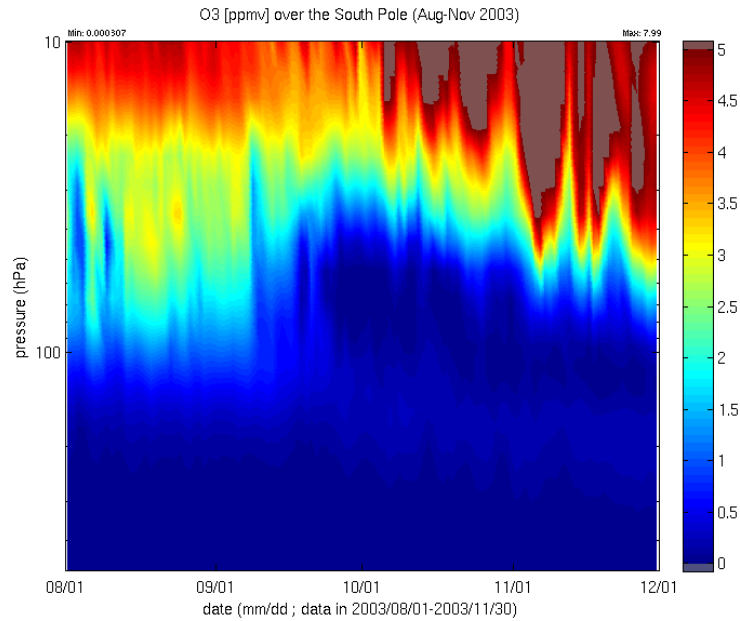
**Figure 10: Time series of O3 profiles above the South Pole from August till November 2003.**

Figure 11 shows the bias and standard deviation of the IFS, IFS-MOZART (*fbov*) and BASCOE O3 reanalyses versus HALOE and POAM satellite profiles at the South Pole during the Antarctic ozone hole season. The larger biases around 10 hPa show that IFS and the coupled system have problems in predicting the ozone hole. In view of the good performance for the total ozone column, it is clear that the assimilation in IFS partially corrects the bias, but the vertical distribution is still wrong.
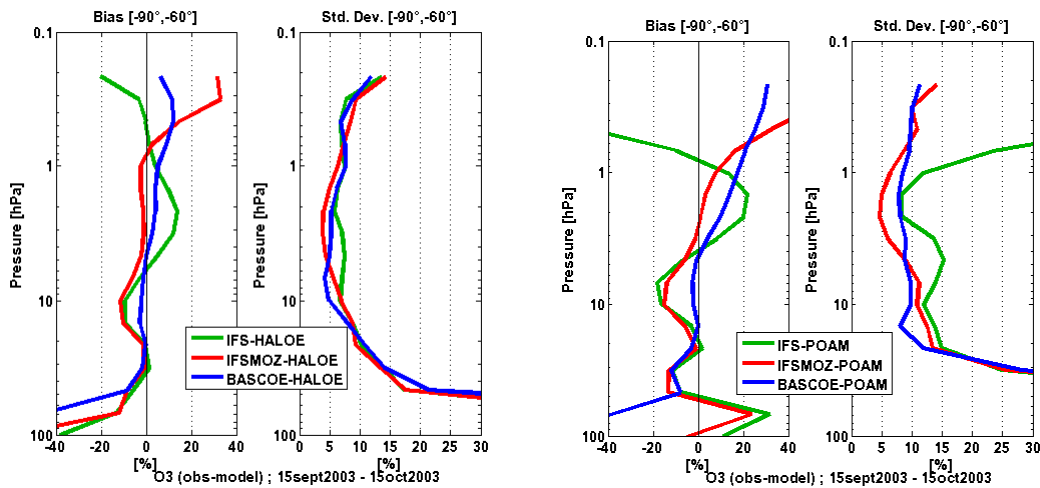


**Figure 11: Bias and standard deviation of IFS, IFS-MOZART (*fbov*) and BASCOE reanalyses against HALOE (left) and POAM (right) satellite observations at the South Pole during the Antarctic ozone hole period (15 Sept-15 Oct 2003). Color code is the same as in Figure 9.**

## 3.5 Ozone-related species: IFS-MOZART versus BASCOE

To understand the processes that lead to the almost-record ozone hole of winter/spring 2003 and to validate them in IFS-MOZART, we evaluate the behavior and evolution of the global stratospheric constituents that play a role in the chemical and dynamical processes of the ozone hole formation. In what follows, we discuss and compare the results for O3, H2O, HNO3, NOx, HCl, ClONO2, N2O as delivered by the IFS-MOZART reanalysis *fbov* with the results from the BASCOE Envisat/MIPAS reanalysis (Errera et al, 2008). The representativeness of the BASCOE model as comparison dataset for 2003 has been proven in Errera et al (2008) and has been illustrated during the FP6 project GEMS several times, so it will not be repeated here. Note that NOx, HCl and ClONO2 were not yet assimilated by BASCOE at that time. As IFS-MOZART only assimilates O3 in the stratosphere, we can consider the output for all other (non-ozone) species as 'model output'.

In the next sections, we will show zonally averaged time series of long- to short-lived species, of chlorine reservoir species and active chlorine compounds for the two above-mentioned models.

**Table 1: Overview of the main characteristics of the different runs that are used to validate the chemical processes in the stratosphere that lead to the 2003 Antarctic ozone hole**

| run | IFS-MOZ fbov | BASCOE analysis MIP_v4q30a |
|---|---|---|
| **start date** | 2002-12-01 | 2002-07-15 |
| **assimilation** *stratospheric* **species** | - O3 profiles: Envisat/MIPAS <br><br> - O3 total columns: SBUV-2 SCIAMACHY | - O3, HNO3, NO2, CH4, H2O, N2O profiles: Envisat/MIPAS |
| **horizontal resolution** | MOZ: 1.125° x 1.125° (160x320) IFS: 1° x 1° (360x181) | 5° x 3.75° (72x49) |

### 3.5.1 Long-lived tracer: nitrous oxide N2O

The BASCOE analysis in Figure 12 clearly confirms that N2O is a long-lived tracer. As it does not chemically react with other species at such short timescales, it almost doesn't vary over the time period Aug-Oct 2003. The variations we observe can be attributed to transport and dynamical effects only. Therefore, we can use N2O to fix the vortex edge at a scaled PV of 1.4x10-4 s-1 (Figure 13).We see a stream of air moving towards the South Pole around the 10th of Oct, when the final stratospheric warming takes place. From early November on, we see more variation, which is due to the break-up of the vortex, which marks the end of the ozone hole season. From this moment on, we start to see mixing of air at lower latitudes with air around the South Pole. The amount of mixing is overestimated by IFS-MOZART. At southern midlatitudes the agreement between IFS-MOZART and BASCOE is very good, but the more southwards, the larger the discrepancy. Southwards of 70°S, IFS-MOZART seriously overestimates the amount of N2O. Discrepancies tend to be larger at the end of and after the ozone hole season.
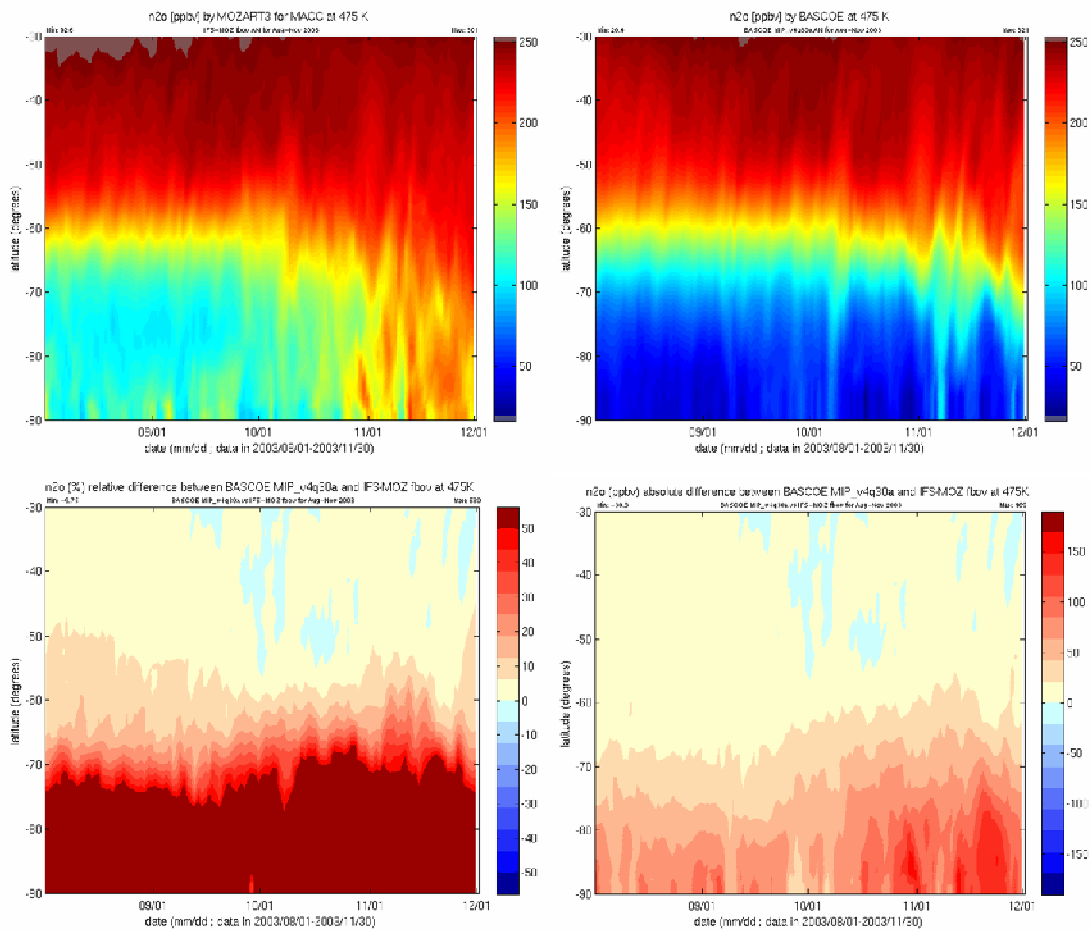
**Figure 12: Same as for Figure 21, but now for N2O.**
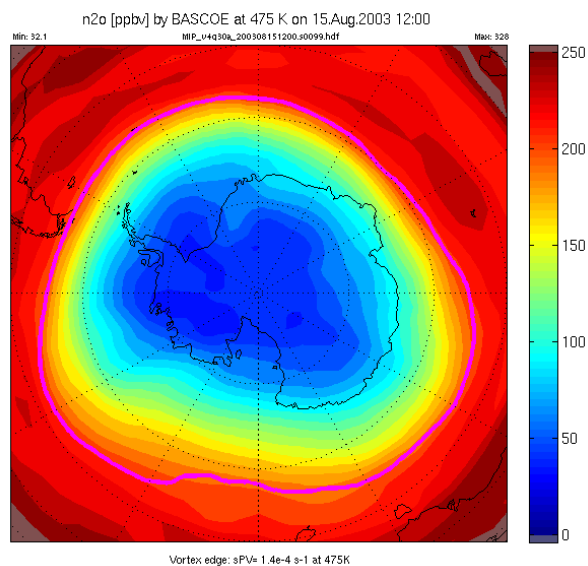


**Figure 13: Vortex edge (magenta) is defined on the basis of N2O and fixed at a scaled PV of 1.4x10-4 s-1 following Manney et al (2007).**

### 3.5.2 Water Vapor H2O

Recalling the temperature time series (Figure 5 and Figure 6), we see that until late September temperatures were low enough to form ice PSCs, and thus to cause dehydration due to the formation of these PSCs. Figure 14 gives obvious proof of dehydration due to the formation of ice PSCs (PSC type II). Although the dehydration is also seen in the IFS-MOZART output, it is seriously underestimated. Outside the polar vortex, H2O values are underestimated, inside the polar vortex, they are overestimated.
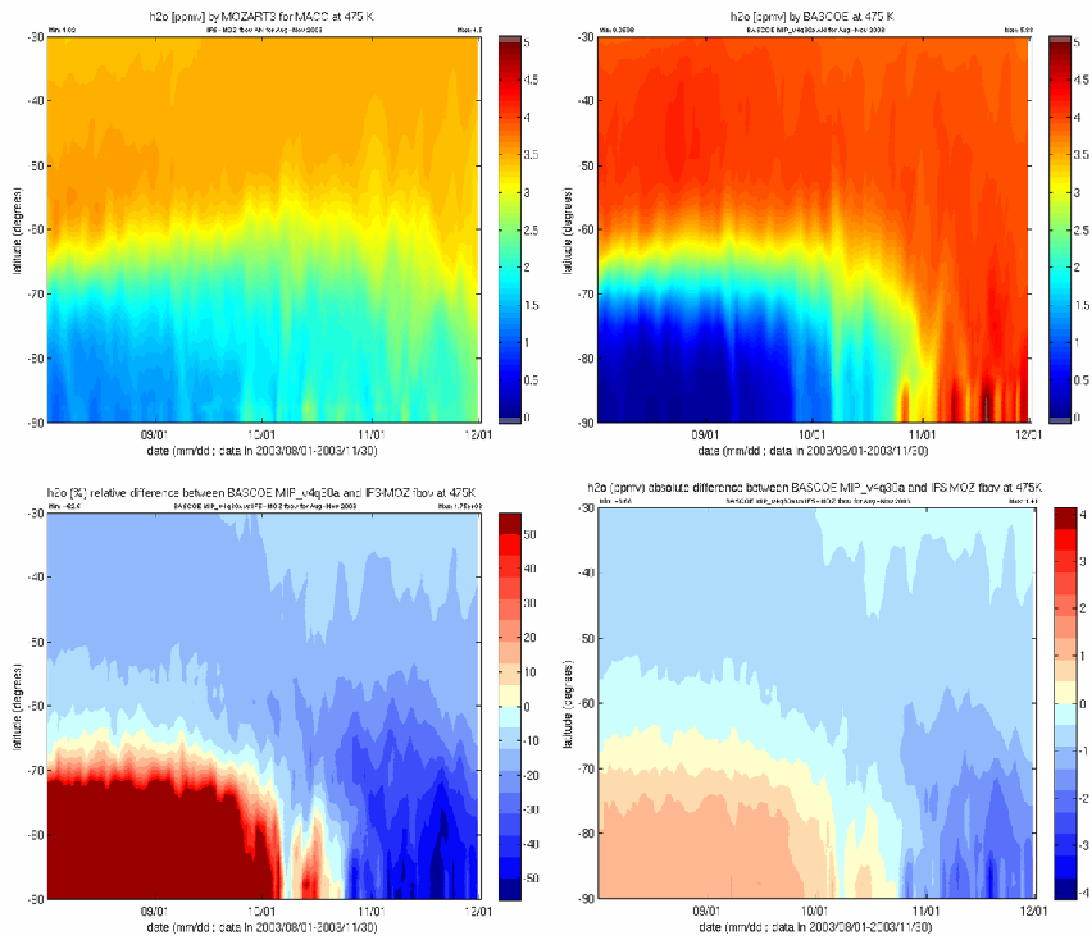


**Figure 14: Same as for Figure 21, but now for H2O.**

### 3.5.3   Reservoir species: nitric acid HNO3

The formation of NAT (HNO3.3H2O) and STS (H2O/H2SO4/HNO3) particles (PSC type I) remove HNO3 from the gaseous phase, causing denitrification. When the temperature rises above the level required for PSCs to exist, HNO3 is released from the PSC back into gas phase and we see an increase in HNO3. Both reanalyses show important denitrification (Figure 15). IFS-MOZART has a global negative bias compared to BASCOE, except for some short time periods at the South Pole, where HNO3 is overestimated. However, HNO3 concentrations are so small that we can neglect these. The absolute differences (bottom right panel of Figure 15) show that there is only an offset of less than 0.5 ppbv. Denitrification seems to extend until lower southern latitudes in IFS-MOZART.
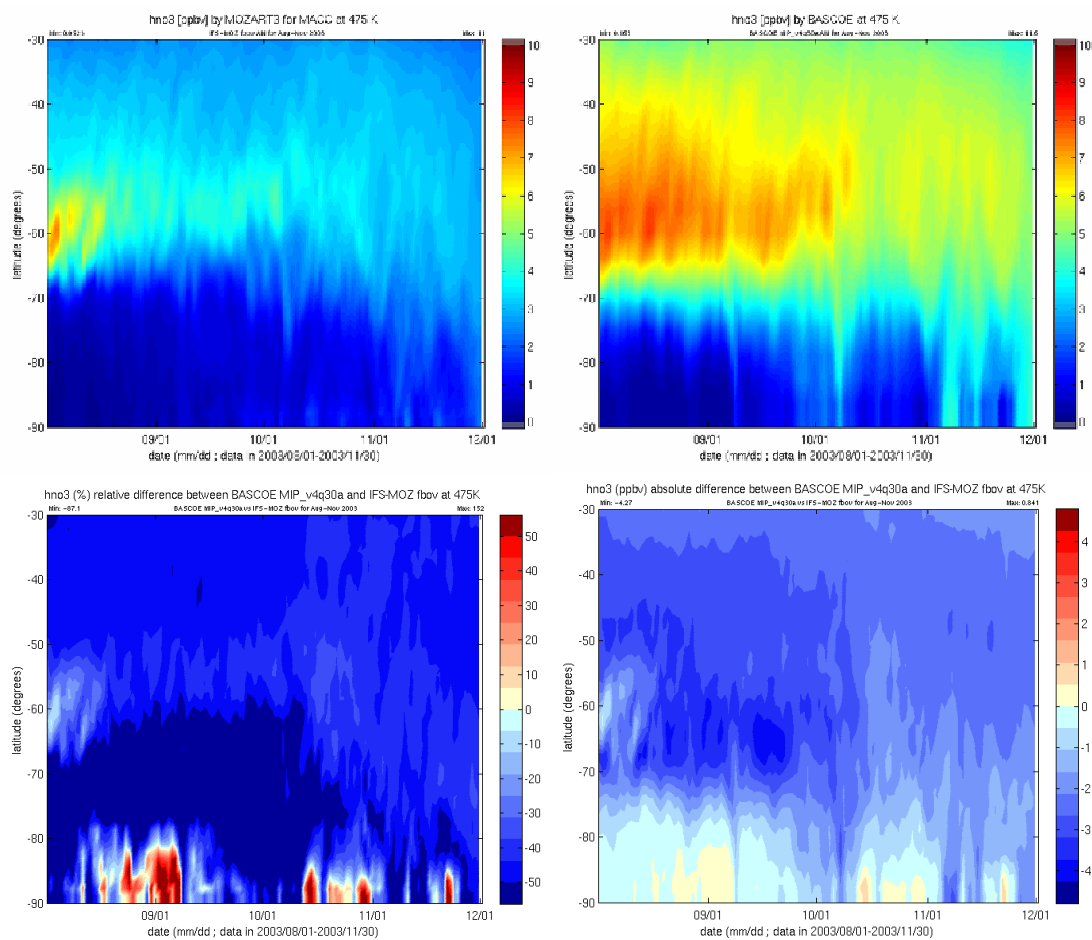


**Figure 15: Same as for Figure 21, but now for HNO3.**

Figure 16 shows that the polar vortex is divided into two area: a strongly mixed inner core, where temperatures can decrease low enough to form PSC particles and reduce HNO3 significantly. Separated from the core, there is a broad ring of weakly mixed air extending to the vortex boundary. A transport barrier between the two areas prevents air from getting mixed. HNO3 is strongly reduced in the inner core of the vortex, where temperatures decrease below +/-195K. Outside of this central part, HNO3 cannot leave the isolated vortex due to the transport barrier at the vortex edge and keeps building up. IFS-MOZART predicts too few of this build up.
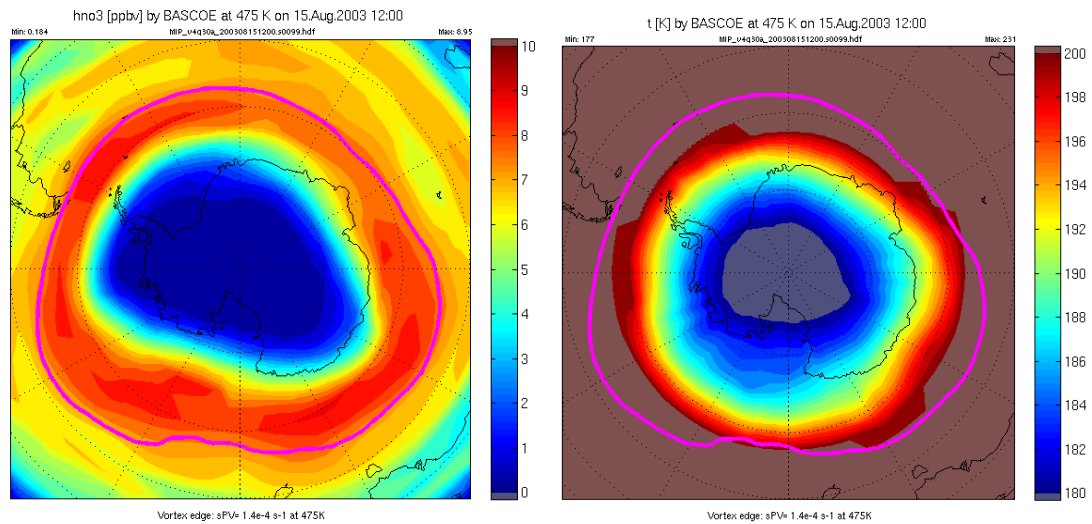


**Figure 16: Snapshot of HNO3 (left) on 15 Aug 2003 at the 475K isentropic level. In magenta, the vortex edge is indicated. In the right panel, a snapshot of the temperature under the same conditions is shown.**

### 3.5.4 Chlorine reservoir species: hydrogen chloride HCl and chlorine nitrate ClONO2

HCl and ClONO2 are two important, respectively long-and intermediate-lived, chlorine reservoirs. The dominant chlorine reservoir before the onset of PSC processing is HCl. Chemical reactions destroying these particles are so slow in the gaseous phase that they normally do not occur. PSC particles, however, can play the role of catalyst of these reactions, converting these chlorine reservoir species into active chlorine species, such as Cl2 and HOCl, through the reactions

$$HCl + ClONO2 \rightarrow HNO3 + Cl2$$
$$ClONO2 + H2O \rightarrow HNO3 + HOCl$$
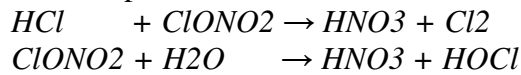
which take place on the surface of the PSC particles (chlorine activation).

Whereas HCl and ClONO2 are removed from gas phase and transformed into active chlorine species, the resulting HNO3 remains in the PSC particles and can either sediment or be released back into gas phase after PSC particles disappear.

The reanalyses indeed show that during the ozone hole conditions, almost all HCl and ClONO2 are lost and transformed into active chlorine due to heterogeneous chemistry (Figure 17 and Figure 18), lasting until the end of September/beginning of October. Chlorine activation at the South Pole stops about 1 week earlier in IFS-MOZART than in BASCOE and about 1 month earlier at latitudes around 60°S.
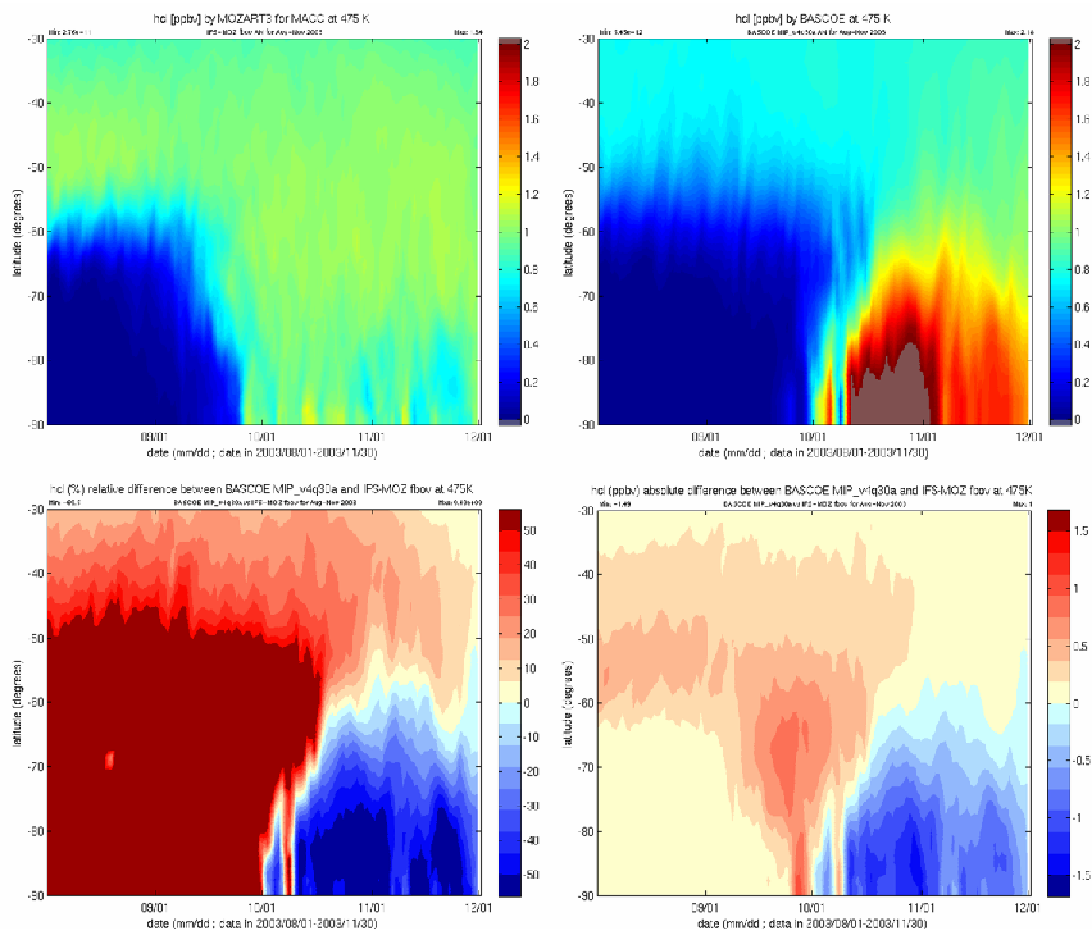


**Figure 17: Same as for Figure 21, but now for HCl.**

Even though the plot with the relative differences between IFS-MOZART and BASCOE gives a dramatic impression due to the almost complete removal of HCl (Figure 17 bottom left panel), the absolute differences (Figure 17 bottom right panel) confirm that IFS-MOZART and BASCOE output agrees very well during August and September 2003 inside the polar vortex. The final sudden stratospheric warming around the 10th of October and the consequent chlorine deactivation brings along a strong boost in HCl in the coarse of October, after which it stabilizes at somewhat lower but more or less constant levels during November. IFS-MOZART also shows a large increase at the end of September, but only half as large as what is simulated by BASCOE, leading to an underestimation of HCl during the months October and November.

Whereas HCl recovers very quickly, ClONO2 recovery happens a lot slower. In the severely denitrified and ozone-depleted conditions characteristic of late Antarctic winter, in the chlorine deactivation process, HCl production is highly favored and ClONO2 production is suppressed.

Around 60°S, BASCOE simulations show elevated values of ClONO2 outside the core of, but still within the polar vortex, similar to what was seen for HNO3 (Figure 16). IFS-MOZART simulations also show elevated values but at latitudes which are a bit shifted (at more southern latitudes) and it already stops at the end of September, where, on the contrary, an increase is observed in BASCOE, for the whole month of September until mid October at latitudes between 55 and 70°S.
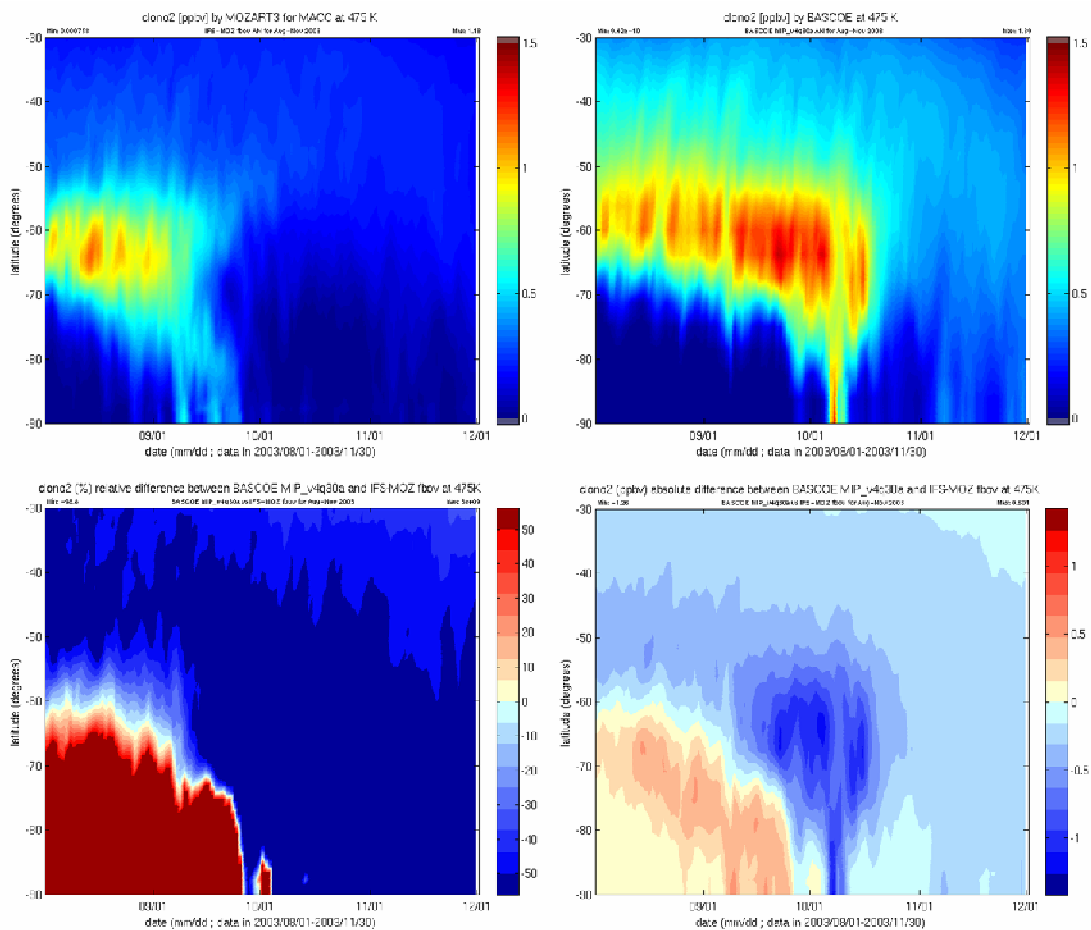


**Figure 18: Same as for Figure 21, but now for ClONO2.**
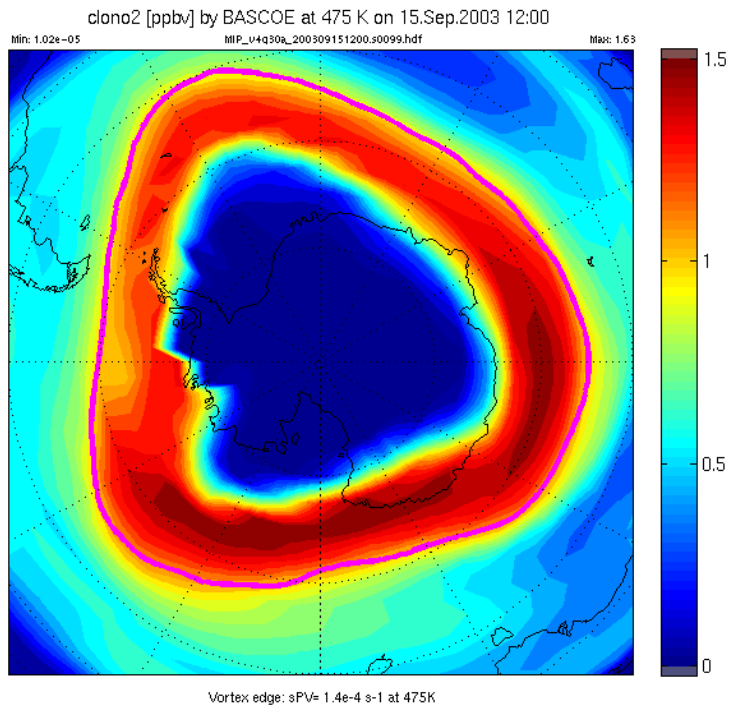
**Figure 19: Snapshot of ClONO2 on 15 Sept 2003 at the 475K isentropic level. In magenta, the vortex edge is indicated.**

### 3.5.5 Short-lived species: nitrogen oxides NOx

In Figure 20 we display the results for NOx (NO+ NO2). In general the agreement between IFS-MOZART and BASCOE is quite good. Only the recovery of NOx from IFS-MOZART starts too early compared to BASCOE and values are at least a half time larger than what is seen in BASCOE.
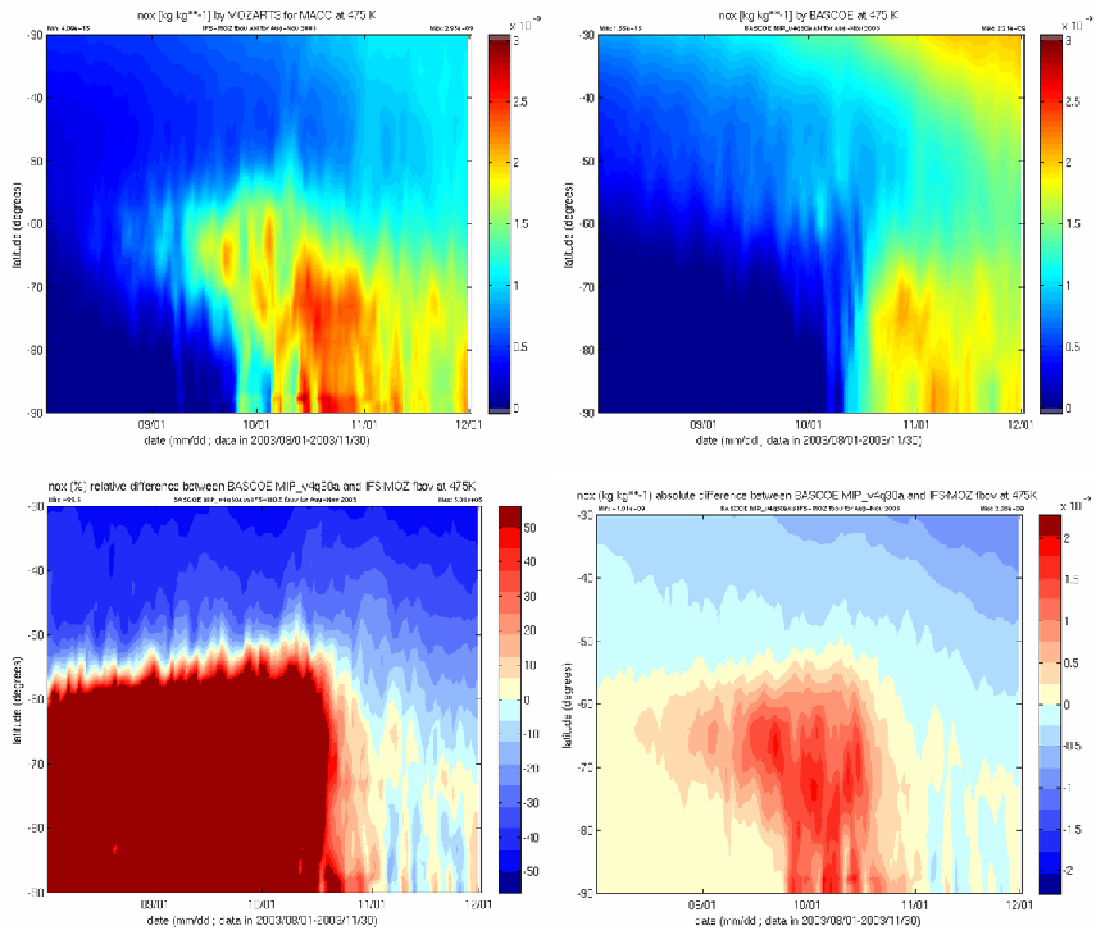


Figure 20: Same as for Figure 21, but now for NOx.

## 3.6    Ozone at 475K: IFS-MOZART versus BASCOE reanalyses

Figure 21 shows the zonally averaged time series of ozone for the Antarctic ozone hole season 2003 (Aug-Nov). Ozone depletion starts mid September and continues until early November, when it slowly starts to recover. Mid November there is a period where there is again more ozone depletion, but late November ozone concentrations are rising again. The behavior is very similar in IFS-MOZART and in BASCOE, although IFS-MOZART clearly underestimates the depth of the ozone hole. Also the onset of the ozone hole in IFS-MOZART is somewhat later than in BASCOE. Early August, IFS-MOZART predicts a period of +/- 5 days, where ozone is a lot lower (+/- 1.5 ppmv) at high latitudes (between 80 and 90°S) which is not seen in the BASCOE analyses. During the months September and October (but most pronounced in September), IFS-MOZART underestimates ozone at 475K between 60 and 75°S.
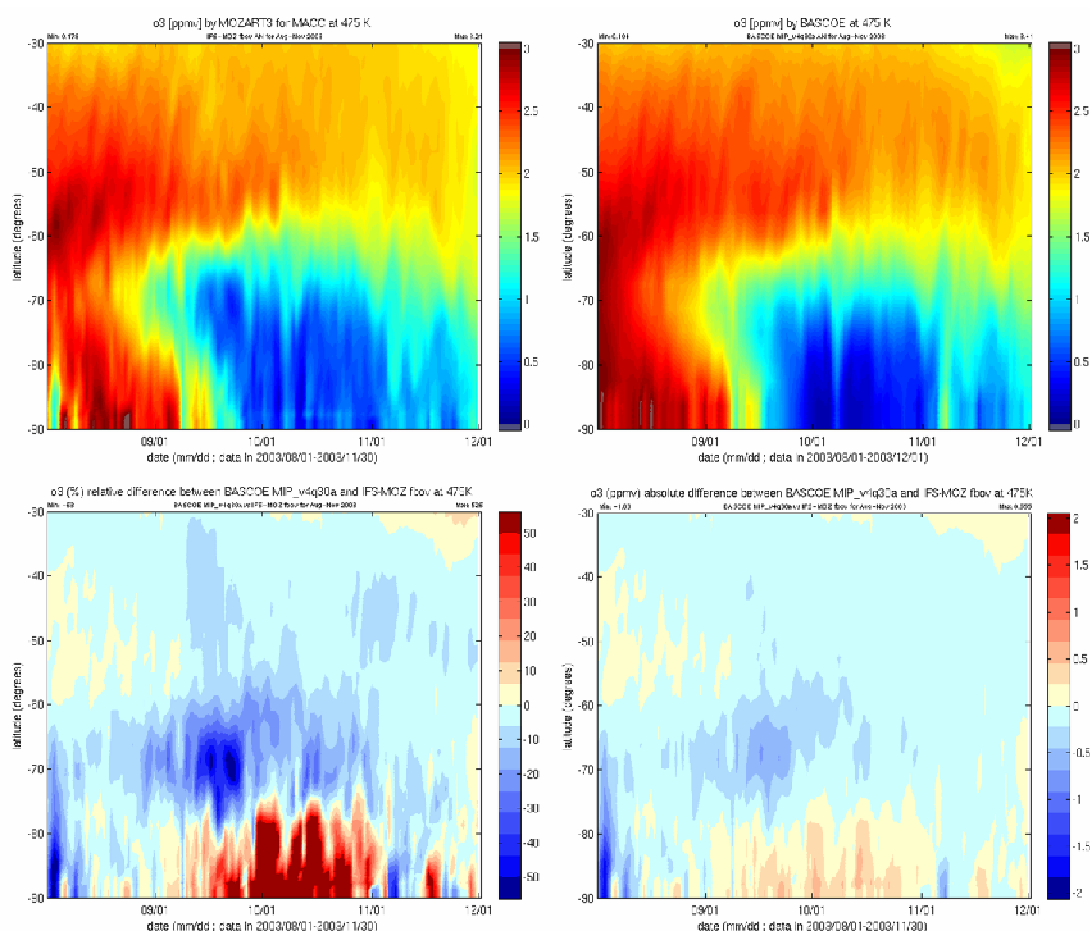


**Figure 21: Zonally averaged O3 time series for Aug-Nov 2003 at the 475K isentropic level, for the IFS-MOZART reanalysis fbov (top left) and the BASCOE reanalysis (top right), and the relative (bottom left) and absolute (bottom right) differences between the two runs.**

# 4 Case study 2: The Arctic ozone depletion event winter/spring 2011

## 4.1 General introduction

Arctic stratospheric temperatures during winter 2011 were lower than usual (Figure 22). Temperatures got cold very early in the winter (in December 2010 already) and continued to be that way until late March 2011. Winter conditions were somewhat similar to the severe stratospheric winter/spring 2004/2005. These long-lasting exceptionally cold conditions prevailing over the Arctic, together with man-made ozone-depleting compounds lingering in the atmosphere, caused the destruction of almost 40% of stratospheric ozone by the end of March. The previous record loss was 30%, which occurred several times over the past 15 years.   Figure 23 compares the monthly mean total ozone column for March this year with those from the previous 8 years. The last record year was winter/spring 2004/2005, when (as stated above) winter temperatures also got very cold, but didn't last for such a long period in time. The ozone depleted area was also clearly displaced from the North Pole.

Figure 24 shows the minimum total ozone values for this winter, compared with the previous 7 years. These clearly show that total ozone reached lower values than usual for the months March and April. The main NRT Forecast System used by MACC to monitor the stratosphere (IFS-MOZART), delivered analyses of ozone volume mixing ratio lower than 0.2 ppmv at the 475K isentropic level. The depletion started more or less at the beginning of March, reaching its maximum around the 27th of March as illustrated by Figure 25. At this moment the vortex is long-stretched, bringing these low values over Scandinavia and northwest Russia, when the ozone layer protects them from harmful UV radiation by values as low as 220DU. From then on, the ozone layer is slowly recovering.
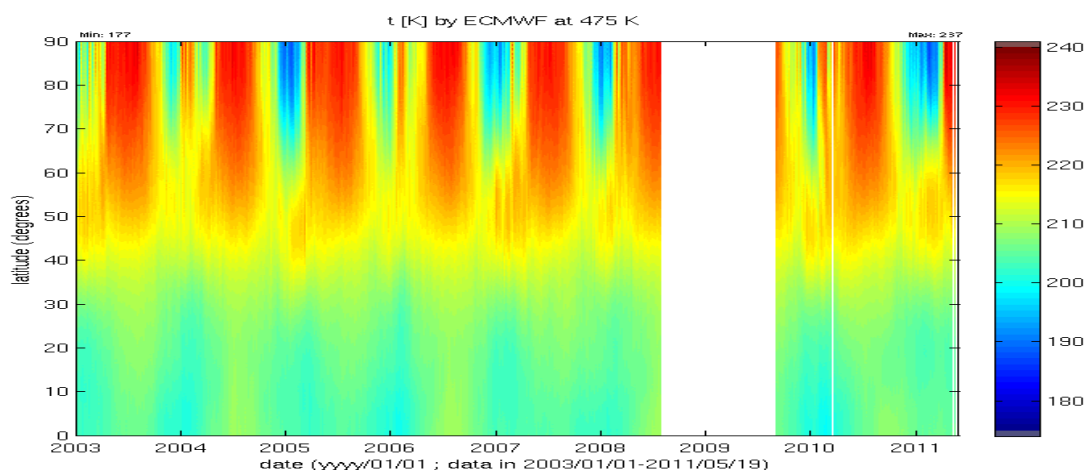


**Figure 22: Temperature evolution at the 475K isentropic level from 2003 to 2011 (temperatures from the MACC reanalysis (which is available until July 2008 at the time of writing), complemented with the temperatures from the MACC NRT analysis (starting as of Aug 2009).**
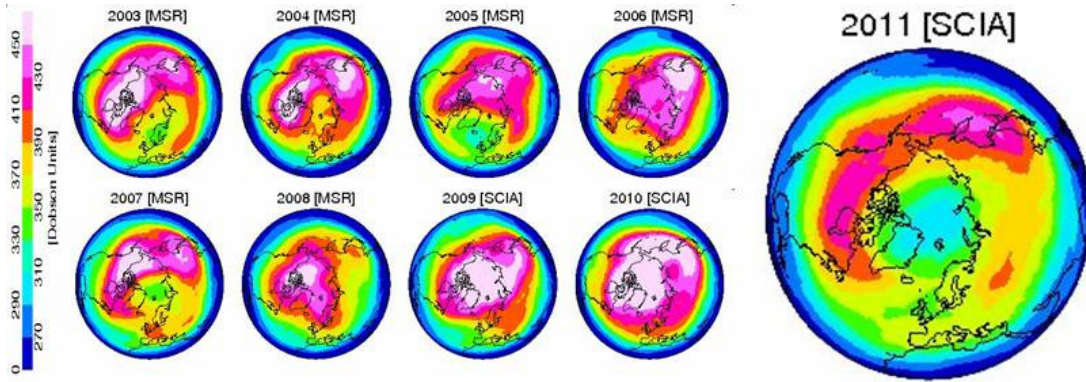
**Figure 23: Monthly mean total ozone for March 2003-2011 from the 30-year Multi Sensor Reanalysis (MSR, 1978-2008), complemented with SCIAMACHY analyses (2009-2011). Figure kindly provided by Ronald van der A.**
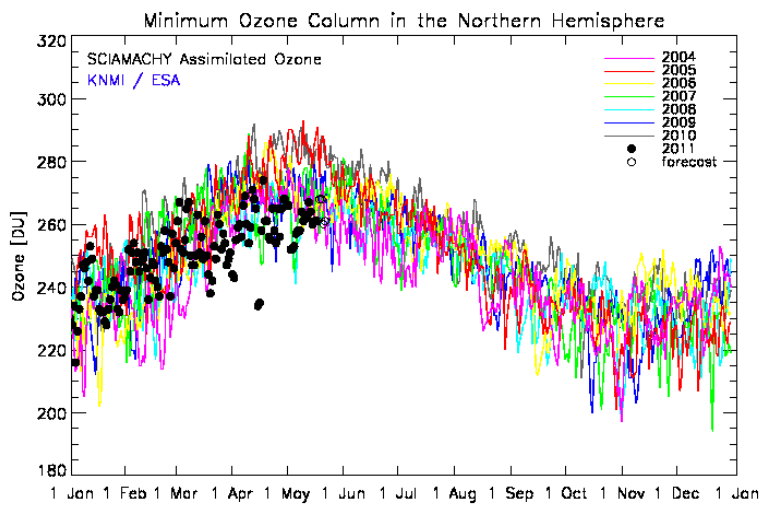


**Figure 24: Minimum ozone columns in the Northern Hemisphere for 2004-2011 from SCIAMACHY analyses. Figure kindly provided by Ronald van der A.**
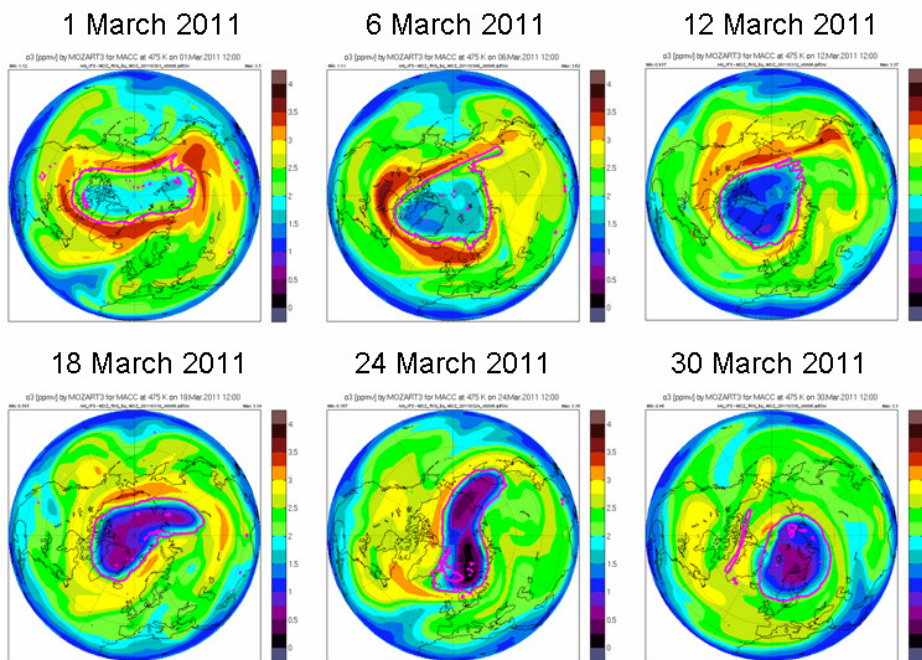


Figure 25: Evolution of ozone volume mixing ratios at 475K during March 2011

## 4.2    Meteorological context Arctic Winter/Spring 2011

Figure 26 shows the zonally-averaged time series for latitudes north of 30°N at the 475K potential temperature level. We will concentrate on this level for most of the rest of this case study for two reasons, first of all because this is exactly the location where ozone depletion appears most obvious, and secondly because it allows us to follow the adiabatic movement of the air parcels through the atmosphere. The two potential temperature contours at 188K and 196K in Figure 26 indicate the approximate temperatures below which different types of polar stratospheric clouds (PSC) can form. As mentioned in Section 3.2, temperatures below approximately 196K set the path to form solid NAT or liquid STS particles. When temperatures decrease even below 188K in the stratosphere, the conditions are right to form ice PSCs.
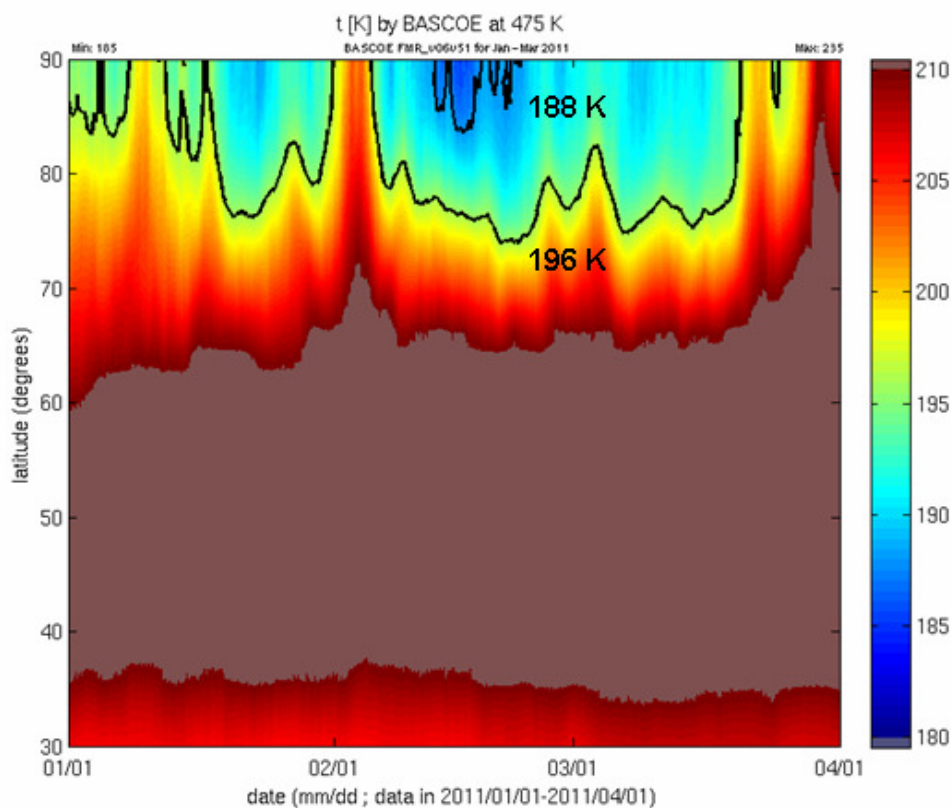


**Figure 26: Temperature evolution at the 475K isentropic level for the period January-March 2011, with the isocontours for T=188K and T=196K indicated by the black lines.**

We observe two periods of sudden stratospheric warming: one starting at the 20th of March which marks the end of the ozone "hole" season when the polar vortex breaks down, but also one at the beginning of February that lasts for 5 days. It coincides with a high pressure region with descending air (Figure 27). Sudden stratospheric warmings (SSW) occur every 1-3 years during the NH winter. They play an important role in the budget of trace species. To understand what is happening during this first stratospheric warming, we look at snapshots of the temperature with the polar vortex indicated (Figure 28). Due to a large growth in wave amplitude, the usual cyclonic polar vortex gets distorted, making it weaker and less stable (we even observe a vortex split at the 475K level), with consequent poleward fluxes of heat and an accompanying increase in temperature.
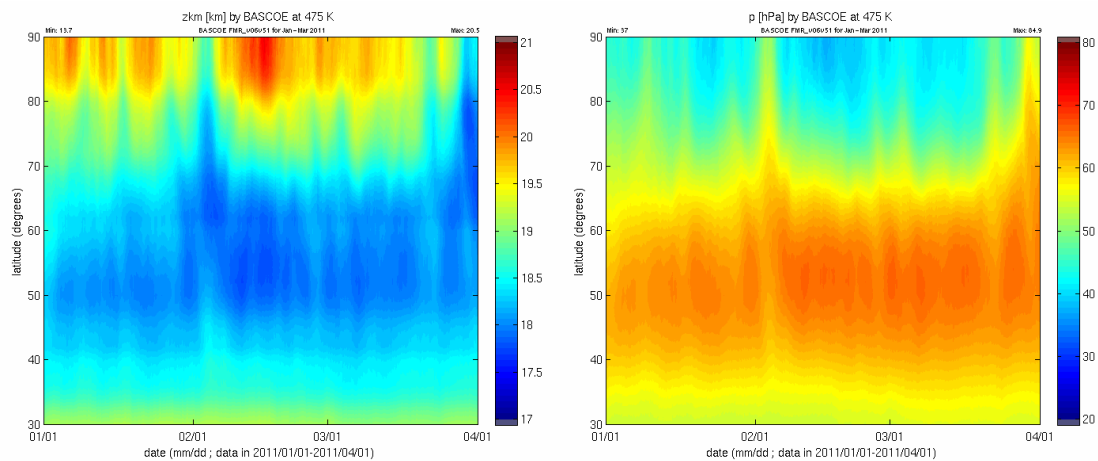


**Figure 27: Height and pressure at the 475K isentropic level.**
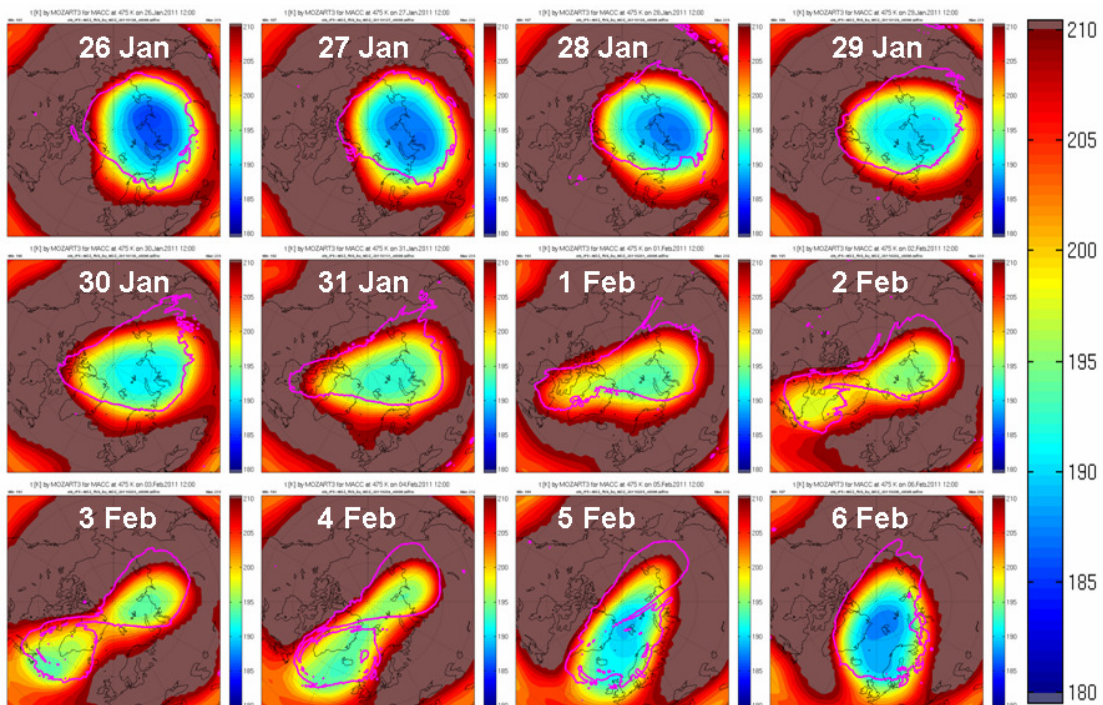


**Figure 28: North Pole snapshots from 26 Jan - 6 Feb. In magenta the polar vortex edge is indicated, calculated with an sPV > 1.7e-4/s.**

## 4.3 Total ozone columns: IFS-MOZART versus observations

In Figure 29 we compare the total ozone columns from the analysis of the coupled system IFS-MOZART with the data received by six SAOZ stations, which are part of the NDACC network: OHP, Salekhard, Sodankyla, Zhigansk, Ny Ålesund and Scoresby Sund[†]. In all cases, the model very nicely reproduces the observations.
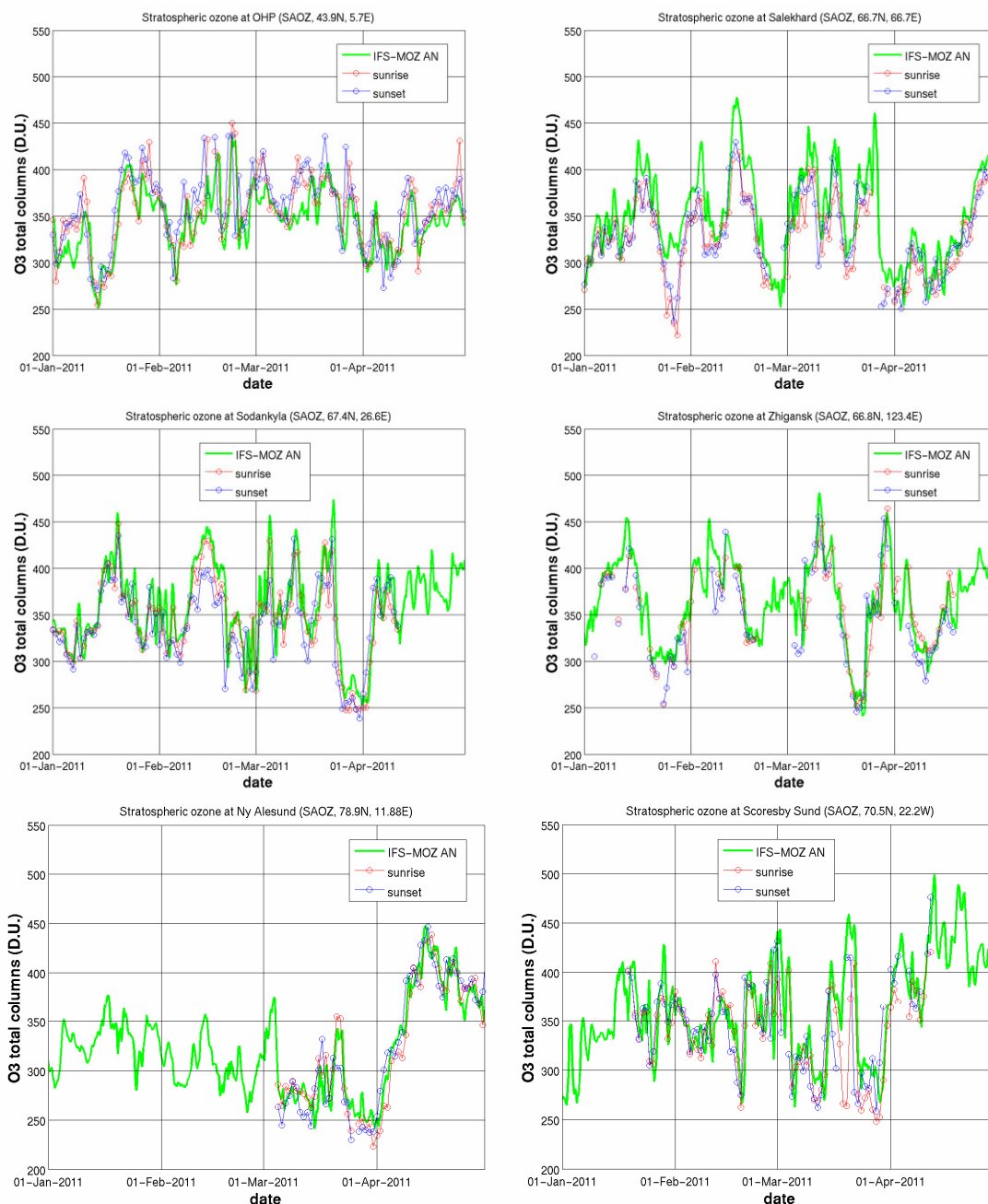


**Figure 29: Comparison total ozone columns (expressed in Dobson Units) for IFS-MOZART NRT AN (f93i, green) versus sunrise (red) and sunset (blue) measurements from six SAOZ stations: OHP, Salekhard, Sodankyla, Zhigansk, Ny Ålesund and Scoresby Sund** *(Data: see text)*.

---

[†] PI for OHP, Salekhard, Sodankyla, Zhigansk, Scoresby Sund: A. Pazmino and F. Goutail, LATMOS, CNRS/UVSQ, France
PI for Ny-Ålesund: K. Stebel, NILU, Norway

Whereas for five out of the six stations, total ozone columns highly vary between 250/300 and 450 D.U., total ozone at Ny Ålesund generally stays at a lower value throughout the winter period January-March 2011, with values between approximately 250 and 350 D.U., increasing very rapidly at the beginning of April with the end of the ozone hole season. After a highly variable winter season, also for Sodankyla and Scoresby Sund, we observe a very steep increase in total ozone at the start of Spring, with values staying above the 350 D.U. level from approximately the 10th of April on. Comparing the position of the stations at e.g. Scoresby Sund and Ny Ålesund w.r.t. the polar vortex, this is immediately understood: Ny Ålesund remains within the polar vortex all the time, while Scoresby Sund is moving in and out of the vortex, causing lower and higher values of ozone. Figure 30 maps the situation for the 11th and 20th of March for comparison.
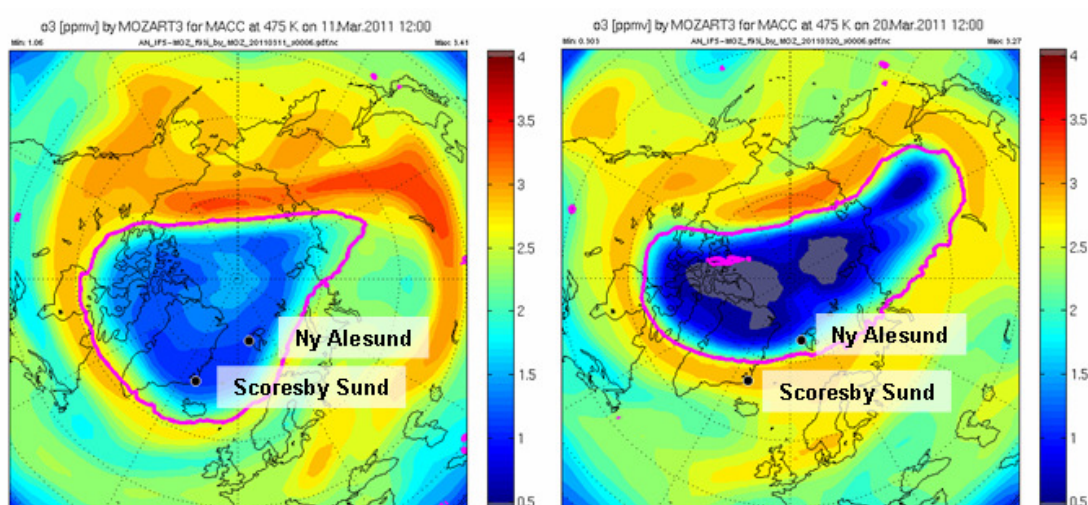


**Figure 30: North Pole O3 noon snapshots at 475K for 11 and 20 March 2011. The position of the 2 SAOZ stations at Ny Ålesund (78.9N, 11.88E, left) and Scoresby Sund (70.5N, 22.2W, right) are indicated, as well as the position of the vortex edge, indicated in magenta.**

## 4.4 Ozone-related species: IFS-MOZART versus BASCOE

### 4.4.1 Introduction

To understand the processes that lead to the ozone depletion record of winter/spring 2011 and to validate them in IFS-MOZART, we evaluate the behavior and evolution of the global stratospheric constituents that play a role in the chemical and dynamical processes of the ozone hole formation. For O3 and NOx, we compare with the "control run" f7kn, which is a forecast run without data assimilation, but which already started earlier than the forecast run *with* data assimilation, f93i, under a different IFS cycle and with a different MOZART version (and which can, for these reasons, not be considered as a true *control* run).

In what follows, we discuss and compare the results for O3, H2O, HNO3, NOx, HCl, ClONO2, N2O as delivered by the IFS-MOZART analysis with the results from the BASCOE Aura/MLS analysis. Figures in Appendix A prove that the analysis of Aura/MLS is close enough to the Aura/MLS observations for it to be considered as representative for them. Note that NOx and ClONO2 are not assimilated by BASCOE

and are therefore not shown in Appendix A. On the other hand, ClO and HOCl *were* assimilated, but shouldn't have. The data quality of these species is insufficient for assimilation and these data are not recommended for scientific use above 22 and 10 hPa respectively. As IFS-MOZART only assimilates O3 in the stratosphere, we can consider the output for all other (non-ozone) species as 'model output', and therefore we have chosen to additionally compare with a free model run of BASCOE, which was started at the beginning of the winter season on the 1st of Dec 2010. The latter is something that should be kept in mind when interpreting the results of the comparison as IFS-MOZART was started on the 1st of August 2009, running freely without any observational correction since then.

On the 26th of March 2011, MLS ceased sending telemetry to the Aura spacecraft and was accordingly placed into a standby mode, until recovery on 2011-04-19. Datasets are missing between these two dates and can/will have an important effect on both the IFS-MOZART and BASCOE analyses of Aura/MLS. Therefore, we limit most of the following discussion to the period extending up to the end of March 2011.

In the next sections, we will show zonally averaged time series of long- to short-lived species, of chlorine reservoir species and active chlorine compounds for the three above-mentioned models.

**Table 2: Overview of the main characteristics of the different runs that are used to validate the chemical processes in the stratosphere that lead to the 2011 Arctic ozone depletion event, with NAT = Nitric Acid Trihydrate, LBS = Liquid Binary Solution, and STS = Supercooled Ternary Solution**

| run | IFS-MOZ f93i | BASCOE FMR | BASCOE AN |
|---|---|---|---|
| **start date** | 2009-08-01 | 2010-12-01 | 2009-12-01 |
| **assimilation *stratospheric* species** | - O3 profiles: Aura/MLS NRT (latency < 1day)<br><br>- O3 total columns: SBUV-2 OMI SCIAMACHY | no assimilation | - O3, N2O, HNO3, HCl, HOCl, H2O profiles: Aura/MLS SCI (latency upto 4 days) |
| **horizontal resolution** | MOZ: 1.875° x 1.875° (191x95)<br>IFS: 1° x 1° (360x181) | 2.5° x 2° (144x91) | 3.75° x 2.5° (96x73) |
| **PSC parameterization** | based on NAT, LBS, STS and ICE<br><br>Described in Auxiliary Material of Kinnison et al. (2007) | based on NAT, LBS, STS and ICE<br><br>Parameterization from the chemical transport model REPROBUS | Cold T limit: T < 194 K → NAT T < 186 K→ ICE |

### 4.4.2 Long-lived tracer: nitrous oxide N2O

As N2O is a long-lived tracer, it is not expected to vary much over the time period Jan-March 2011 and any variations that may occur, could be attributed to transport. Both IFS-MOZART and BASCOE FMR overestimate N2O within the vortex. We can think of three possible explanations for this overestimation.

- When a model runs freely for too long, transport can adds spurious mixing across the vortex edge, resulting in horizontal gradients that are too weak w.r.t. the analysis
- The diabatic downward velocities may be stronger than what is found from the meteorological analyses
- Wrong loss rate

We suspect that IFS-MOZART f93i has some transport problems, e.g. during the events of sudden stratospheric warming early February and at the end of March, the upward air movement should bring *more* N2O, while we observe a decrease in N2O at these moments.
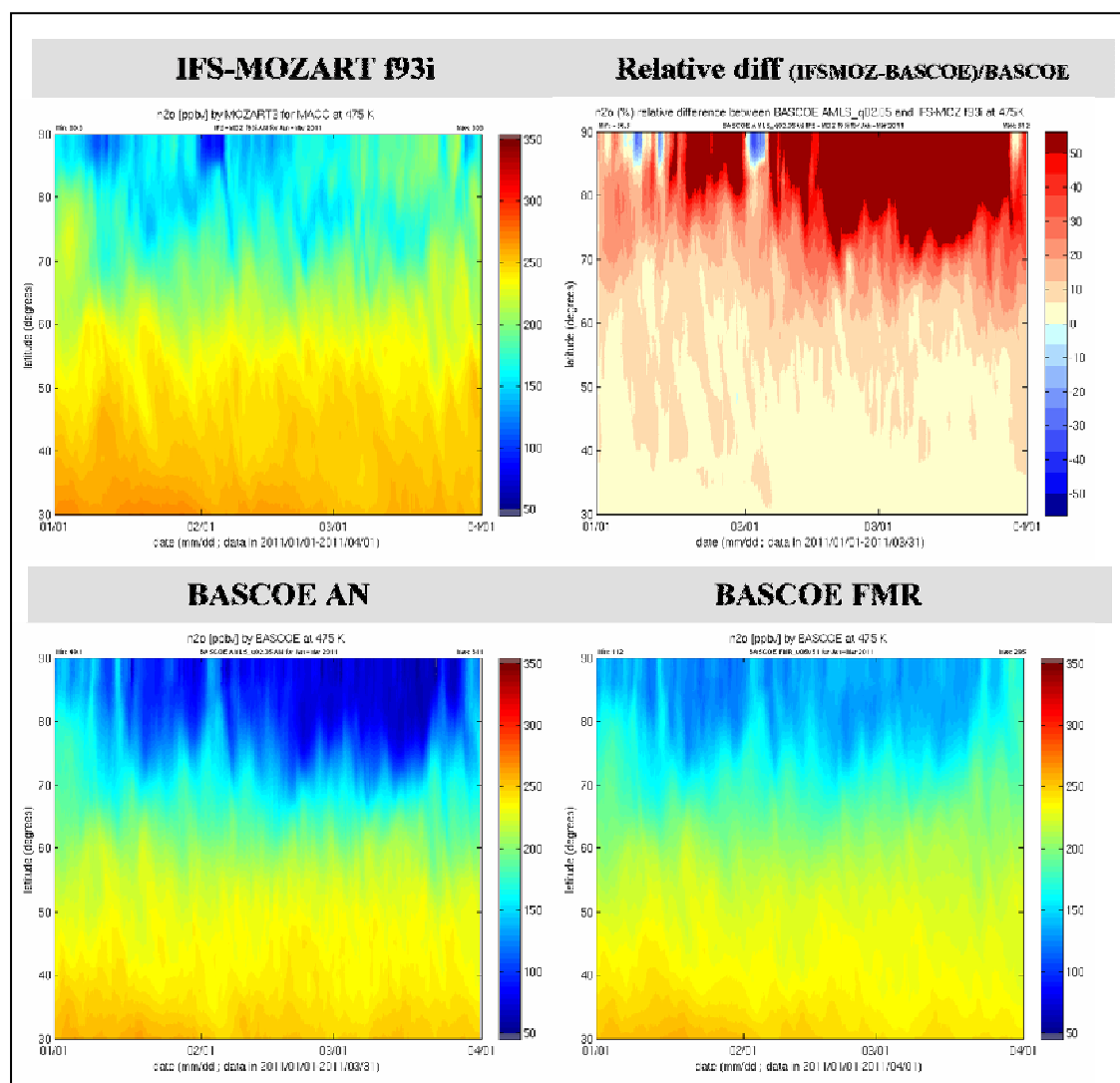


**Figure 31: Zonally averaged N2O time series for Jan-March 2011 at the 475K isentropic level, for the IFS-MOZART run f93i (top left), the BASCOE analysis (bottom left), the relative difference between the two (top right), and the BASCOE free model run (bottom right).**

### 4.4.3 Water Vapor H2O

Recalling the temperature time series (Figure 26), we see that only during a 5-day period in mid February temperatures were low enough to form ice PSCs and thus to possibly cause dehydration due to the formation of these ice clouds. Whereas the BASCOE free model run simulates some dehydration during this period, it is not observed. The BASCOE H2O analysis suggests that there was no or only very little ice PSC formation. Water vapor in IFS-MOZART is globally too low compared to the analyses. This may however be due to the fact that the IFS-MOZART run already starts with a bias, as it was already running freely since the 1st of August 2009, without any further bias correction towards the observations.
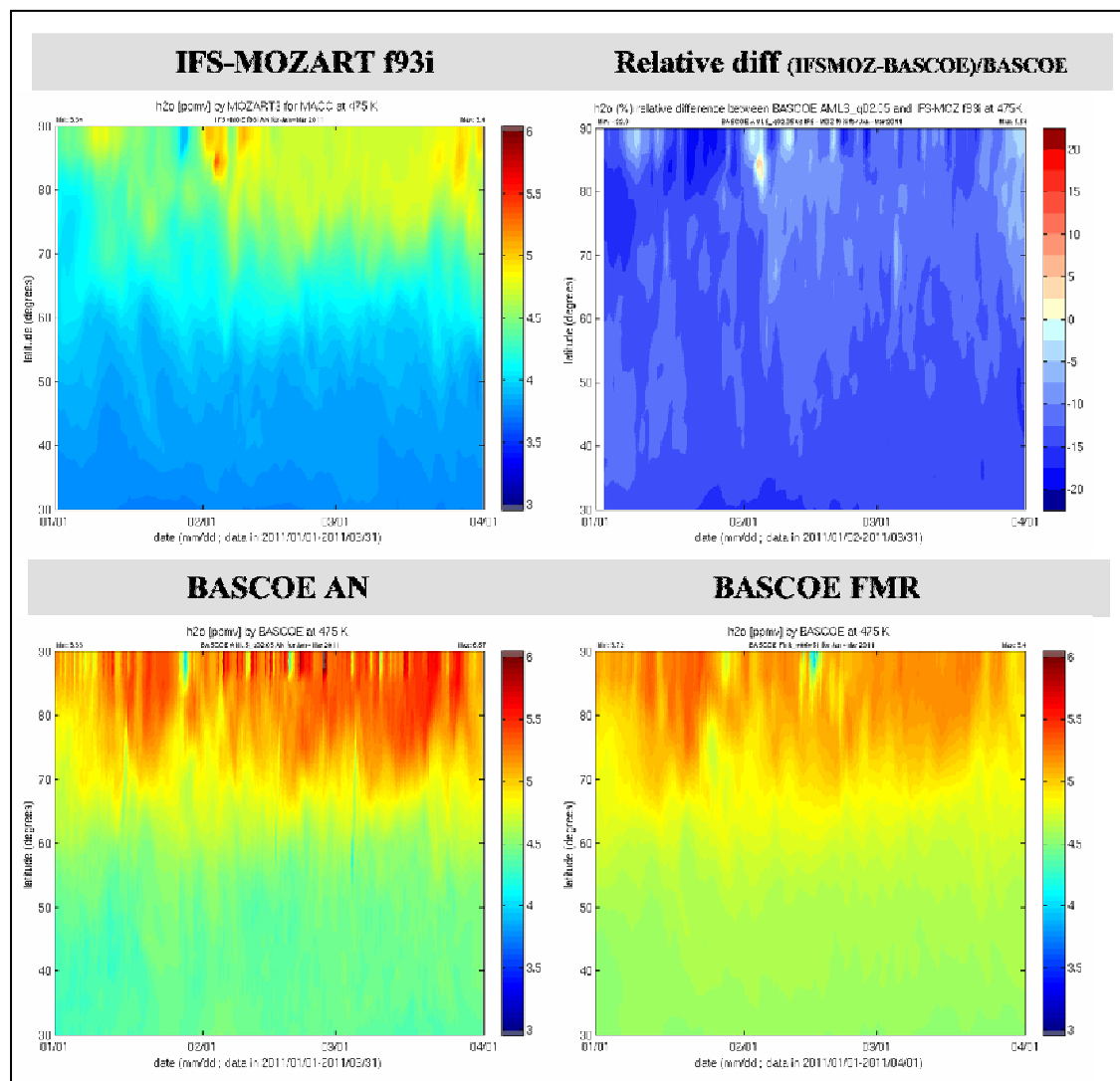


**Figure 32: Same as for Figure 31 but now for H2O.**

### 4.4.4 Reservoir species: nitric acid HNO3

The BASCOE analysis shows important denitrification. The formation of NAT (HNO3.3H2O) and STS (H2O/H2SO4/HNO3) remove HNO3 from the gaseous phase. Denitrification is mainly caused by the formation (and then partly by the sedimentation) of NAT particles. Whereas the REPROBUS parameterization clearly overestimates this denitrification, Figure 34 shows that the parameterization in IFS-MOZART performs very well. Taking into account the initial bias at the start of the winter season, the HNO3 trend followed by IFS-MOZART is very similar to the BASCOE analysis.

When the temperature rises above the level required for PSCs to exist, HNO3 is released from the PSC back into gas phase and we see an increase in HNO3. This increase is highly overestimated by the BASCOE free model run. Probably the model predicted too many small NAT particles, not large enough to sediment and fall out and consequently a too large restore of HNO3 into gas phase. Another explanation could be that, once the polar vortex gets weaker, the air from the central core of the vortex gets mixed with the air at lower latitudes which has elevated abundances of HNO3 (see further).
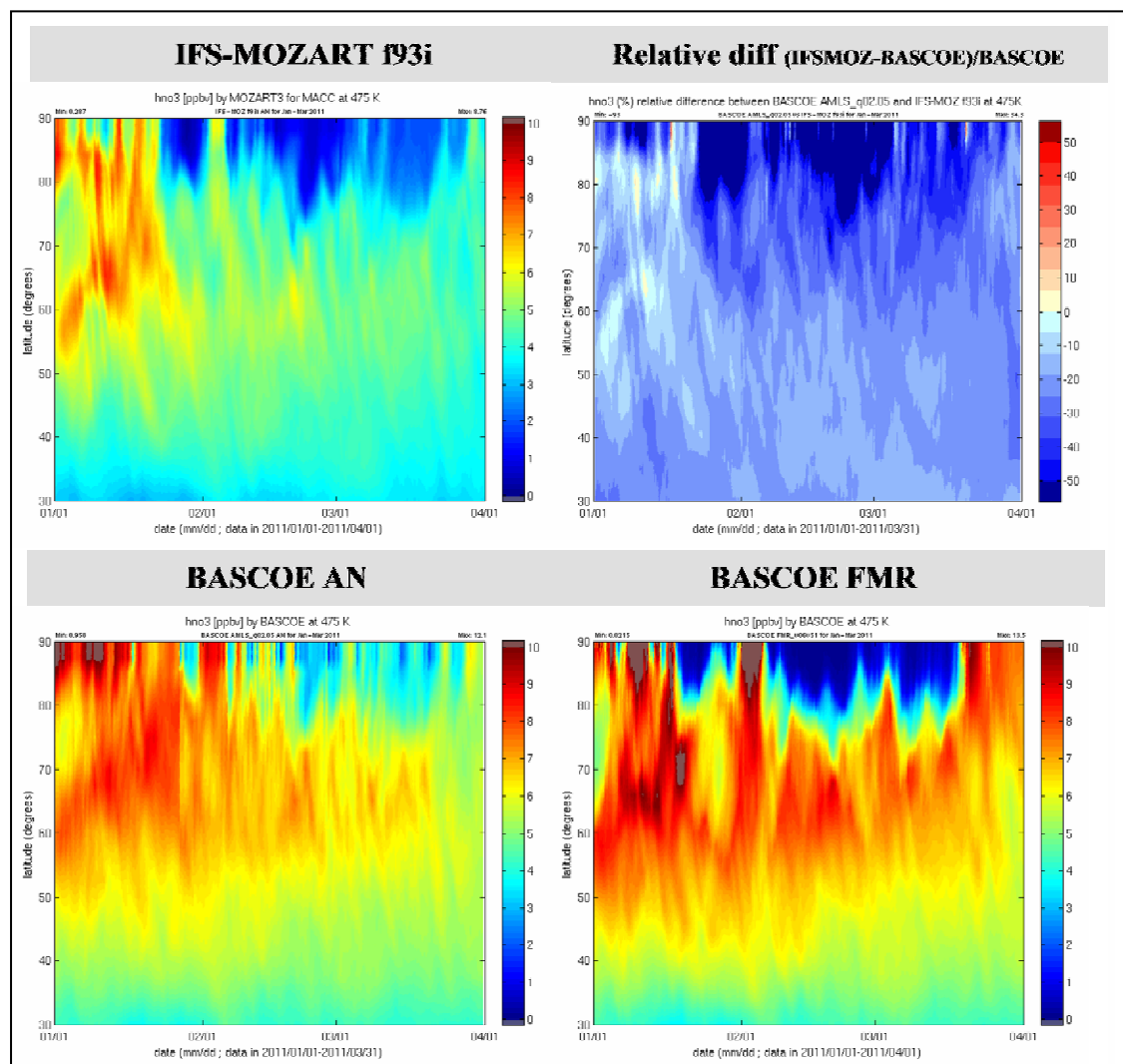


**Figure 33: Same as for Figure 31 but now for HNO3.**
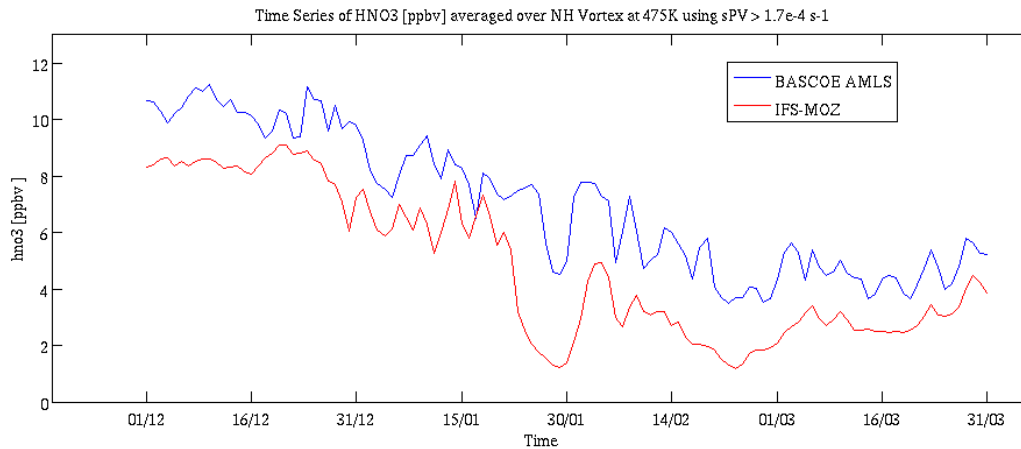
**Figure 34: Time series of nitric acid averaged over the northern hemisphere vortex at 475K using an sPV > 1.7e-4 s-1**

Figure 35 shows that the polar vortex is divided into two area's. On the one hand, there is the strongly mixed inner core, where temperatures can decrease low enough to form PSC particles and reduce HNO3 significantly. Separated from the core, there is a broad ring of weakly mixed air extending to the vortex boundary. A transport barrier between the two areas prevents air from getting mixed. This is something which is usually seen in the Antarctic vortex, which is much stronger, but can also be seen from the HNO3 snapshots. HNO3 is strongly reduced in the inner core of the vortex, where temperatures decrease below +/-195K. Outside of this central part, HNO3 cannot leave the isolated vortex due to the transport barrier at the vortex edge and keeps building up. While IFSMOZ predicts too few of this build up (which, again, may be related to the initial bias), BASCOE FMR has too much of it compared to the analysis. Once the vortex gets weaker and air gets mixed, this overestimation of HNO3 in the ring around the core of the polar vortex may play a role in the overestimation of HNO3 at the poles.
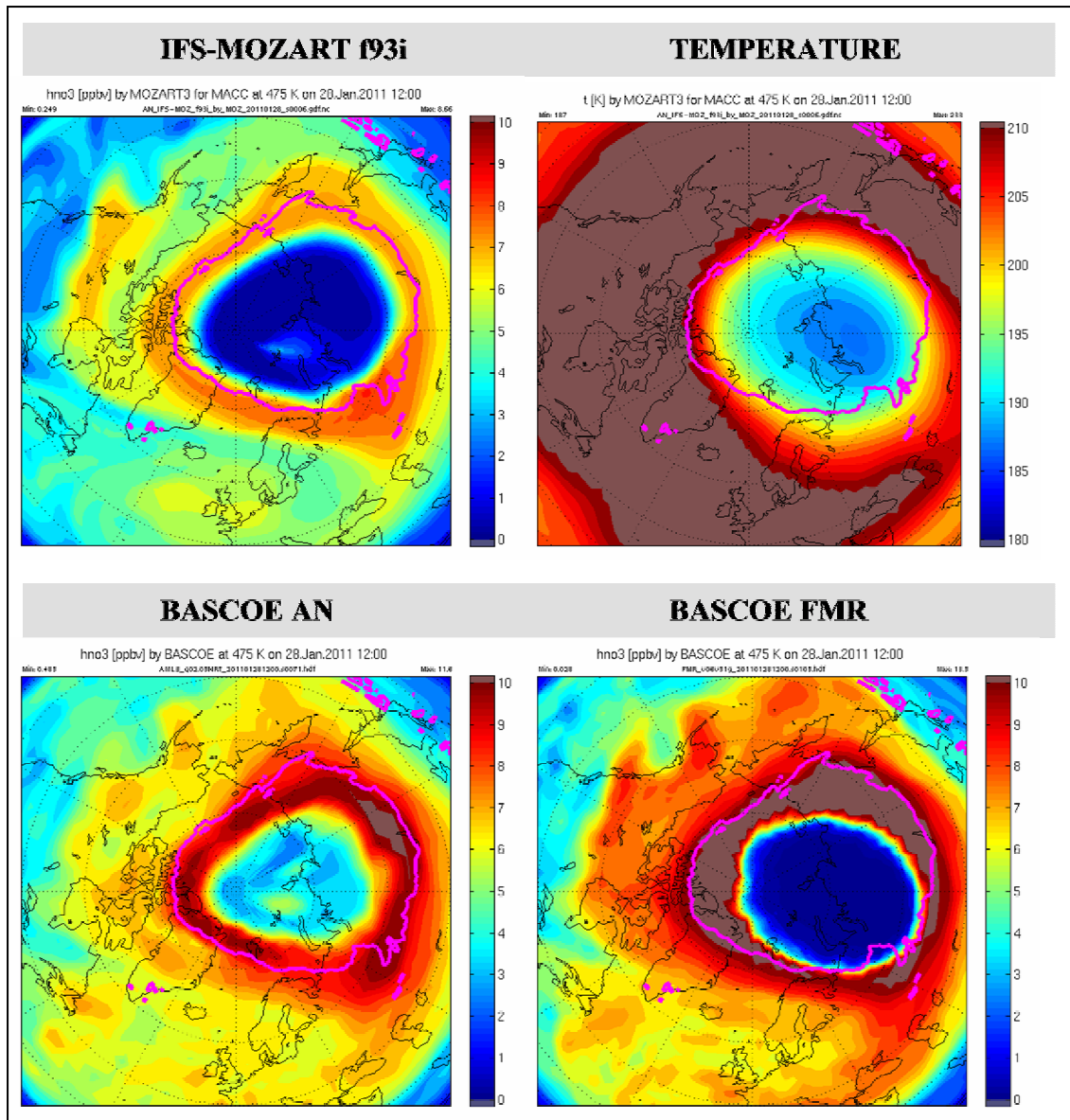
**Figure 35: North Pole snapshots for the 28th of January 2011: HNO3 from IFS-MOZART (top left), BASCOE Aura/MLS AN (bottom left), BASCOE free model run (bottom right), with the temperature (top right). This illustrates the division of the polar vortex into two areas: a strongly mixed inner core and isolated from it a broad ring of weakly mixed air extending to the vortex boundary, leading to a completely different HNO3 behaviour.**

### 4.4.5 Chlorine reservoir species: hydrogen chloride HCl and chlorine nitrate ClONO2

HCl and ClONO2 are two important, respectively long-and intermediate-lived, chlorine reservoirs. Figure 38 shows that HCl is actually the dominant chlorine reservoir before the onset of PSC processing. Chemical reactions destroying these particles are so slow in the gaseous phase that they normally do not occur. PSC particles, however, can play the role of catalyst of these reactions, converting these chlorine reservoir species into active chlorine species, such as Cl2 and HOCl, through the reactions    *HCl      + ClONO2 → HNO3 + Cl2*
        *ClONO2 + H2O      → HNO3 + HOCl*
which take place on the surface of the PSC particles (chlorine activation).
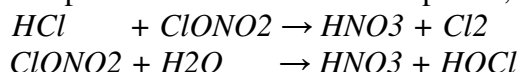
Whereas HCl and ClONO2 are removed from gas phase and transformed into active chlorine species, the resulting HNO3 remains in the PSC particles and can either sediment or be released back into gas phase after PSC particles disappear.

The BASCOE analysis indeed shows important HCl and ClONO2 losses due to heterogeneous chemistry (Figure 37 and Figure 39). The BASCOE FMR overestimates this loss for HCl. Even though the FMR starts with the same initial conditions as BASCOE AN on the 1st of December, the simulation removes HCl much too quickly and the reformation at the end of March is too slow. For IFS-MOZART it is exactly the opposite: the HCl removal is too slow in the beginning and the reformation too fast at the end (Figure 36). The PSC parameterization in IFS-MOZART seems too sensitive to the temperature increase during the two sudden stratospheric warming events at the beginning of February and at the end of March.

Figure 38 supports the canonical picture of chlorine deactivation in the Arctic, with the primary pathway the reformation of ClONO2, followed by slow repartitioning between ClONO2 and HCl.
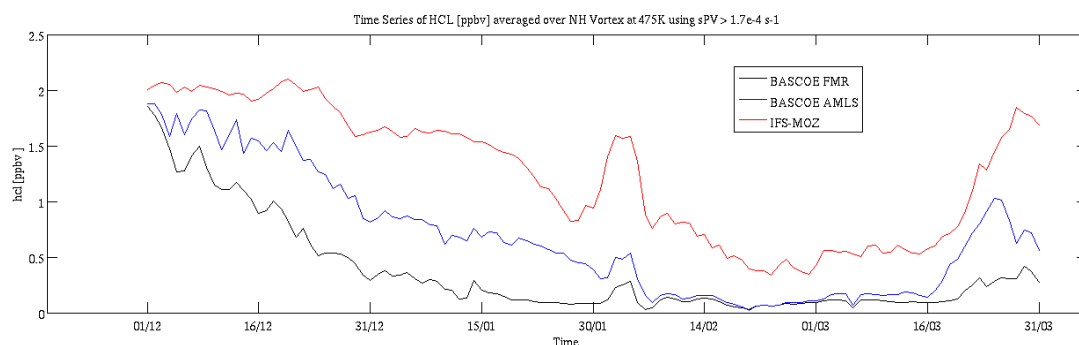


**Figure 36: Time series of hydrogen chloride averaged over the northern hemisphere vortex at 475K using an sPV > 1.7e-4 s-1 for IFS-MOZART compared to BASCOE FMR and BASCOE AN.**
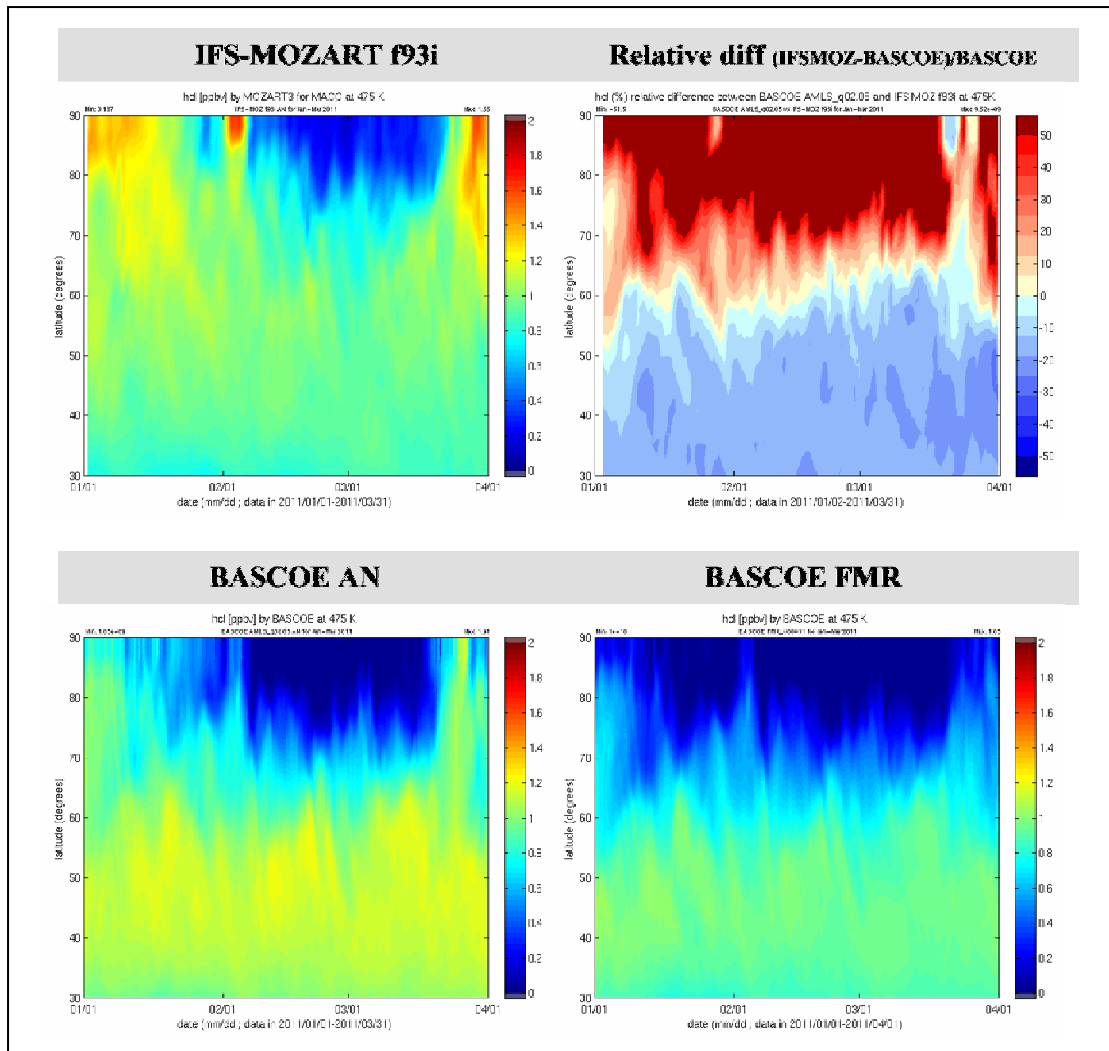
**Figure 37: Same as for Figure 31 but now for HCl.**
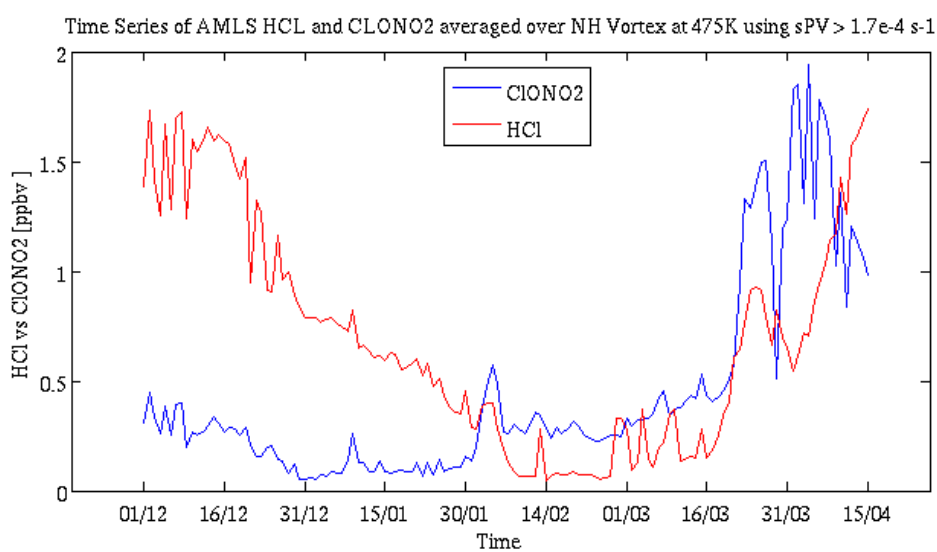


**Figure 38: BASCOE HCl and ClONO2 AN time series, averaged over the northern hemisphere vortex at 475K using an sPV > 1.7e-4 s-1.**
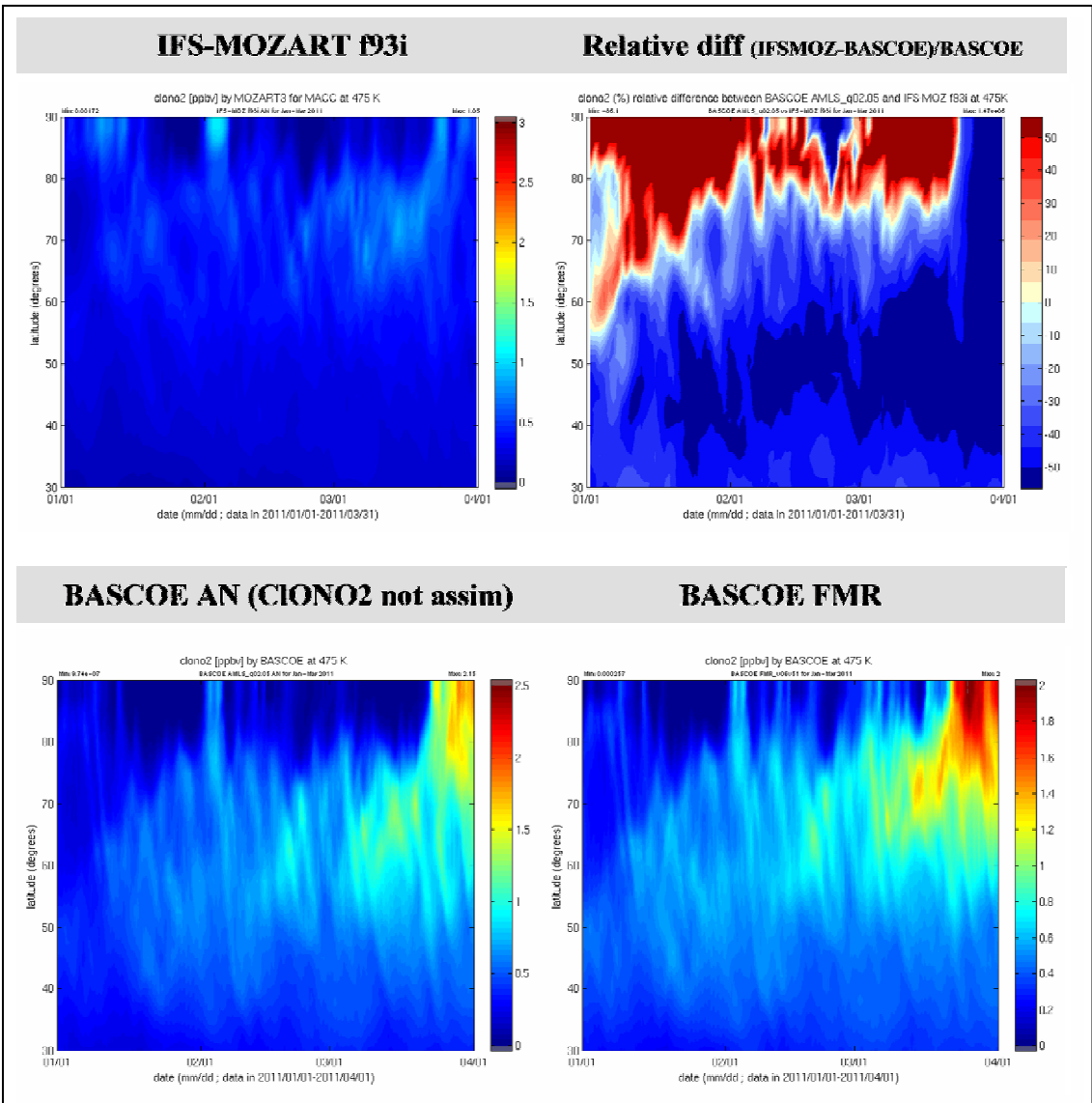
**Figure 39: Same as for Figure 31 but now for ClONO2. Note that ClONO2 is not one of the Aura/MLS species that is assimilated by BASCOE.**

### 4.4.6 Short-lived species: nitrogen oxides NOx

In Figure 40 we display the results for NOx (NO+ NO2). This time, we also compare the IFS-MOZART analysis with the IFS-MOZART control run. They seem to agree very well, except for the two periods of sudden stratospheric warming. This is particularly clear for the final stratospheric warming, where NOx values for *f93i* are at least three times as high as in the control run *f7kn*. Even though the control run is not a proper control run, we nevertheless had a closer look at what was happening in the analysis during this period by investigating the snapshots (Figure 41). These show that at the end of March, the polar vortex is already elongated and weakening. At the 22nd of March, in the upper (on the figure) part of the vortex (above Asia) a structure of elevated NOx values starts to form, rising in values, extending in area and spreading from there over the entire vortex by the 27th of March. Similar patterns are seen in the control run, even though less pronounced, but values don't rise in a similar way as the NRT run. It is not entirely clear what may be the cause of this. For completeness and consistency with the previously discussed figures, we also show the BASCOE analysis, even though NO and NO2 are also not assimilated by BASCOE (which is also the case for *f93i*). It must be noted though that BASCOE does assimilate observations of N2O, which is the main source of NOx in the stratosphere.
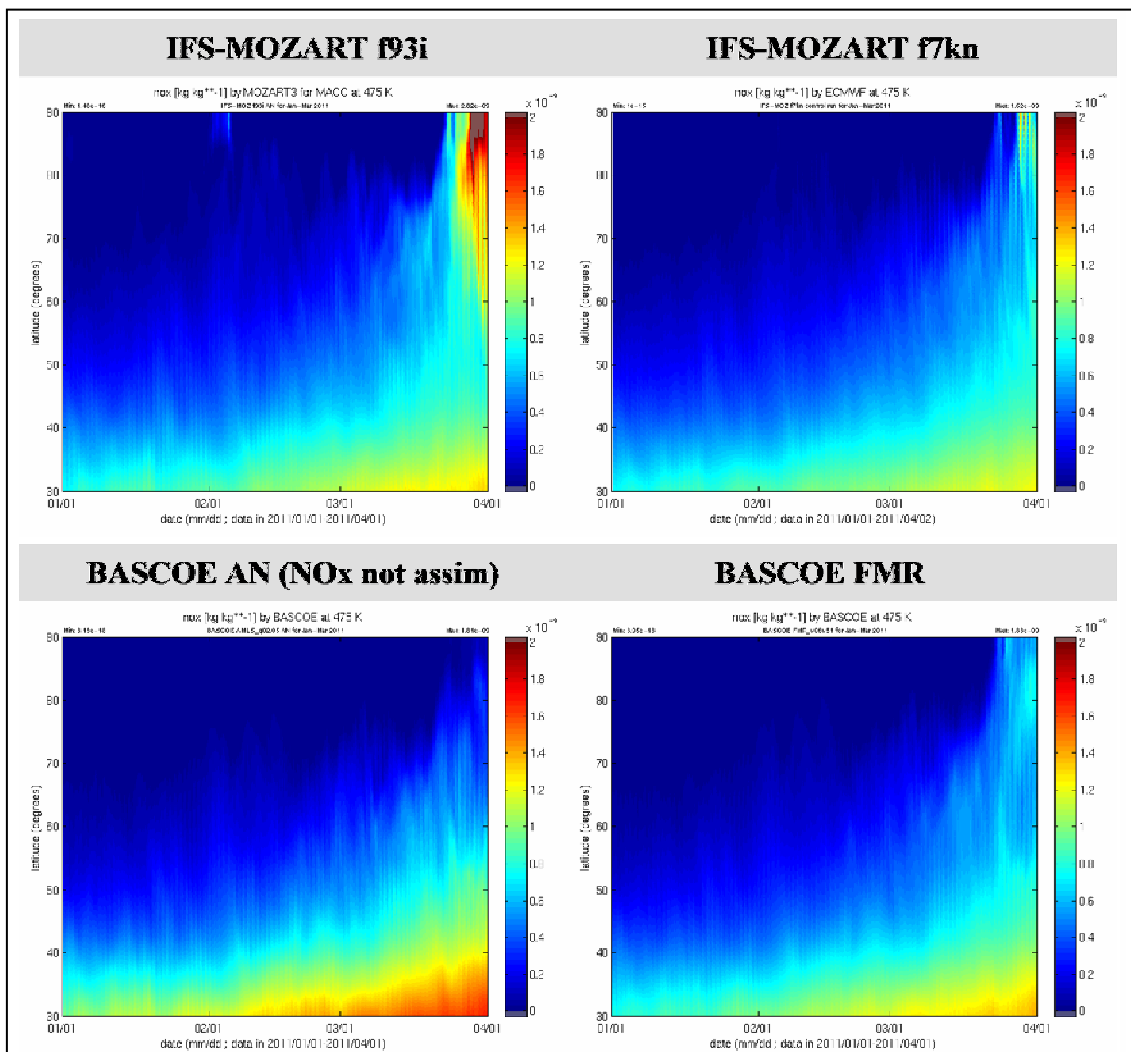


**Figure 40: Same as for Figure 31 but now for NOx. Instead of relative differences, we plot the IFS-MOZART control run f7kn.**
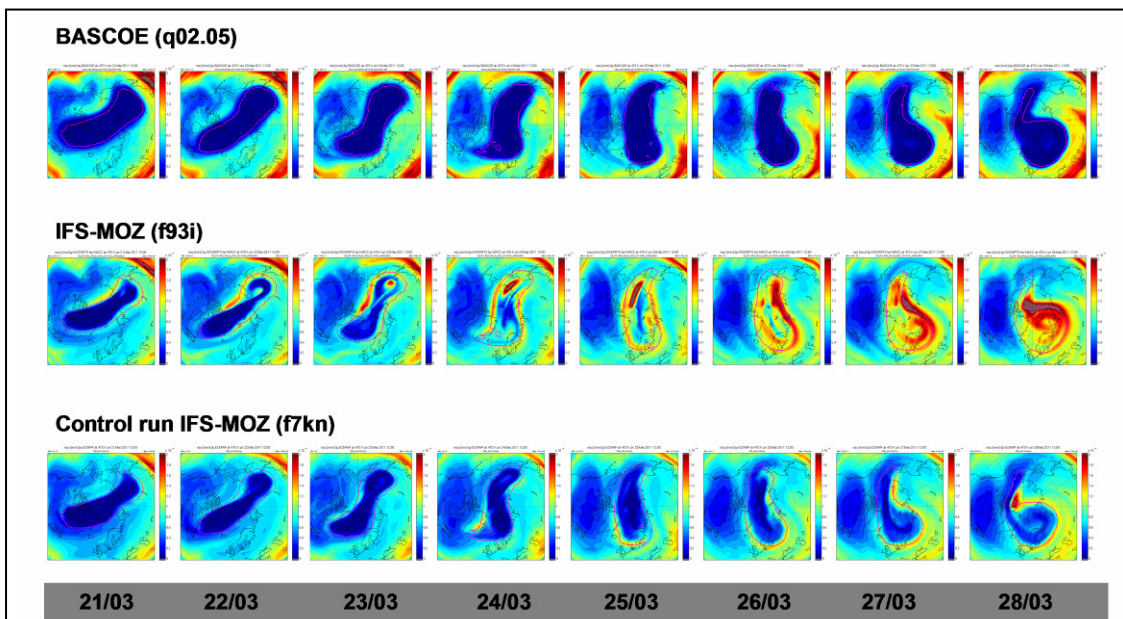
**Figure 41: NOx model snapshots for BASCOE "analysis", the IFS-MOZ "analysis" and the IFS-MOZ "control run" for the period 21-28 March 2011.**

## 4.5 Ozone at 475K: IFS-MOZART versus BASCOE

The MACC ozone analyses nicely reproduce the Arctic ozone depletion (top panels of Figure 42). It slowly starts at the beginning of March when heterogeneous reactions on the surface of PSCs take place and chlorine radicals are produced due to the return of sunlight after the long polar night. Near the 20th of March, ozone depletion reaches its maximum after which the ozone depleted area slowly recovers and finally disappears in the coarse of April, when the polar vortex weakens and finally breaks up.

Whereas the ozone hole is well captured by the analyses, the corresponding control runs do not simulate the ozone depletion correctly (Figure 42). On the one hand, the performance of the IFS-MOZART run f93i is hard to interpret if it starts more than a year before this particular event, without any intermediate correction by observations. Conclusive evaluation of stratospheric processes in IFS-MOZART requires a new FC run from 2010/12/01 starting from BASCOE analyses.

On the other hand, polar ozone depletion in models was validated mainly for Antarctic ozone hole and is probably not well adjusted for such unusual events at the North Pole. Changes to PSC parameterizations for a better simulation of Arctic ozone depletion events are clearly needed. The previous discussion of the IFS-MOZART parameterization in comparison with the BASCOE analysis (representative for the Aura/MLS observations) and the BASCOE FMR (independent free model run) for ozone-related species might be a first step in this direction.
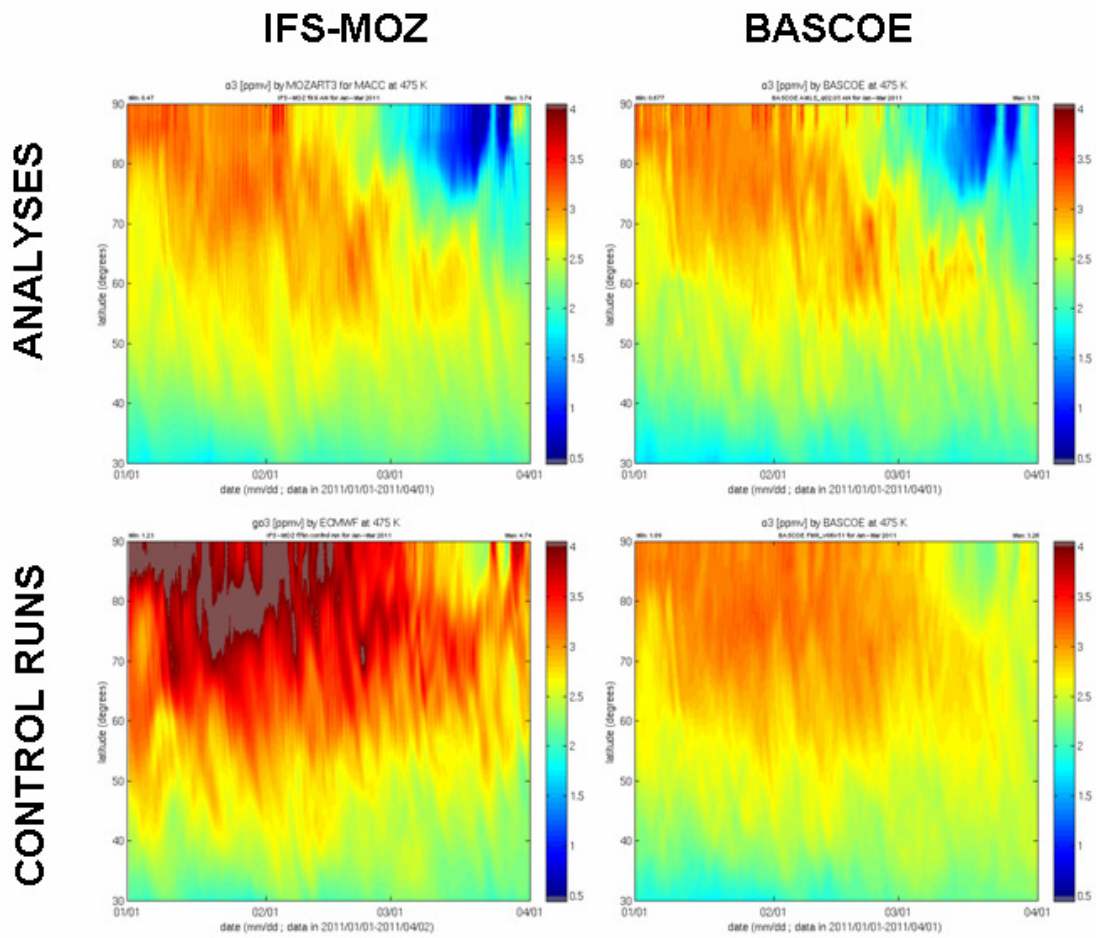
**Figure 42: Zonally averaged O3 time series for Jan-March 2011 at the 475K isentropic level, for the IFS-MOZART run f93i (top left), the BASCOE analysis (top right) and their respective "control runs": IFS-MOZART without data assimilation (bottom left) and BASCOE free model run (bottom right).**

## 4.6 NRT Validation of IFS-MOZART and IFS-TM5 using O3 soundings

*Annette Wagner, Harald Flentje, and Werner Thomas*

### 4.6.1 Validation data

Model profiles of the Near-Real-Time forecast runs IFS-MOZART without data assimilation (f7kn), IFS-MOZART with data assimilation (f93i) and IFS-TM5 (f9nd) were compared to balloon sonde measurement data of 10 stations taken from the data bases NDACC (Network for the Detection of Atmospheric Composition Change), WOUDC (World Ozone and Ultraviolet Radiation Data Centre), NILU (Norwegian Institute for Air Research) and SHADOZ (Southern Hemisphere Additional Ozone Sondes) for the validation of the arctic ozone hole conditions in spring 2011.
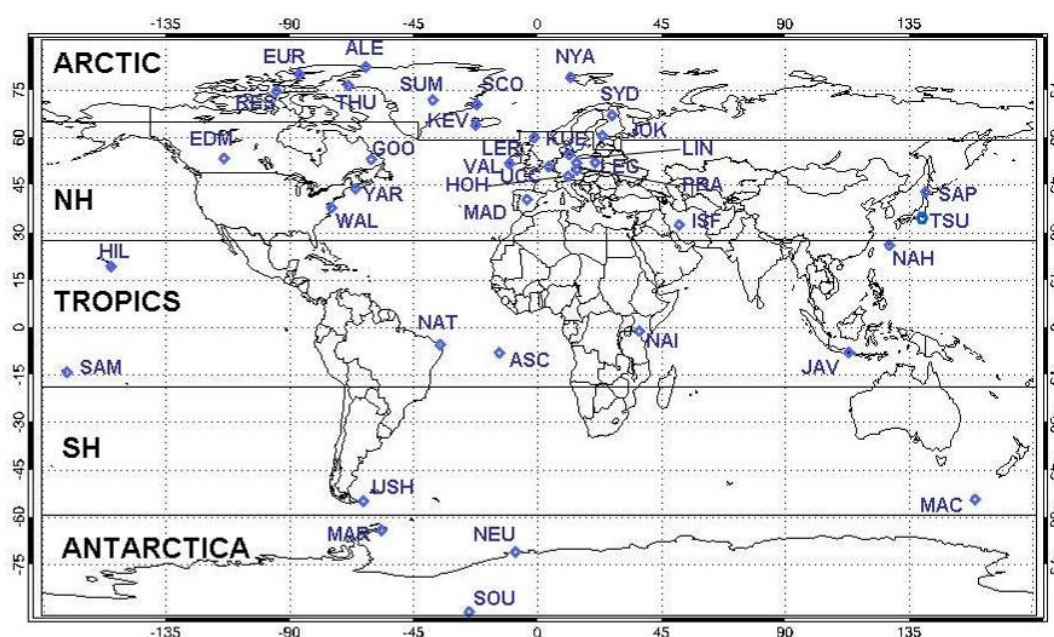


**Figure 43: Map of the NDACC stations. The 10 stations located in the Arctic region were used for the validation of the Arctic ozone hole conditions in spring 2011.**

### 4.6.2 Methodologies

Model values at the station's locations in the horizontal are interpolated linearly from the model gridded data. To make the measurement results comparable to model data, first of all the sonde ozone units are converted from partial pressure to mass mixing ratio using the following conversion formula: ppmm = $p_{O3}$ * 10/p * M with M the molecular ratio $O_3$/air = 1.657 and secondly, the sonde profiles are fitted to the model levels. The latter is done by linearly interpolating the sonde values to the model levels, after which they are averaged between the model levels. No temporal interpolation is done. Instead, we only compare the sonde profiles with the forecast to which it is closest in time.

From these individual comparisons, monthly mean profiles of

$$\text{Bias}(p) = 1/N \, \Sigma_i \, (O_{3 \, \text{Model}}(p)_i - O_{3 \, \text{Sonde}}(p)_i), \tag{1}$$

$$\text{NMBias}(p) = 1/N \, \Sigma_i \, (O_{3 \, \text{Model}}(p)_i - O_{3 \, \text{Sonde}}(p)_i)/( O_{3 \, \text{Sonde}}(p)_i), \tag{2}$$

$$\text{MNMBias}(p) = 2/N \, \Sigma_i \, \text{Bias}(p)_i/(O_{3 \, \text{Sonde}}(p)_i + O_{3 \, \text{Model}}(p)_i), \text{ and} \tag{3}$$

$$\text{FGE}(p) = 2/N \, \Sigma_i \, (|\text{Bias}(p)_i/(O_{3 \, \text{Sonde}}(p)_i + O_{3 \, \text{Model}}(p)_i)|) \tag{4}$$

are derived, where $i$ denotes the individual profile measurement at pressure level $p$. For monthly averages, $N$ describes the number of profiles of one station per month; for monthly regional averages, $N$ describes the number of all measured $O_3$ profile within the considered region within a month. These calculations are only performed provided that at least two single comparison results per month are available. The lowest 6 levels are not included in the validation as sonde measurements in the first levels might suffer from measurement artefacts. Further information about the methodologies was described in J. Cammas et al. (2009).

To get an overview of the main performance of the three model runs, spatial averaging is applied. Table 3 lists the geographical regions and the associated latitude band. Additionally, monthly averages have been calculated for three different altitude ranges: the free troposphere, the UTLS region and the stratosphere. The respective pressure levels are listed in Table 4.

**Table 3: Geographical Regions and the Associated Latitude Band**

| Region | Latitude band |
|---|---|
| Arctic | 60° – 90° N |
| Northern Hemisphere mid latitudes (NH) | 30° – 60° N |
| Tropics | 30° S – 30° N |
| Southern Hemisphere mid latitudes (SH) | 30° – 60° S |
| Antarctic | 60° – 90° S |

**Table 4: Altitude ranges used for the vertical averaging**

| Region | Free Troposphere | UTLS | Stratosphere |
|---|---|---|---|
| **Tropics** | 750 – 200 hPa | 100 – 60 hPa | 60 – 10 hPa |
| **High latitudes** | 750 – 350 hPa | 300 – 100 hPa | 90 – 10 hPa |
| **Mid latitudes** | 750 – 350 hPa | 300 – 100 hPa | 90 – 10 hPa |

### 4.6.3 Validation results

In the stratosphere, the IFS-MOZART forecast run without assimilation (f7kn) overestimates ozone mixing ratios by around 20%. In the UTLS overestimation of measured mixing ratios reaches up to 65% in April. Good results could be obtained in the free troposphere with relative biases less than 10%.

The model forecast runs with data assimilation could correctly reproduce the ozone hole conditions between January and April 2011 with relative biases mostly below 10% in the stratosphere, UTLS region and troposphere. IFS-MOZART with data assimilation (f93i) shows a better performance with smaller relative biases in the stratosphere and UTLS, whereas IFS-TM5 (f9nd) obtains slightly better results in the free troposphere (see Figure 44). Statistic scores for the stratosphere, UTLS and troposphere region are listed in Table 5. Monthly mean profiles are displayed in Figure 45 to Figure 47.
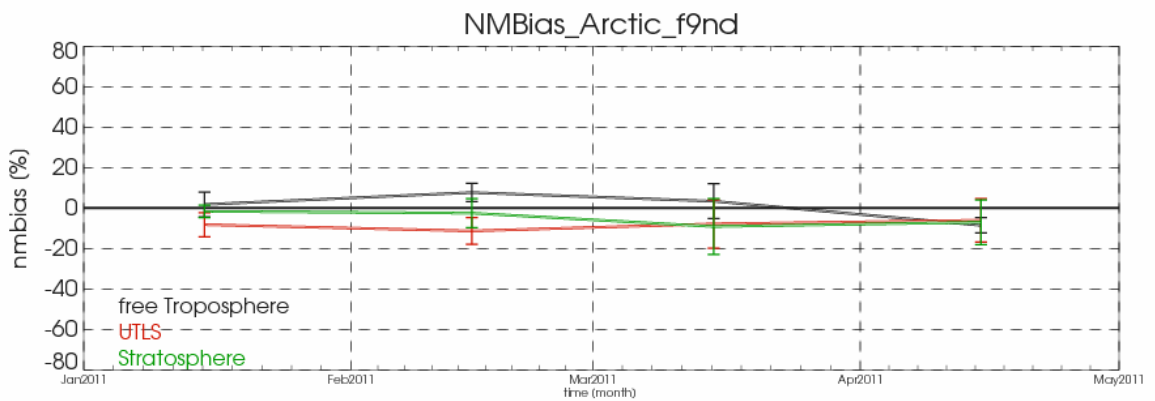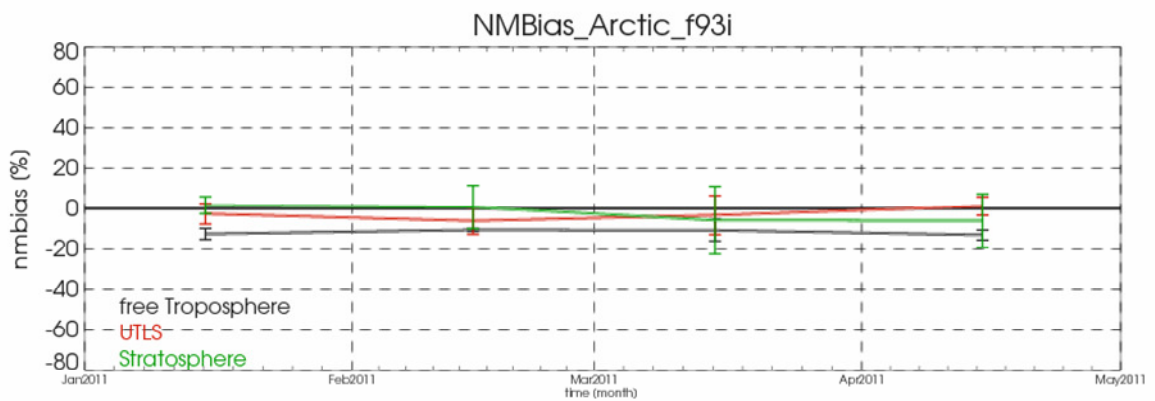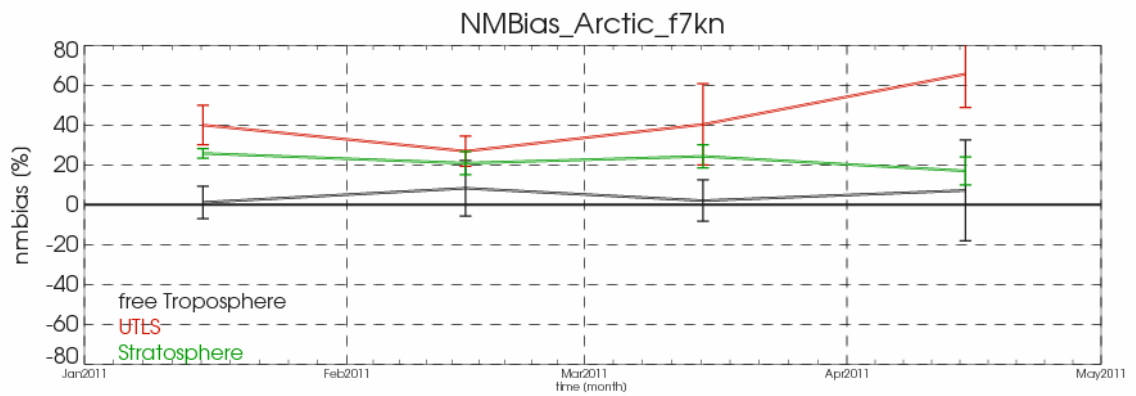
**Figure 44: Monthly averaged relative bias (expressed in percent) of run f7kn (upper panel), run f93i (middle panel) and run f9nd (lower panel) between the Arctic ozone soundings and the forecast runs, January 2011 to April 2011. Color codes denote the three altitude regions free troposphere in black, the UTLS region in red and the stratosphere in green.**

**Table 5: Statistical scores for IFS-MOZART without (f7kn) and with (f93i) data assimilation and IFS-TM5 run (f9nd) for the Arctic ozone depletion event 2011**

| Month | Level | FGE_f7kn | FGE_f93i | FGE_f9nd | Bias_f7kn [ppmm] | Bias_f93i [ppmm] | Bias_f9nd [ppmm] | RELBias_f7kn [%] | RELBias_f93i [%] | RELBias_f9nd [%] |
|-------|-------|----------|----------|----------|------------------|------------------|------------------|------------------|------------------|------------------|
| JAN | TROPOSPHERE | 0.157 | 0.141 | 0.1 | 0.002 | -0.011 | 0.001 | 1.2 | -12.4 | 1.8 |
| FEB | TROPOSPHERE | 0.194 | 0.14 | 0.118 | 0.008 | -0.009 | 0.006 | 8.3 | -10.4 | 7.7 |
| MAR | TROPOSPHERE | 0.171 | 0.147 | 0.127 | 0.003 | -0.011 | 0.002 | 2.1 | -10.6 | 3.4 |
| APR | TROPOSPHERE | 0.215 | 0.167 | 0.135 | 0.011 | -0.013 | -0.009 | 7.2 | -12.9 | -8.5 |
| | | | | | | | | | | |
| JAN | UTLS | 0.391 | 0.167 | 0.184 | 0.381 | -0.003 | -0.088 | 40 | -2.5 | -8.2 |
| FEB | UTLS | 0.208 | 0.219 | 0.24 | 1.087 | -0.001 | -0.071 | 26.9 | -6 | -11.3 |
| MAR | UTLS | 0.398 | 0.265 | 0.259 | 0.398 | 0.046 | -0.012 | 40.3 | -3.2 | -7.8 |
| APR | UTLS | 0.489 | 0.214 | 0.219 | 0.656 | 0.056 | -0.033 | 65.6 | 1.3 | -6 |
| | | | | | | | | | | |
| JAN | STRATOSPHERE | 0.244 | 0.096 | 0.096 | 1.365 | 0.095 | -0.091 | 25.8 | 1.7 | -1.6 |
| FEB | STRATOSPHERE | 0.208 | 0.096 | 0.104 | 1.087 | 0.056 | -0.153 | 20.9 | 0.8 | -2.5 |
| MAR | STRATOSPHERE | 0.263 | 0.179 | 0.226 | 0.893 | -0.152 | -0.34 | 24.3 | -5.7 | -9.1 |
| APR | STRATOSPHERE | 0.236 | 0.151 | 0.176 | 0.749 | -0.351 | -0.211 | 17 | -5.9 | -7 |
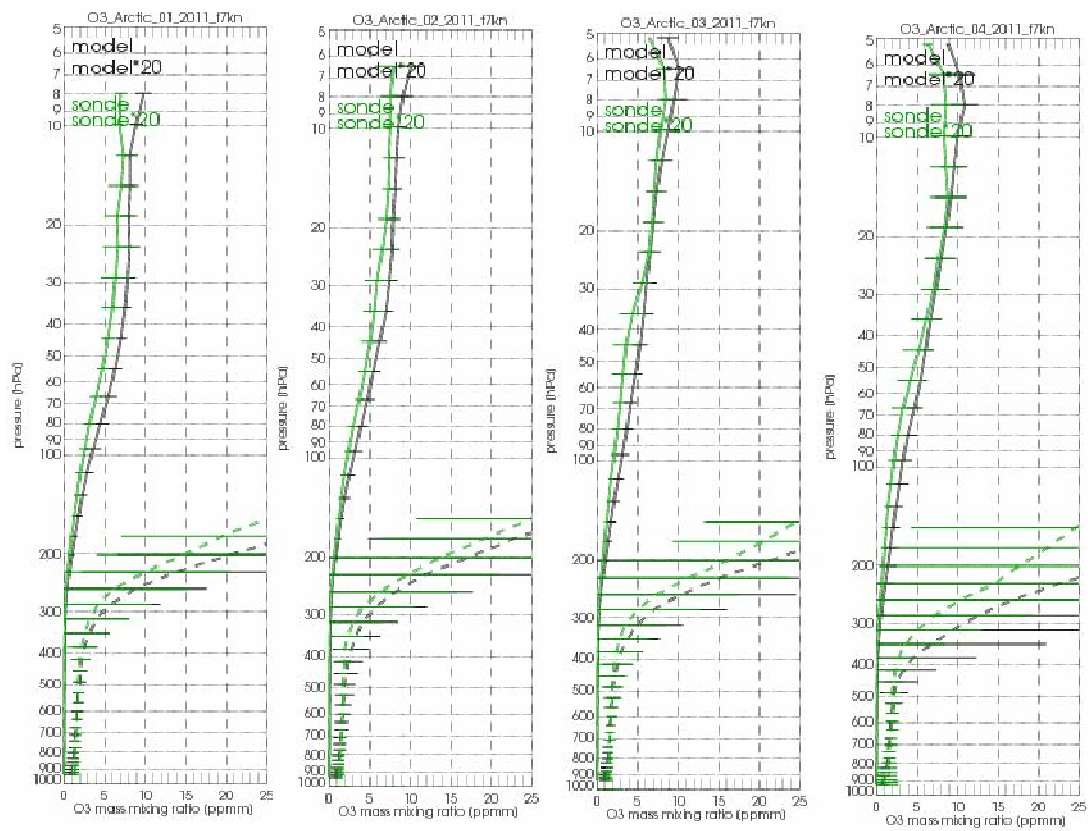


**Figure 45: Comparison between the mean O3 profiles of the model run f7kn (black) with those of the sonde measurements (green) for January, February, March and April 2011 in the Arctic region. The UTLS region is displayed separately by applying a magnification factor.**
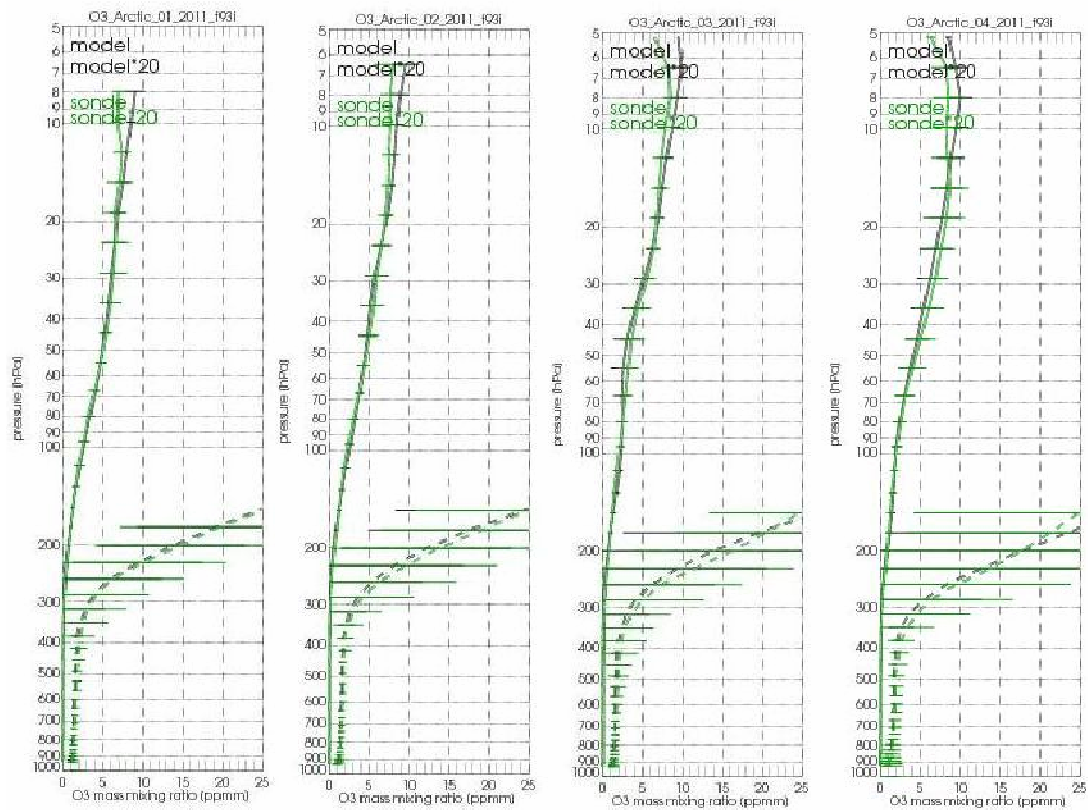
**Figure 46: Same as for Figure 45 but now for the IFS-MOZART run *with* assimilation f93i.**
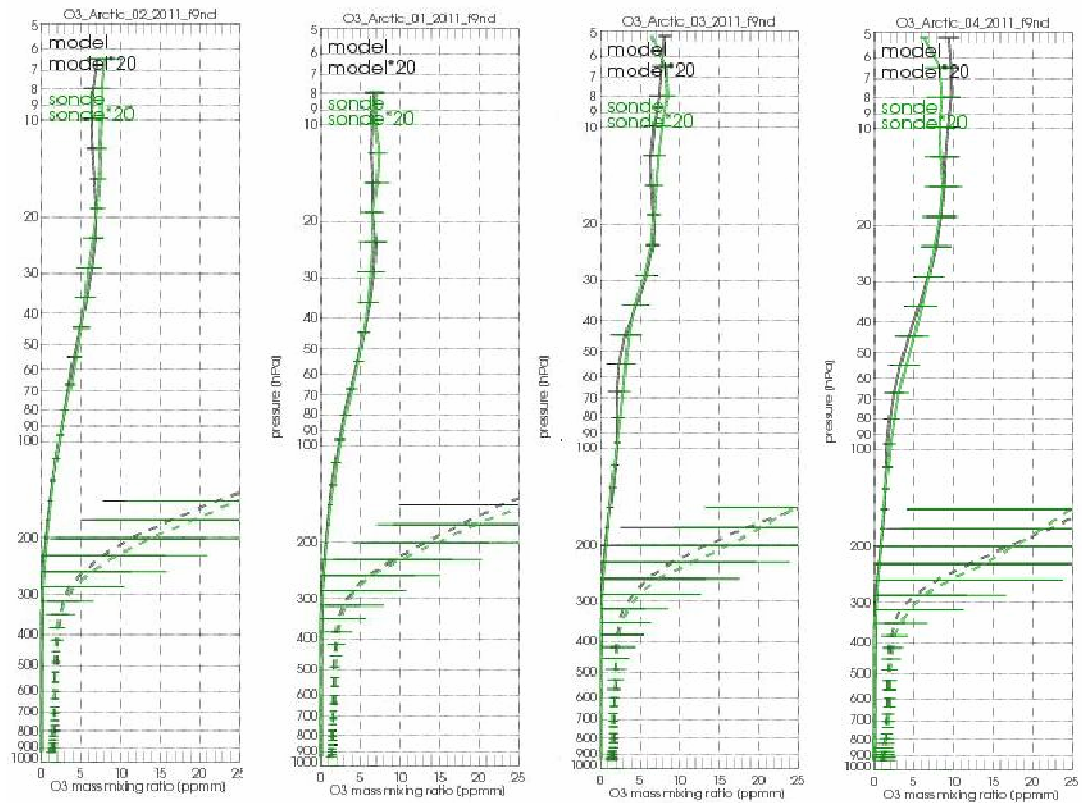


**Figure 47: Same as for Figure 45 but now for the IFS-TM5 analysis f9nd.**

# 5  NRT evaluation of IFS-MOZART and IFS-TM5 2010

## 5.1  NRT validation using O3 soundings

*Annette Wagner, Harald Flentje, and Werner Thomas*

### 5.1.1  Validation Data

Model profiles of the Near-Real-Time forecast runs IFS-MOZART without data assimilation (*f7kn*), IFS-MOZART with data assimilation (*f93i*) and IFS-TM5 (*f9nd*) were compared to balloon sonde measurement data of 38 stations taken from the data bases NDACC, WOUDC, NILU and SHADOZ for the year 2010. Figure 43 displays the location of the stations together with the geographical region where they are attributed to. Table 6 lists the details of the sounding stations, the number of profiles and the measurement period that was used for the evaluation in 2010.

As can be seen from Figure 43, there is a sufficient number of stations available in the northern midlatitudes (NH), Artic and tropical region, providing a good basis for a representative estimation of model quality. In the southern midlatitude (SH) and Antarctic region however, there is only a limited number of ozone sounding stations available in Near-Real-Time, which makes the evaluation of model results less representative. Additionally, the amount of soundings available is decreasing towards the end of the year due to the fact that Near-Real-Time data arrive with a certain delay and are not yet available at the time of evaluation.

The gross of soundings are performed with ECC sondes, except for Hohenpeissenberg (Brewer Mast). The sondes have a precision of 3-5% (~10% in the troposphere for Brewer Mast) and an accuracy of 5-10%. For further detail see J. Cammas et al. (2009), T. Deshler et al. (2008) and H.G.J. Smit et al (2007).

### 5.1.2  Methodologies

The methodologies used are the same as for the case study "Arctic ozone hole 2011" and are described in detail in section 4.6.2.

### 5.1.3  Validation Results

#### 5.1.3.1  Arctic Region

In the Arctic region, there is a good accordance between measured and modelled ozone concentrations. Due to insufficient ozone soundings in December, the validation could only be carried out until November 2010. For the whole validation period, **stratospheric** ozone mixing ratios are slightly overestimated by the IFS-MOZART forecast without assimilation (*f7kn*) and slightly underestimated by both model runs with data assimilation, with relative biases of less than 20% for *f7kn*, and less than -10% and -20% for IFS-MOZART (*f93i*) and IFS-TM5 (*f9nd*), respectively (Figure 48). The Arctic ozone depletion during winter/spring 2010 is slightly underestimated by the IFS-MOZART forecast run without data assimilation (f7kn) and slightly overestimated by both model runs with data assimilation.

**Table 6: Ozone sounding stations and number of ozone profiles used for the comparisons with the different model runs**

| Station | Country | LON | LAT | Data Source | Measurement Period 2010 | Number of profiles |
|---|---|---|---|---|---|---|
| Alert | Canada | -62.3 | 82.4 | NILU | 08.01.2010-03.03.2010 | 11 |
| Ascension Isl. STN 328 | UK | -14 | -8 | WOUDZ | 04.01.2010-27.12.2010 | 19 |
| Edmonton | Canada | -114 | 53.5 | NILU | 06.01.2010-03.03.2010 | 8 |
| Eureka | Canada | -86.5 | 80 | NILU | 06.01.2010-04.03.2010 | 18 |
| Goose Bay | Canada | -60.5 | 53.2 | NILU | 06.01.2010-03.03.2010 | 10 |
| Hilo | Hawaii USA | -155 | 19.4 | SHADOZ | 06.01.2010-04.08.2010 | 28 |
| Hohenpeissenberg | Germany | 11 | 48 | NILU | 04.01.2010-29.10.2010 | 52 |
| Isfahan STN 336 | Iran | 51.43 | 32.48 | WOUDZ | 16.01.2010-16.11.2010 | 16 |
| Java (Watukosek) | Indonisia | 113 | -8 | SHADOZ | 23.02.2010-25.08.2010 | 7 |
| Joikoinen | Finland | 60.814 | 23.5 | NILU | 08.01.2010-13.02.2010 | 5 |
| Kevlawik | Island | -22.5 | 63.97 | NILU | 14.01.2010-24.03.2010 | 11 |
| Kühlungsborn | Germany | 54.12 | 11.77 | NILU | 06.01.2010-26.01.2010 | 2 |
| Legionow | Poland | 52.4 | 20.9 | NILU | 06.01.2010-06.10.2010 | 42 |
| Lerwick | England | -1.19 | 60.14 | NILU | 06.01.2010-24.11.2011 | 46 |
| Lindenberg | Germany | 52.21 | 14.12 | NILU | 03.02.2010-10.02.2010 | 2 |
| Macquarie Island STN 29 | Australia | 158.9 | -54.5 | WOUDZ | 05.01.2010-24.08.2010 | 31 |
| Madrid STN 308 | Spain | -3.8 | 40.5 | WOUDZ | 07.01.2010-29.12.2010 | 50 |
| Marambio STN 233 | Antarctica/ Argentina | -56.62 | -64.23 | WOUDZ | 06.01.2010-29.12.2010 | 73 |
| Naha STN 190 | Japan | 127.7 | 26.2 | WOUDZ | 03.03.2010-22.12.2010 | 29 |
| Nairobi | Kenia | 37 | -1 | WOUDZ | 06.03.2010-22.12.2010 | 36 |
| Natal | Brazil | -35.38 | -5.42 | NILU | 13.01.2010-05.10.2010 | 18 |
| Neumayer STN 323 | Antarctica/ Germany | -8 | -71 | WOUDZ | 08.01.2010-30.12.2010 | 49 |
| Ny Alesund | Svalbard / Norway | 12 | 79 | NILU | 01.01.2010-24.11.2010 | 67 |
| Prag | Czech Republic | 14.4 | 50 | NILU | 04.01.2010-30.04.2010 | 45 |
| Resolute | Canada | -94.98 | 74.72 | NILU | 11.01.2010-27.02.2010 | 6 |
| Samoa (Cape Matatula) | USA | -171 | -14 | SHADOZ | 08.01.2010-19.08.2010 | 12 |
| Sapporo STN 12 | Japan | 141 | 43 | WOUDZ | 04.03.2010-27.12.2010 | 31 |
| Scoresbysund | Greenland (Denmark) | -22 | 70.5 | NILU | 06.01.2010-30.12.2010 | 49 |
| Sodankyla | Finland | 27 | 67 | NILU | 06.01.2010-24.11.2010 | 61 |
| SouthPole | Antarctica | -24.8 | -90 | NDAC | 07.01.2010-29.07.2010 | 29 |
| Summit | Greenland (Denmark) | 38 | 72 | NDAC | 08.01.2010-30.07.2010 | 23 |
| Tateno/Tsukuba STN 14 | Japan | 140.1 | 36.06 | | 03.03.2010-24.08.2011 | 21 |
| Thule | Greenland (Denmark) | -68.8 | 76.5 | NILU | 19.01.2010-01.03.2010 | 2 |
| Uccle | Belgium | 4 | 51 | NILU | 29.01.2010-23.08.2010 | 4 |
| Ushuaia STN 339 | Argentina | -63.31 | -54.85 | WOUDZ | 07.01.2010-29.12.2010 | 27 |
| Valentia STN 318 | Ireland | -10.3 | 51.9 | WOUDZ | 06.01.2010-30.06.2010 | 25 |
| Wallops Isl. STN 107 | USA | -75 | 38 | WOUDZ | 06.01.2010-01.10.2010 | 41 |
| Yarmouth | Canada | -66.1 | 43.8 | NILU | 06.01.2010-03.03.2010 | 9 |

Mean O3 profiles for the model forecasts in the Arctic region from January to April are displayed in Figure 49 and Figure 50.

For the **UTLS** similar results are obtained: the IFS-MOZART run without data assimilation (f7kn) shows a weak overestimation, whereas the runs with assimilation underestimate measured mixing ratios by less than -20%. Maximum errors occur in June/July (around -17%).

In the **troposphere**, both IFS-MOZART runs mostly underestimate measured O3 mixing ratios throughout the year by 20-30%. The IFS-TM5 run (f9nd) underestimates ozone mixing ratios in the troposphere from January to July by less than -20%, between September and December modelled mixing ratios exceed measured ratios slightly (relative biases < 10%). Data assimilation clearly improves the IFS-MOZART results in the stratosphere and UTLS region.

Statistical scores for the stratosphere, UTLS and troposphere region are listed in Table 7 to Table 9.
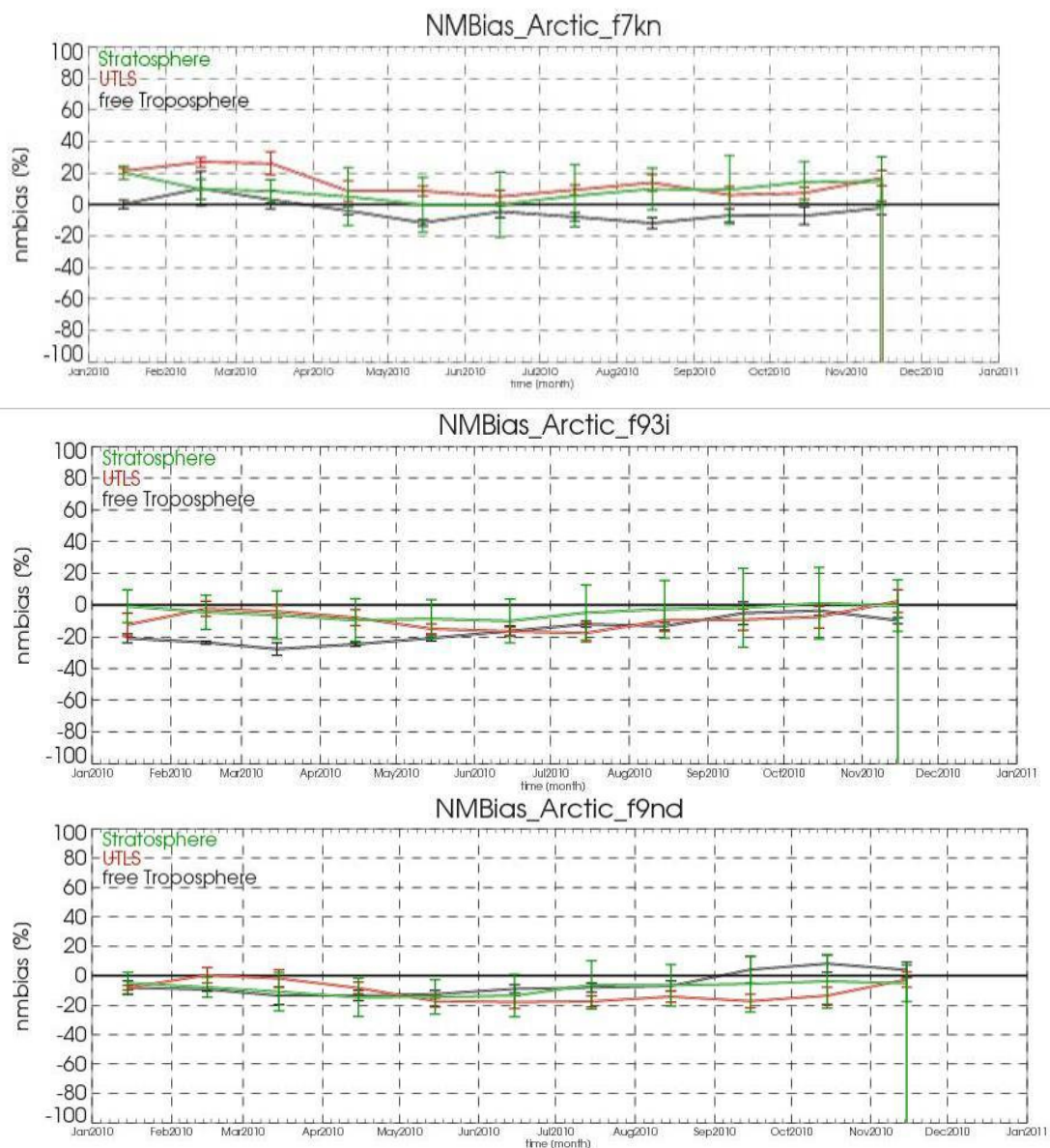


**Figure 48: Monthly averaged relative bias of model runs f7kn (top panel), f93i (middle panel) and f9nd (lower panel) in percent between the Arctic ozone soundings and the forecast runs for January 2010 to November 2010, for the free troposphere (black), the UTLS region (red), and the stratosphere (green).**

**Figure 49: Comparison of the mean O3 profiles for January (top) and February (bottom) 2010 in the Arctic region for model run f7kn (left), f93i (middle) and f9nd (right). Modeled results are in black, sonde measurements in green. The UTLS region is displayed separately with a factor.**

**Figure 50: Same as for Figure 49 but now for March and April 2010.**

**Table 7: Statistical scores for IFS-MOZART without (f7kn) and with (f93i) data assimilation and IFS-TM5 run (f9nd) for the Arctic stratosphere**

| STRATOSPHERE | Region | FGE_f7kn | FGE_f93i | FGE_f9nd | Bias_f7kn [ppmm] | Bias_f93i [ppmm] | Bias_f9nd [ppmm] | RELBias_f7kn [%] | RELBias_f93i [%] | RELBias_f9nd [%] |
|---|---|---|---|---|---|---|---|---|---|---|
| JAN | Arctic | 0.224 | 0.133 | 0.131 | 1.154 | -0.029 | -0.287 | 20.2 | -0.7 | -4.9 |
| FEB | Arctic | 0.147 | 0.126 | 0.139 | 0.66 | -0.376 | -0.66 | 9.6 | -4.5 | -7.8 |
| MAR | Arctic | 0.145 | 0.121 | 0.148 | 0.484 | -0.487 | -0.865 | 8.5 | -6.3 | -10.8 |
| APR | Arctic | 0.166 | 0.142 | 0.177 | 0.295 | -0.538 | -0.923 | 4.9 | -9.5 | -14.7 |
| MAY | Arctic | 0.159 | 0.134 | 0.183 | -0.026 | -0.551 | -0.948 | -0.1 | -8.7 | -2.6 |
| JUN | Arctic | 0.137 | 0.147 | 0.167 | -0.051 | -0.608 | -0.847 | -0.1 | -10 | -13.5 |
| JUL | Arctic | 0.135 | 0.109 | 0.088 | 0.268 | -0.239 | -0.34 | 5.5 | -4.8 | -6.2 |
| AUG | Arctic | 0.103 | 0.075 | 0.078 | 0.448 | -0.083 | -0.335 | 9.8 | -8.3 | -17.4 |
| SEP | Arctic | 0.108 | 0.081 | 0.08 | 0.411 | -0.086 | -0.308 | 9.3 | -1.7 | -5.5 |
| OCT | Arctic | 0.138 | 0.081 | 0.085 | 0.652 | 0.044 | -0.18 | 14.2 | 1.2 | -3.7 |
| NOV | Arctic | 0.152 | 0.091 | 0.088 | 0.773 | -0.031 | -0.261 | 14.8 | -0.3 | -5.1 |
| DEC | Arctic | - | - | | - | - | | - | - | |

**Table 8: Statistical scores for IFS-MOZART without (f7kn) and with (f93i) data assimilation and IFS-TM5 run (f9nd) for the Arctic UTLS region.**

| UTLS | Region | FGE_f7kn | FGE_f93i | FGE_f9nd | Bias_f7kn [ppmm] | Bias_f93i [ppmm] | Bias_f9nd [ppmm] | RELBias_f7kn [%] | RELBias_f93i [%] | RELBias_f9nd [%] |
|---|---|---|---|---|---|---|---|---|---|---|
| JAN | Arctic | 0.341 | 0.326 | 0.309 | 0.175 | -0.046 | -0.028 | 21.2 | -12.4 | -8 |
| FEB | Arctic | 0.339 | 0.26 | 0.243 | 0.272 | 0.036 | 0.039 | 26.8 | -2.4 | 0.4 |
| MAR | Arctic | 0.341 | 0.246 | 0.234 | 0.371 | 0.041 | 0.052 | 26.1 | -4 | -1.8 |
| APR | Arctic | 0.305 | 0.288 | 0.294 | 0.176 | -0.032 | -0.04 | 8.5 | -7.9 | -8.3 |
| MAY | Arctic | 0.335 | 0.255 | 0.278 | 0.161 | -0.11 | -0.138 | 8.5 | -15 | -17.2 |
| JUN | Arctic | 0.315 | 0.309 | 0.308 | 0.123 | -0.126 | -0.136 | 5 | -16.6 | -17.9 |
| JUL | Arctic | 0.332 | 0.319 | 0.279 | 0.131 | -0.091 | -0.093 | 9.2 | -17.6 | -17.4 |
| AUG | Arctic | 0.276 | 0.222 | 0.223 | 0.139 | -0.014 | -0.062 | 13.8 | -9.6 | -14.2 |
| SEP | Arctic | 0.244 | 0.238 | 0.259 | 0.088 | 0.015 | -0.047 | 6 | -9.2 | -17.2 |
| OCT | Arctic | 0.219 | 0.263 | 0.27 | 0.072 | 0.017 | -0.035 | 7.2 | -7.4 | -13.5 |
| NOV | Arctic | 0.265 | 0.212 | 0.19 | 0.146 | 0.061 | 0.004 | 16.7 | 2.5 | 0.4 |
| DEC | Arctic | - | - | | - | - | | - | - | |

**Table 9: Statistical scores for IFS-MOZART without (f7kn) and with (f93i) data assimilation and IFS-TM5 run (f9nd) for the Arctic troposphere**

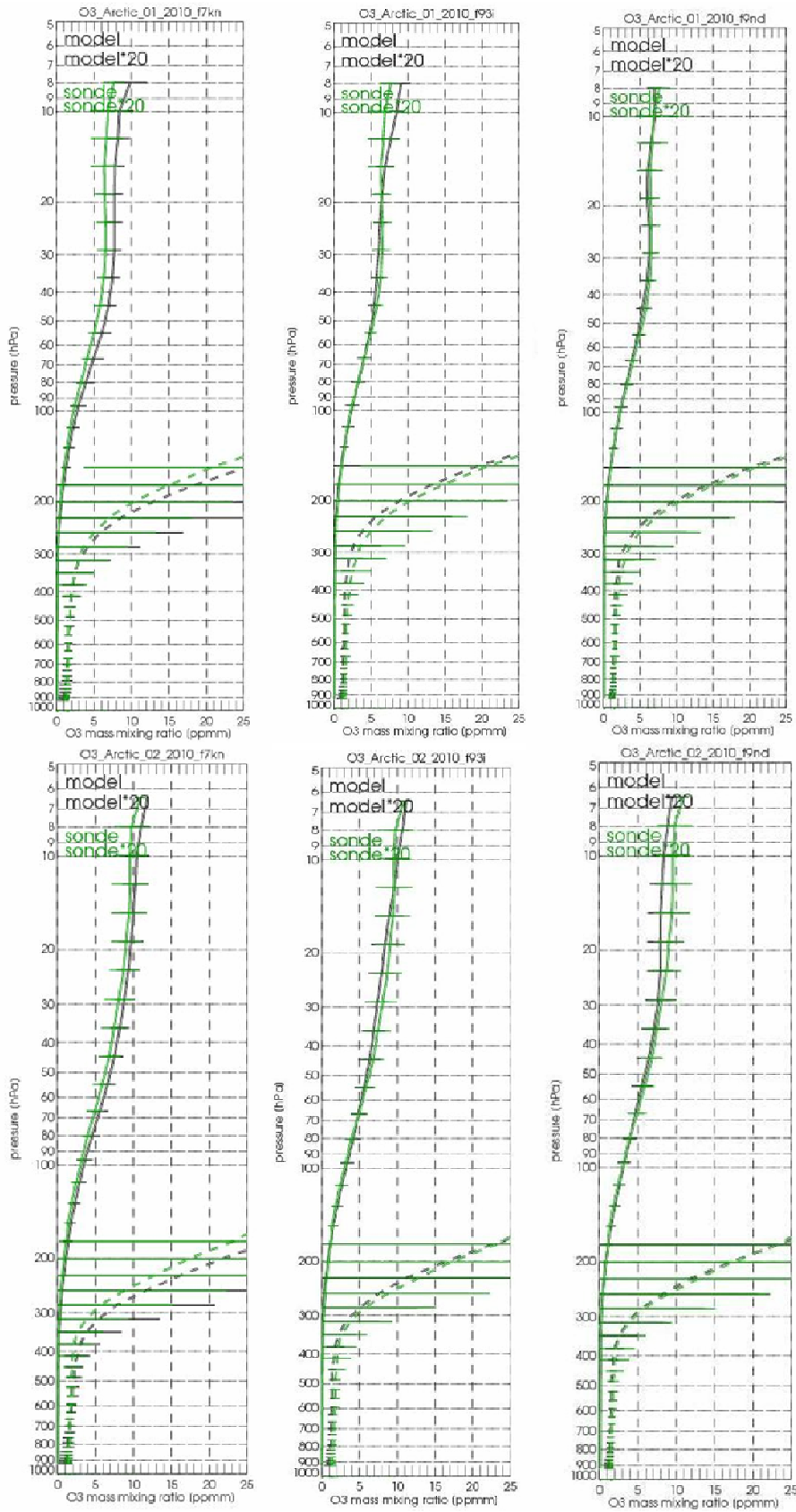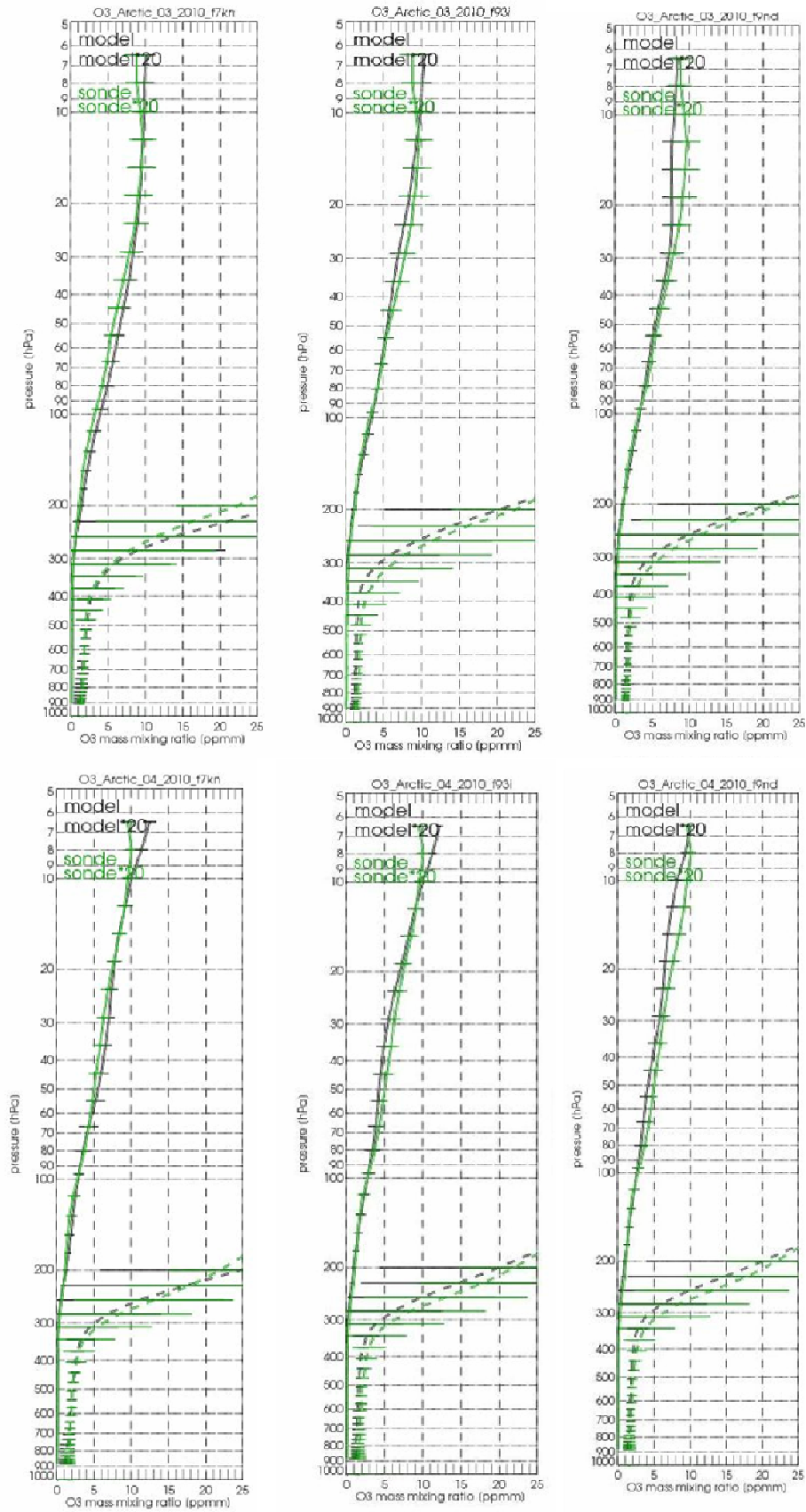| TROPOSPHERE | Region | FGE_f7kn | FGE_f93i | FGE_f9nd | Bias_f7kn [ppmm] | Bias_f93i [ppmm] | Bias_f9nd [ppmm] | RELBias_f7kn [%] | RELBias_f93i [%] | RELBias_f9nd [%] |
|---|---|---|---|---|---|---|---|---|---|---|
| JAN | Arctic | 0.12 | 0.228 | 0.113 | 0 | -0.018 | -0.007 | 0.1 | -20.9 | -8.1 |
| FEB | Arctic | 0.168 | 0.265 | 0.126 | 0.01 | -0.021 | -0.008 | 10.1 | -23.6 | -9.3 |
| MAR | Arctic | 0.153 | 0.305 | 0.15 | 0.004 | -0.029 | -0.015 | 3 | -27.7 | -13.5 |
| APR | Arctic | 0.103 | 0.278 | 0.15 | -0.004 | -0.026 | -0.015 | -4 | -24.7 | -13.4 |
| MAY | Arctic | 0.174 | 0.222 | 0.16 | -0.014 | -0.025 | -0.015 | -11.6 | -20.8 | -12.4 |
| JUN | Arctic | 0.134 | 0.201 | 0.151 | -0.004 | -0.016 | -0.009 | -4.6 | -16.4 | -8.9 |
| JUL | Arctic | 0.128 | 0.149 | 0.133 | -0.008 | -0.012 | -0.009 | -7.9 | -12 | -8 |
| AUG | Arctic | 0.153 | 0.165 | 0.127 | -0.013 | -0.015 | -0.008 | -11.9 | -13.3 | -6.9 |
| SEP | Arctic | 0.118 | 0.115 | 0.121 | -0.007 | -0.006 | 0.003 | -7 | -5.1 | 4.2 |
| OCT | Arctic | 0.132 | 0.089 | 0.118 | -0.006 | -0.003 | 0.006 | -7.2 | -3.5 | 8.2 |
| NOV | Arctic | 0.11 | 0.13 | 0.103 | -0.002 | -0.009 | 0.003 | -2.2 | -9.7 | 4 |
| DEC | Arctic | - | - | | - | - | | - | - | |

### 5.1.3.2 Northern Midlatitudes (NH)

For all runs, there is a very good accordance between measured and modelled ozone mixing ratios in the **stratosphere** throughout the year 2010 (relative bias < ±5%). Monthly relative bias values are displayed in Figure 51. The data assimilation still improves the results for the IFS-MOZART run in the stratosphere.

In the **UTLS** region, the IFS-MOZART run is overestimating measured mixing rations between January and July by around 20%. Both model runs with assimilation show an underestimation of measured ozone concentrations between April and December with a maximum of -20% (f93i) and -27% (f9nd) in August. For both model runs maximum relative biases appear in the summer months from June to

September. *Figures 5a-d* show the mean O3 profiles for all model runs at the northern midlatitudes for the summer period May to August.

In the **troposphere**, measured ozone mixing ratios are mostly slightly underestimated by all model runs. Data assimilation seems to downgrade the results of IFS-MOZART.

The quality of the results varies strongly between the stations: a comparison between the stations at Lerwick (lat = 60°) and Hohenpeissenberg (lat = 48°) is shown in Figure 54. Statistical scores for the stratosphere, UTLS and troposphere region are listed in Table 10 to Table 12.
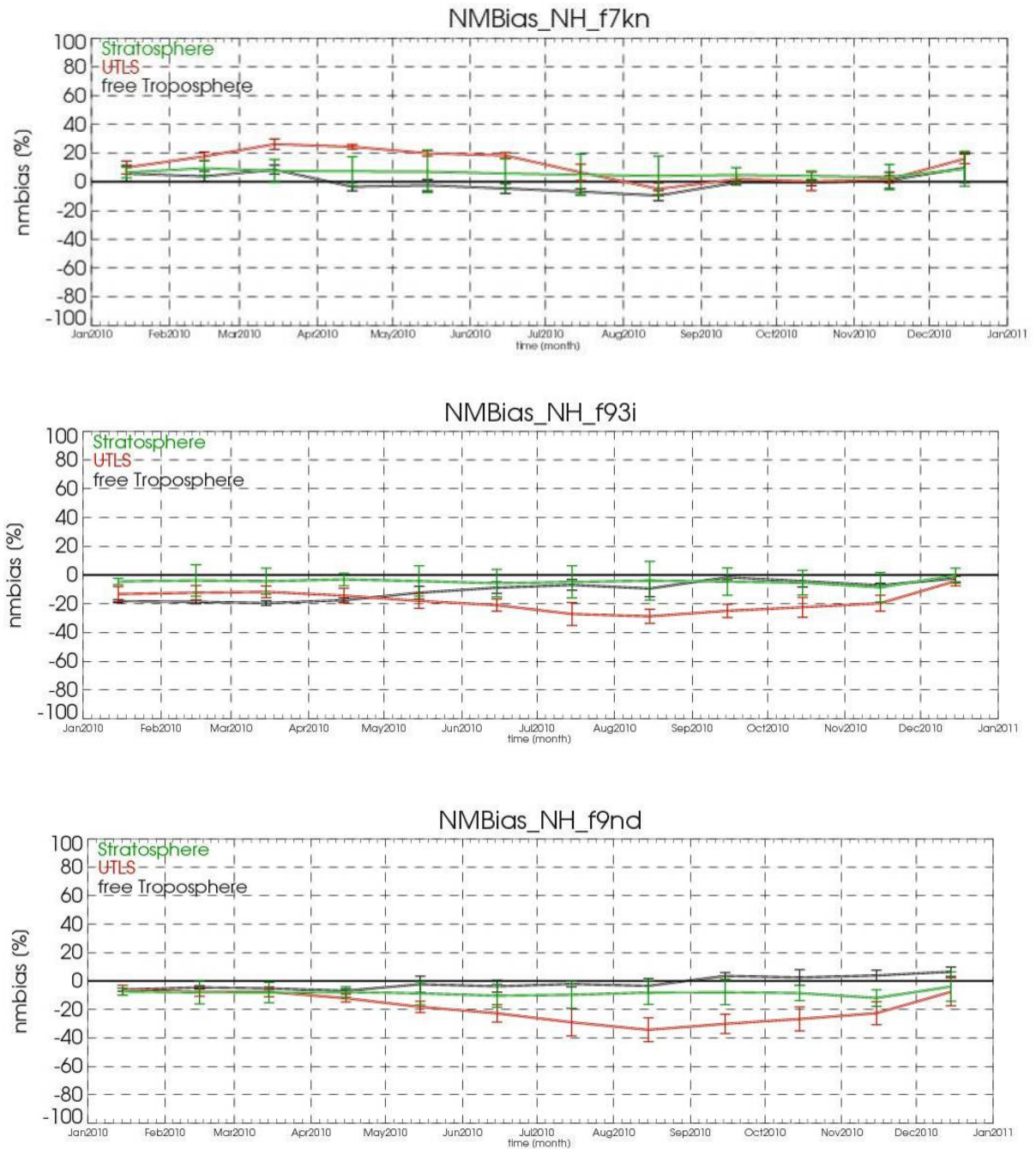


**Figure 51: Monthly averaged relative bias of run f7kn (upper panel), f93i and run f9nd (lower panel) in percent between the northern hemisphere ozone soundings and the forecast runs, January 2010 to December 2010. Colour codes denote the three altitude regions free troposphere in black, the UTLS region in red and the stratosphere in green.**
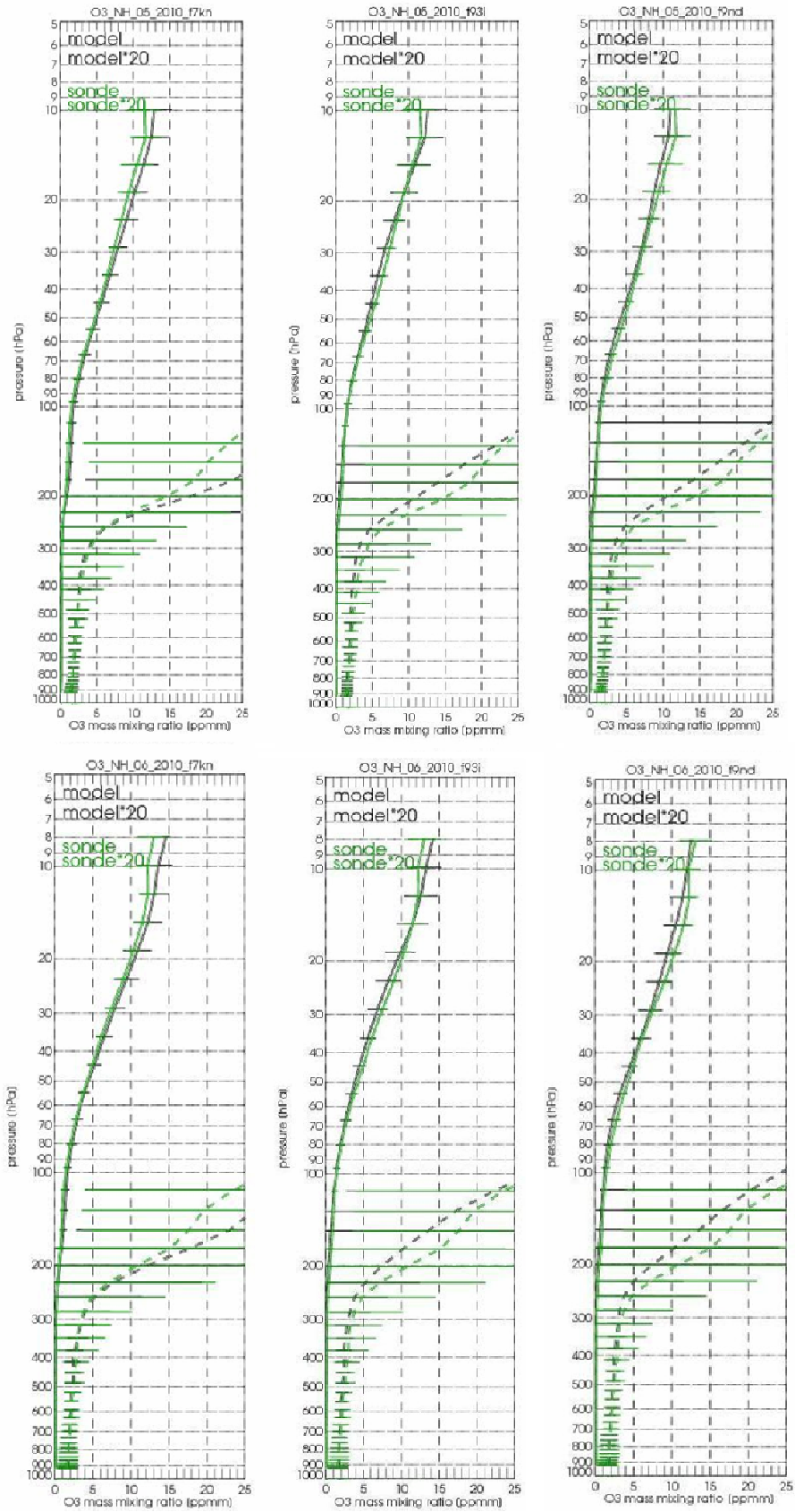
**Figure 52: Comparison of the mean O3 profiles for May (top) and June (bottom) 2010 at the northern midlatitudes for model run f7kn (first panel), f93i (second panel) and f9nd (third panel). Modeled results are in black, sonde measurements in green. The UTLS region is displayed separately with a factor.**

**Figure 53:** Same as for but now for July and August 2010

**Figure 54: Comparison of validation results between the two stations Lerwick (top) and Hohenpeissenberg (bottom) for the 28th of July 2010. Modeled results are in black, sonde measurements in red and green (mean profiles). The UTLS region is displayed separately with a factor.**

**Table 10: Statistical scores for IFS-MOZART without (f7kn) and with (f93i) data assimilation and IFS-TM5 run (f9nd) for the northern midlatitude stratosphere**

| STRATOSPHERE | Region | FGE_f7kn | FGE_f93i | FGE_f9nd | Bias_f7kn [ppmm] | Bias_f93i [ppmm] | Bias_f9nd [ppmm] | RELBias_f7kn [%] | RELBias_f93i [%] | RELBias_f9nd [%] |
|---|---|---|---|---|---|---|---|---|---|---|
| JAN | NH | 0.156 | 0.131 | 0.137 | 0.495 | -0.317 | -0.562 | 6.5 | 2.5 | -3.1 |
| FEB | NH | 0.15 | 0.122 | 0.13 | 0.624 | -0.26 | -0.589 | 9.5 | 2.3 | -2 |
| MAR | NH | 0.127 | 0.118 | 0.132 | 0.497 | -0.317 | -0.648 | 7.6 | -0.7 | -4.8 |
| APR | NH | 0.125 | 0.111 | 0.116 | 0.501 | -0.169 | -0.55 | 7.3 | 4.8 | 0 |
| MAY | NH | 0.137 | 0.133 | 0.142 | 0.498 | -0.197 | -0.529 | 7.1 | 3.1 | -1.9 |
| JUN | NH | 0.147 | 0.152 | 0.17 | 0.405 | -0.318 | -0.596 | 5.8 | 1.3 | -2.9 |
| JUL | NH | 0.17 | 0.16 | 0.187 | 0.481 | -0.135 | -0.394 | 5 | 5 | -0.4 |
| AUG | NH | 0.161 | 0.14 | 0.162 | 0.388 | -0.135 | -0.355 | 4.1 | 5.5 | 0.9 |
| SEP | NH | 0.155 | 0.127 | 0.147 | 0.397 | -0.203 | -0.391 | 4.8 | 3.9 | -0.4 |
| OCT | NH | 0.163 | 0.149 | 0.178 | 0.441 | -0.161 | -0.335 | 4.1 | 6.6 | -3.5 |
| NOV | NH | 0.155 | 0.149 | 0.192 | 0.258 | -0.443 | -0.614 | 3.3 | -8.5 | -11.9 |
| DEC | NH | 0.102 | 0.063 | 0.111 | 0.593 | -0.008 | -0.215 | 9 | -0.8 | -3.9 |

**Table 11: Statistical scores for IFS-MOZART without (f7kn) and with (f93i) data assimilation and IFS-TM5 run (f9nd) for the northern midlatitude UTLS**

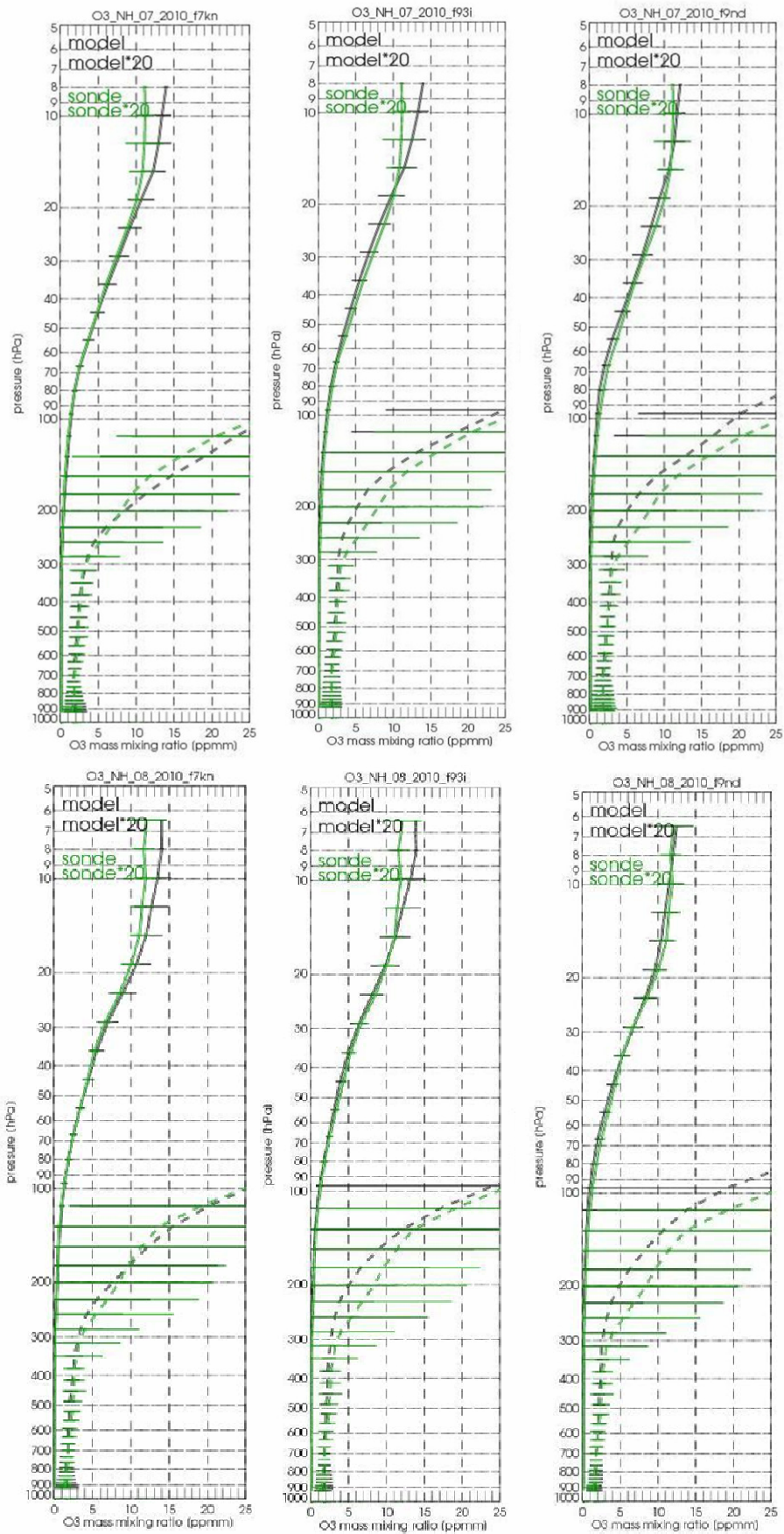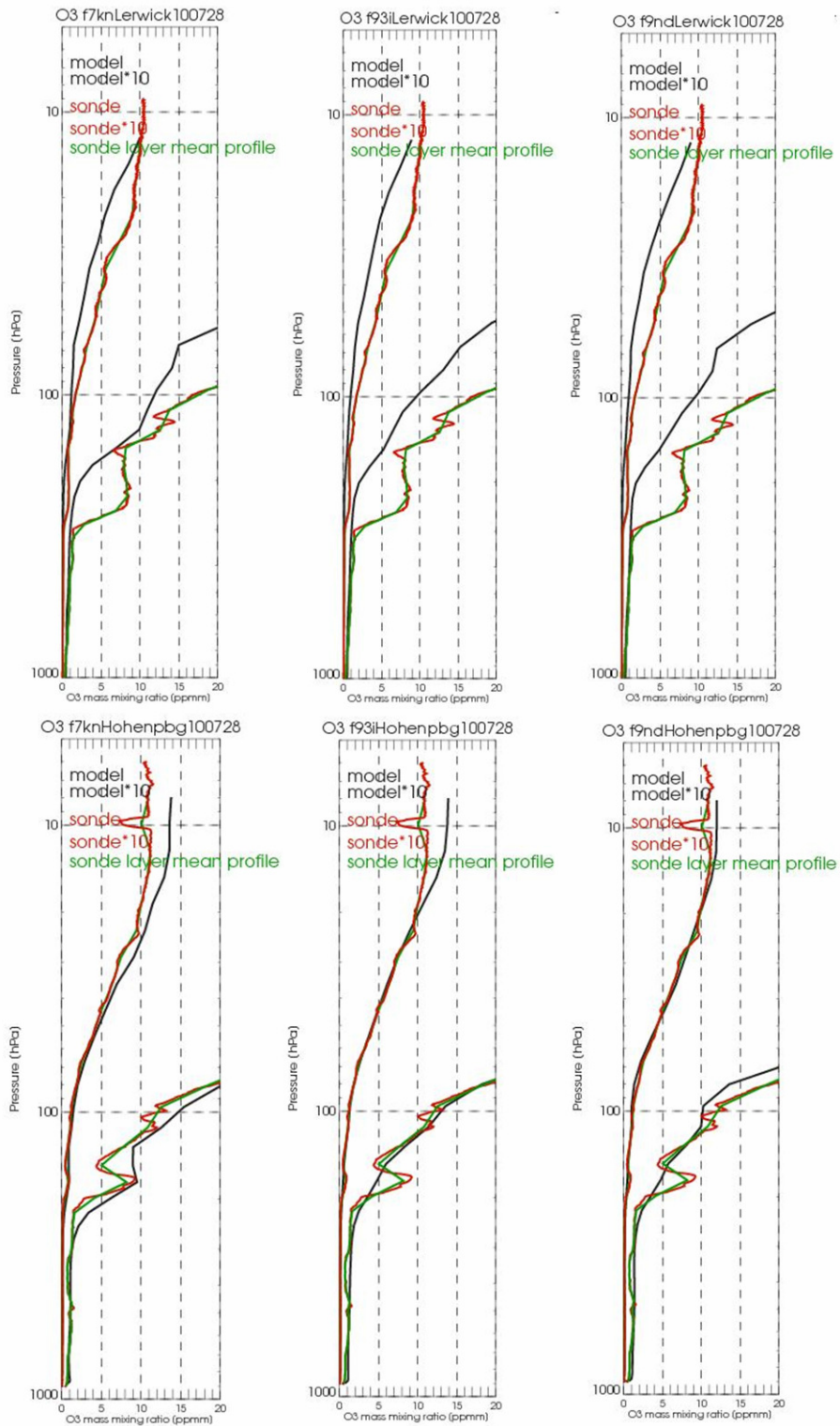| UTLS | Region | FGE_f7kn | FGE_f93i | FGE_f9nd | Bias_f7kn [ppmm] | Bias_f93i [ppmm] | Bias_f9nd [ppmm] | RELBias_f7kn [%] | RELBias_f93i [%] | RELBias_f9nd [%] |
|---|---|---|---|---|---|---|---|---|---|---|
| JAN | NH | 0.332 | 0.377 | 0.35 | 0.057 | -0.088 | -0.055 | 10 | -8 | -3.6 |
| FEB | NH | 0.329 | 0.34 | 0.331 | 0.152 | -0.058 | -0.039 | 17.7 | -6.3 | -1.2 |
| MAR | NH | 0.367 | 0.349 | 0.326 | 0.244 | -0.062 | -0.04 | 26.2 | -6.6 | -2.5 |
| APR | NH | 0.441 | 0.353 | 0.347 | 0.222 | -0.098 | -0.087 | 24.4 | -8.5 | -6 |
| MAY | NH | 0.368 | 0.344 | 0.338 | 0.198 | -0.108 | -0.118 | 19.9 | -11.8 | -11.7 |
| JUN | NH | 0.352 | 0.329 | 0.337 | 0.148 | -0.121 | -0.139 | 18.3 | -16.3 | -17.1 |
| JUL | NH | 0.349 | 0.348 | 0.352 | 0.057 | -0.115 | -0.132 | 6.6 | -18.9 | -20.5 |
| AUG | NH | 0.289 | 0.363 | 0.419 | 0 | -0.117 | -0.158 | -4.9 | -20.4 | -26.5 |
| SEP | NH | 0.279 | 0.351 | 0.411 | 0.012 | -0.084 | -0.114 | 1.9 | -18.1 | -24.4 |
| OCT | NH | 0.281 | 0.341 | 0.373 | 0.005 | -0.066 | -0.089 | 0.4 | -5.6 | -23.4 |
| NOV | NH | 0.309 | 0.382 | 0.383 | 0.022 | -0.073 | -0.101 | 1.8 | -19.6 | -22.6 |
| DEC | NH | 0.274 | 0.226 | 0.241 | 0.092 | -0.034 | -0.071 | 16 | -3.4 | -7.6 |

**Table 12: Statistical scores for IFS-MOZART without (f7kn) and with (f93i) data assimilation and IFS-TM5 run (f9nd) for the northern midlatitude troposphere**

| TROPOSPHERE | Region | FGE_f7kn | FGE_f93i | FGE_f9nd | Bias_f7kn [ppmm] | Bias_f93i [ppmm] | Bias_f9nd [ppmm] | RELBias_f7kn [%] | RELBias_f93i [%] | RELBias_f9nd [%] |
|---|---|---|---|---|---|---|---|---|---|---|
| JAN | NH | 0.131 | 0.203 | 0.102 | 0.005 | -0.016 | -0.005 | 5.8 | -18.2 | -6.1 |
| FEB | NH | 0.122 | 0.212 | 0.104 | 0.004 | -0.017 | -0.004 | 3.8 | -18.6 | -4.5 |
| MAR | NH | 0.134 | 0.232 | 0.119 | 0.009 | -0.019 | -0.005 | 8.5 | -19.5 | -5.2 |
| APR | NH | 0.144 | 0.224 | 0.151 | -0.004 | -0.019 | -0.007 | -3.4 | -17.5 | -6.8 |
| MAY | NH | 0.16 | 0.194 | 0.153 | -0.003 | -0.015 | -0.004 | -2.4 | -12.3 | -2.3 |
| JUN | NH | 0.162 | 0.175 | 0.16 | -0.006 | -0.011 | -0.005 | -4.6 | -8.8 | -3.7 |
| JUL | NH | 0.162 | 0.165 | 0.149 | -0.008 | -0.008 | -0.002 | -6.8 | -6.9 | -2.1 |
| AUG | NH | 0.169 | 0.17 | 0.148 | -0.011 | -0.011 | -0.005 | -9.5 | -9.4 | -3.4 |
| SEP | NH | 0.143 | 0.133 | 0.136 | -0.001 | -0.002 | 0.003 | -0.5 | -1.6 | 3.6 |
| OCT | NH | 0.121 | 0.121 | 0.129 | 0 | -0.004 | 0.002 | -0.5 | -4.3 | 2.5 |
| NOV | NH | 0.135 | 0.13 | 0.105 | 0.001 | -0.006 | 0.003 | 1 | -7.1 | 3.9 |
| DEC | NH | 0.16 | 0.106 | 0.117 | 0 | -0.002 | 0.005 | 9.8 | -2.4 | 6.5 |

### 5.1.3.3  Tropics

In the tropics all model runs show a slight underestimation of measured **stratospheric** ozone concentrations of less than 10% except for the months June and July, where ozone levels are overestimated by around 30-50% (Figure 55). However, the results are not consistent at the beginning of the year where a huge variability between the individual stations appears, even if they are spatially close; see the example for the soundings at Ascension, Natal and Samoa in Figure 58 and Figure 59. Data assimilation decreases the relative bias in summer.

For the **UTLS** region results are less satisfying. The IFS-MOZART forecast run f7kn underestimates mixing ratios in February and from August onwards up to -60%. The

rest of the year mixing ratios are overestimated by around 20-45% (maximum in July). Both model runs with data assimilation underestimate the ozone mixing rations by around -40% (f93i) and -60% (f9nd) with peaks in the months February and September. These discrepancies could have their origin in a too high modelled tropopause altitude (Figure 56 and Figure 57).

All modelled **tropospheric** ozone concentrations are overestimating measured concentrations, with maxima of up to 60% (IFS-MOZART) and 70% in June. Data assimilation reduces the relative biases for IFS-MOZART. IFS-MOZART with data assimilation generally obtains lower biases than IFS-TM5 with data assimilation in all three levels. Statistical scores for the stratosphere, UTLS and troposphere region are listed in Table 13 to Table 15.
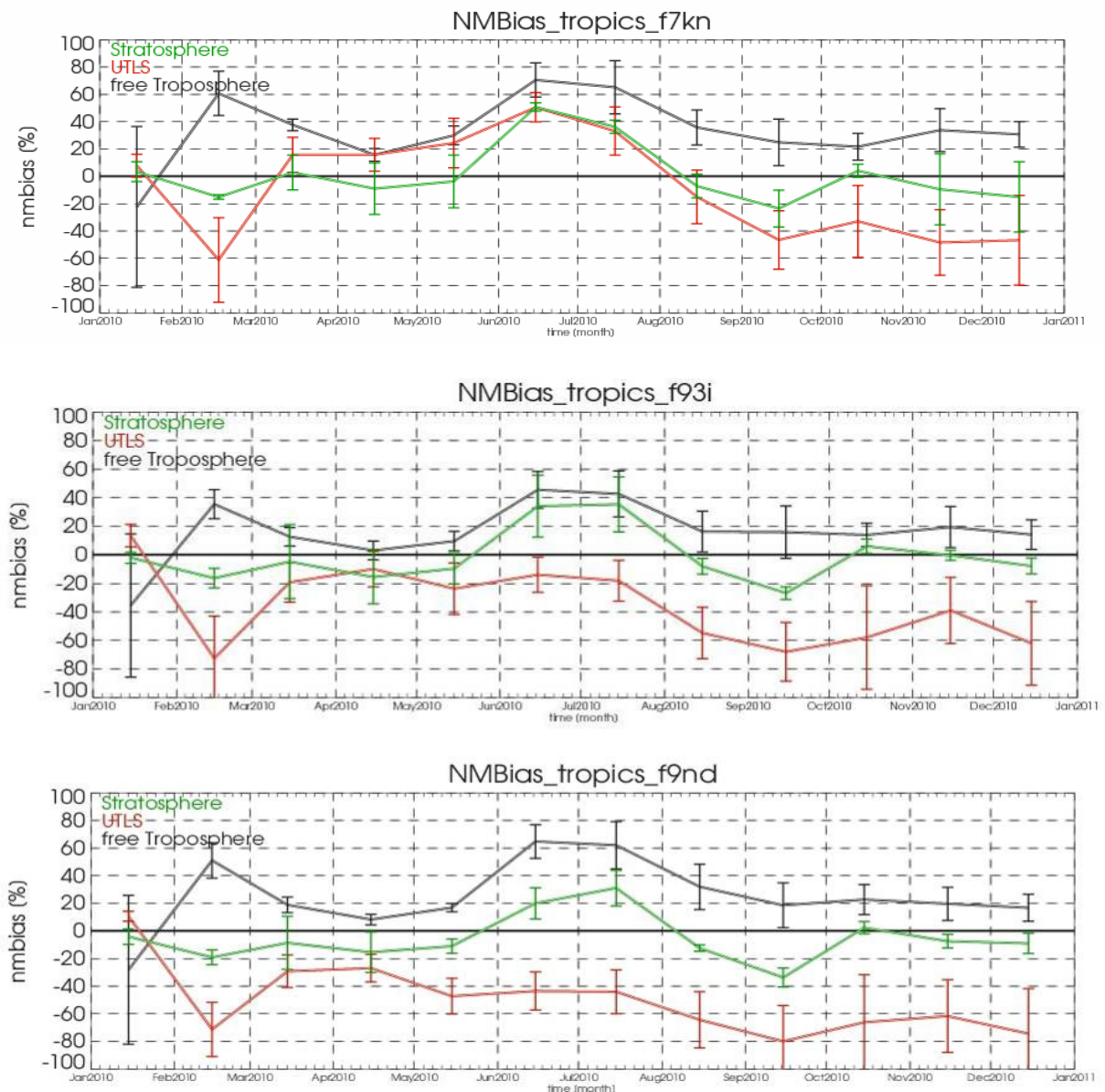


**Figure 55: Monthly averaged relative bias of run f7kn (upper panel), f93i and run f9nd (lower panel) in percent between the tropical ozone soundings and the forecast runs, January 2010 to December 2010. Colour codes denote the three altitude regions free troposphere in black, the UTLS region in red and the stratosphere in green.**
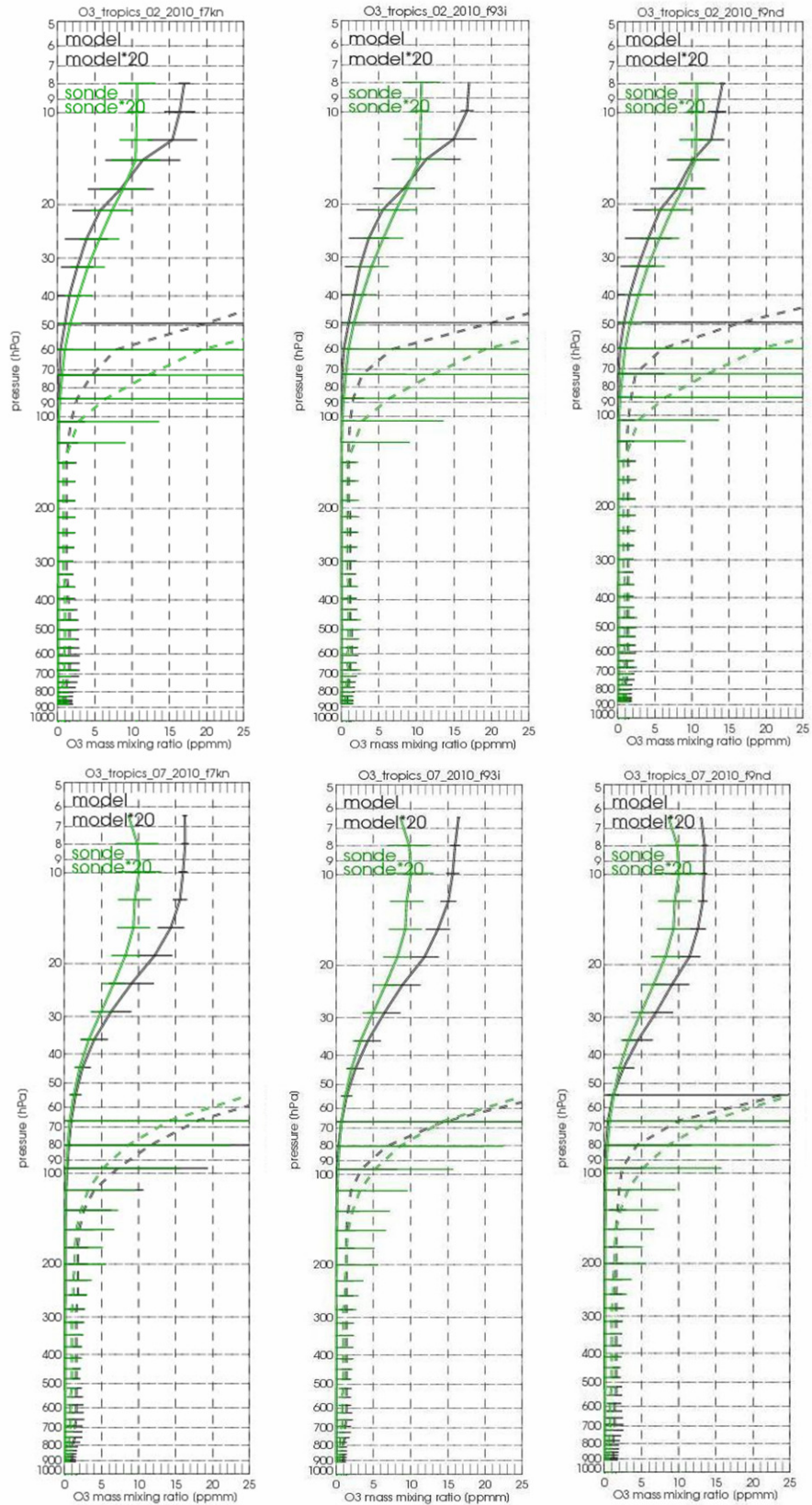
**Figure 56: Comparison of the mean O3 profiles for February (top) and July (bottom) 2010 in the tropics for model run f7kn (left), f93i (middle) and f9nd (right). Modeled results are in black, sonde measurements in green. The UTLS region is displayed separately with a factor.**
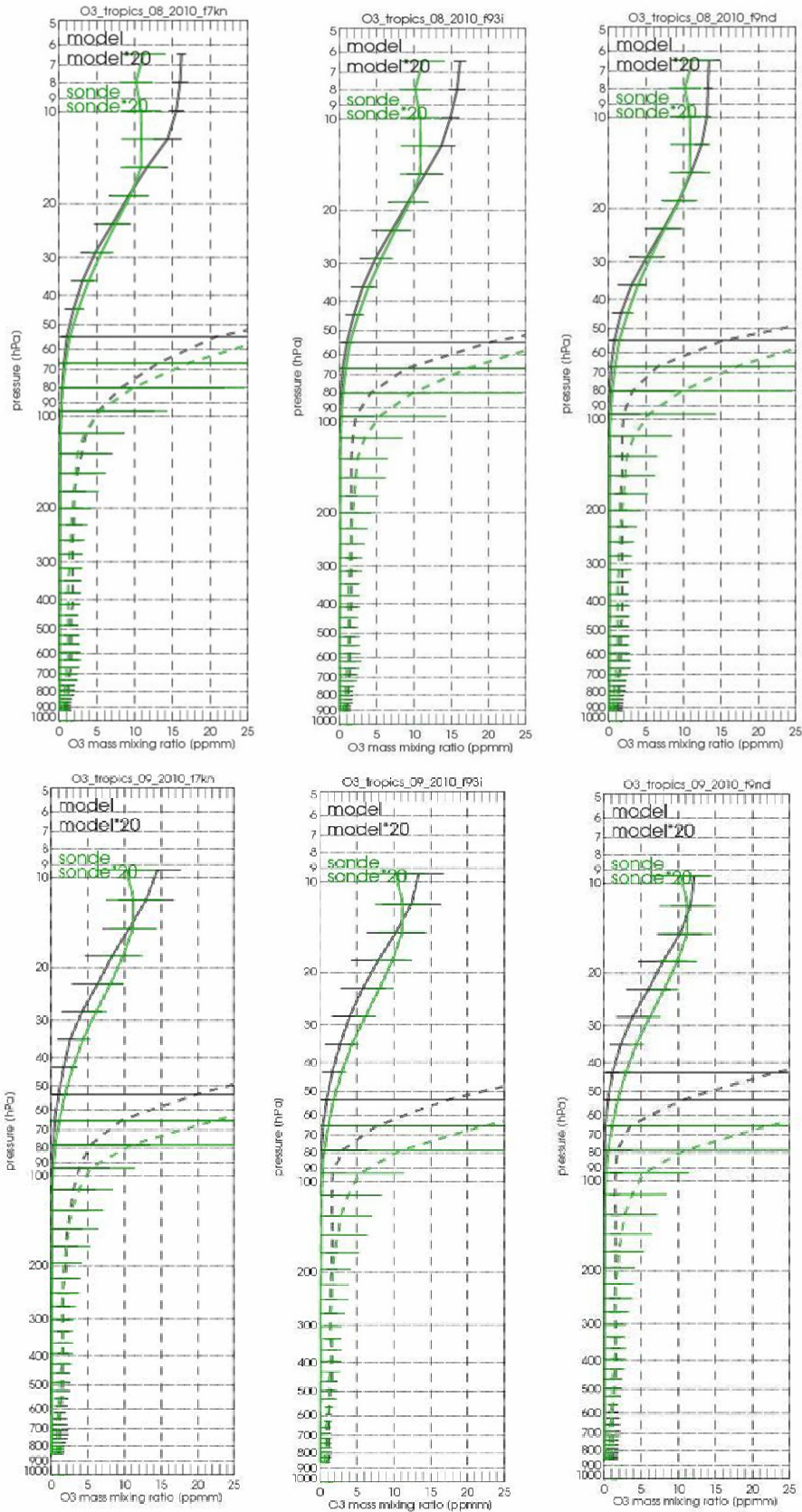
**Figure 57: Comparison of the mean O3 profiles for August (top) and September (bottom) 2010 in the tropics for model run f7kn (first panel), f93i (second panel) and f9nd (third panel). Modeled results are in black, sonde measurements in green. The UTLS region is displayed separately with a factor.**
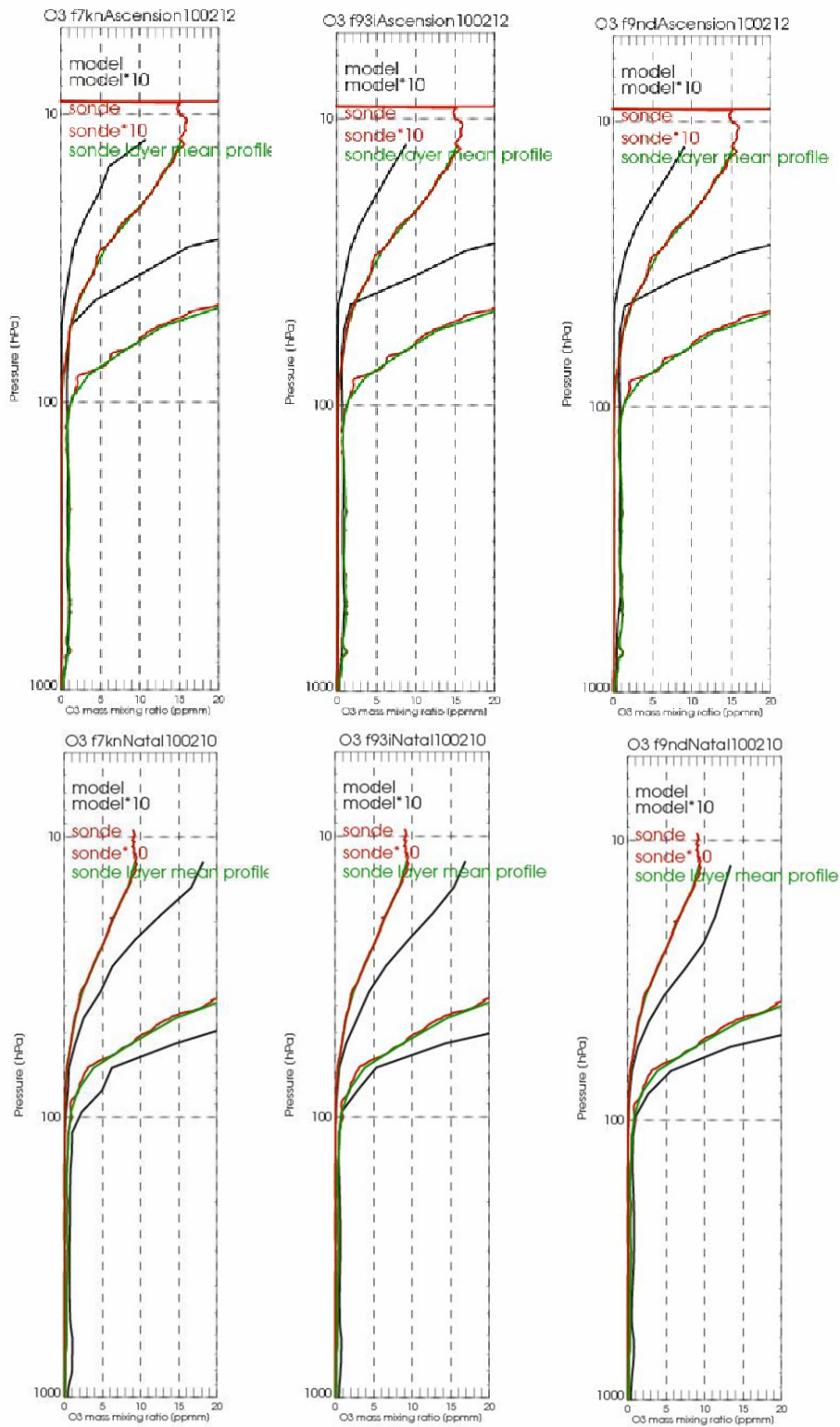
**Figure 58: Comparison of validation results between the two stations Ascension (top) and Natal (bottom) at respectively 12 and 10 Feb 2010. Modeled results are in black, sonde measurements in red and green (mean profiles). The UTLS region is displayed separately with a factor.**

**Figure 59: Comparison of validation results between the two stations Samoa (top) and Natal (bottom) at respectively 25 and 24 June 2010. Modeled results are in black, sonde measurements in red and green (mean profiles). The UTLS region is displayed separately with a factor.**

**Table 13: Statistical scores for IFS-MOZART without (f7kn) and with (f93i) data assimilation and IFS-TM5 run (f9nd) for the tropical stratosphere**

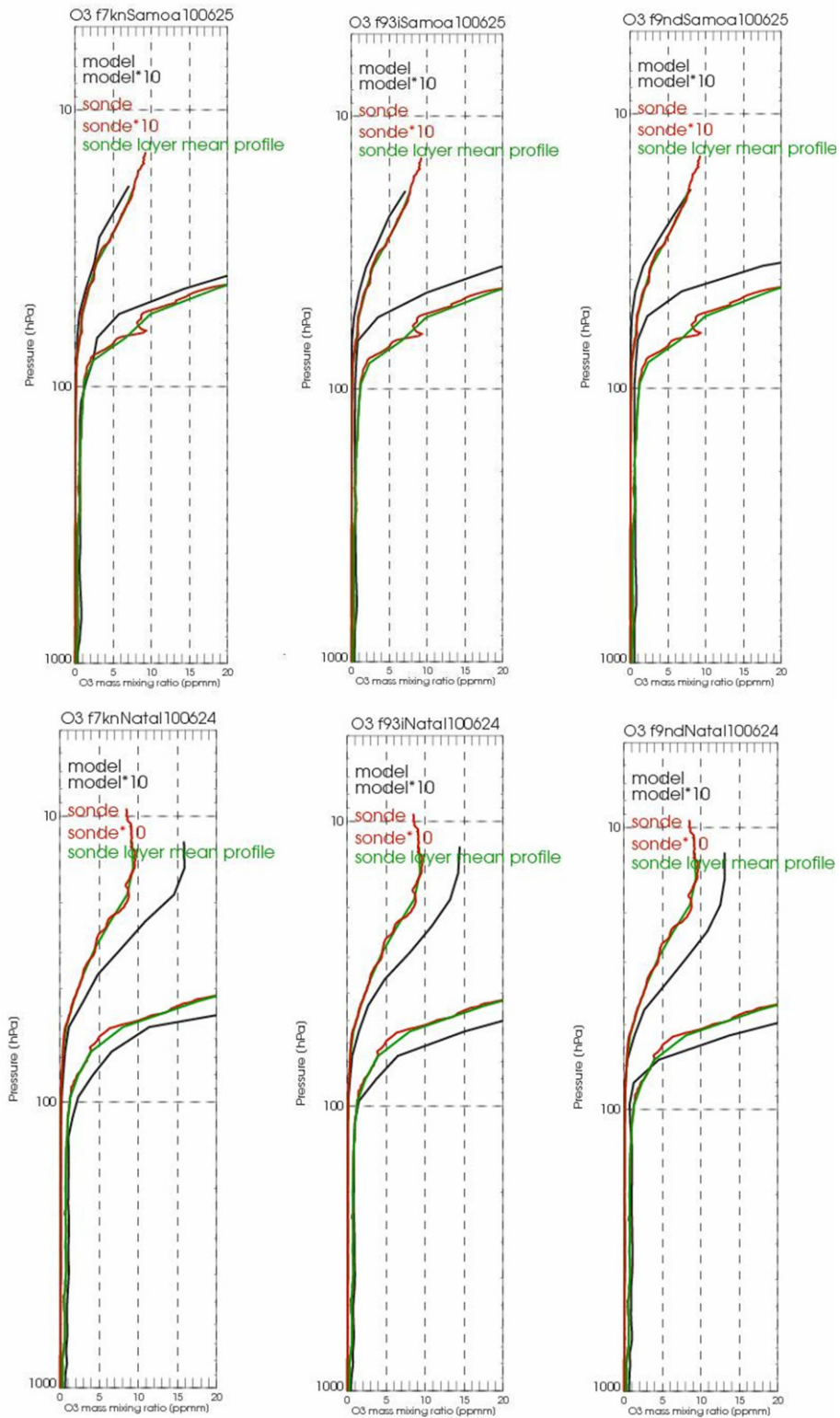| STRATOSPHERE | Region | FGE_f7kn | FGE_f93i | FGE_f9nd | Bias_f7kn [ppmm] | Bias_f93i [ppmm] | Bias_f9nd [ppmm] | RELBias_f7kn [%] | RELBias_f93i [%] | RELBias_f9nd [%] |
|---|---|---|---|---|---|---|---|---|---|---|
| JAN | Tropics | 0.752 | 0.761 | 0.75 | 0.434 | -0.043 | -0.36 | 3.4 | -2 | -5.8 |
| FEB | Tropics | 0.831 | 0.823 | 0.81 | -0.151 | -0.269 | -0.686 | -15.2 | -16.3 | -20.8 |
| MAR | Tropics | 0.681 | 0.717 | 0.726 | 0.593 | 0.161 | -0.204 | 2.9 | -4.8 | -9.5 |
| APR | Tropics | 0.757 | 0.825 | 0.814 | -0.19 | -0.62 | -0.914 | -9 | -15.5 | -18.9 |
| MAY | Tropics | 0.71 | 0.749 | 0.744 | 0.323 | -0.097 | -0.454 | -3.7 | -9.6 | -13.5 |
| JUN | Tropics | 0.534 | 0.531 | 0.547 | 3.036 | 2.181 | 1.887 | 50.7 | 34.1 | 30.1 |
| JUL | Tropics | 0.522 | 0.523 | 0.545 | 2.524 | 2.385 | 2.055 | 36.2 | 35.4 | 31.1 |
| AUG | Tropics | 0.482 | 0.523 | 0.542 | 0.115 | 0.021 | -0.18 | -7.1 | -8 | -12.4 |
| SEP | Tropics | 0.665 | 0.686 | 0.692 | -0.988 | -1.248 | -1.522 | -23.5 | -26.8 | -33.7 |
| OCT | Tropics | 0.396 | 0.368 | 0.395 | 0.948 | 1.298 | 1.08 | 4.1 | 6 | 2.4 |
| NOV | Tropics | 0.43 | 0.511 | 0.5 | 0.043 | 0.657 | 0.287 | -9.5 | -0.3 | -7.4 |
| DEC | Tropics | 0.4 | 0.409 | 0.457 | -0.091 | 0.282 | 0.314 | -15.1 | -7.8 | -9 |

**Table 14: Statistical scores for IFS-MOZART without (f7kn) and with (f93i) data assimilation and IFS-TM5 run (f9nd) for the tropical UTLS region**

| UTLS | Region | FGE_f7kn | FGE_f93i | FGE_f9nd | Bias_f7kn [ppmm] | Bias_f93i [ppmm] | Bias_f9nd [ppmm] | RELBias_f7kn [%] | RELBias_f93i [%] | RELBias_f9nd [%] |
|---|---|---|---|---|---|---|---|---|---|---|
| JAN | Tropics | 0.743 | 0.841 | 0.758 | 0.049 | 0.103 | 0.086 | 7.9 | 13.5 | 12.5 |
| FEB | Tropics | 0.98 | 0.946 | 0.892 | -0.383 | -0.444 | -0.461 | -61.1 | -72.5 | -73.9 |
| MAR | Tropics | 0.711 | 0.856 | 0.836 | 0.069 | -0.024 | -0.07 | 15.7 | -19.2 | -28.9 |
| APR | Tropics | 0.862 | 0.958 | 0.946 | 0.04 | -0.055 | -0.13 | 15.8 | -9.9 | -23.5 |
| MAY | Tropics | 0.759 | 0.784 | 0.748 | 0.093 | -0.101 | -0.223 | 24.4 | -23.7 | -45.9 |
| JUN | Tropics | 0.544 | 0.549 | 0.628 | 0.181 | -0.023 | -0.142 | 50.5 | -13.9 | -43 |
| JUL | Tropics | 0.603 | 0.639 | 0.711 | 0.147 | -0.056 | -0.186 | 33.1 | -18.1 | -44 |
| AUG | Tropics | 0.569 | 0.867 | 0.983 | -0.098 | -0.286 | -0.346 | -15 | -54.7 | -64.3 |
| SEP | Tropics | 0.858 | 1.054 | 1.28 | -0.335 | -0.438 | -0.533 | -46.5 | -67.9 | -79.9 |
| OCT | Tropics | 0.729 | 0.734 | 0.904 | -0.156 | -0.263 | -0.306 | -32.9 | -57.8 | -66.1 |
| NOV | Tropics | 0.742 | 0.722 | 0.908 | -0.271 | -0.172 | -0.281 | -48.4 | -38.9 | -61.6 |
| DEC | Tropics | 0.747 | 0.907 | 1.179 | -0.246 | -0.268 | -0.33 | -46.7 | -61.9 | -74.3 |

**Table 15: Statistical scores for IFS-MOZART without (f7kn) and with (f93i) data assimilation and IFS-TM5 run (f9nd) for the tropical troposphere**

| TROPOSPHERE | Region | FGE_f7kn | FGE_f93i | FGE_f9nd | Bias_f7kn [ppmm] | Bias_f93i [ppmm] | Bias_f9nd [ppmm] | RELBias_f7kn [%] | RELBias_f93i [%] | RELBias_f9nd [%] |
|---|---|---|---|---|---|---|---|---|---|---|
| JAN | Tropics | 0.534 | 0.46 | 0.513 | -0.178 | -0.192 | -0.183 | -22.4 | -35.5 | -25.5 |
| FEB | Tropics | 0.591 | 0.515 | 0.618 | 0.027 | 0.016 | 0.023 | 60.7 | 35.5 | 51.9 |
| MAR | Tropics | 0.418 | 0.333 | 0.371 | 0.024 | 0.008 | 0.014 | 37.7 | 12.7 | 21.9 |
| APR | Tropics | 0.319 | 0.301 | 0.322 | 0.012 | 0.002 | 0.007 | 15.7 | 3.1 | 8.9 |
| MAY | Tropics | 0.411 | 0.351 | 0.399 | 0.024 | 0.007 | 0.014 | 30 | 9.6 | 18.2 |
| JUN | Tropics | 0.532 | 0.402 | 0.498 | 0.034 | 0.022 | 0.031 | 70.5 | 45.6 | 63.6 |
| JUL | Tropics | 0.57 | 0.45 | 0.573 | 0.03 | 0.02 | 0.029 | 65.2 | 42.7 | 62.1 |
| AUG | Tropics | 0.461 | 0.393 | 0.444 | 0.021 | 0.009 | 0.019 | 35.8 | 16.3 | 32 |
| SEP | Tropics | 0.341 | 0.296 | 0.313 | 0.013 | 0.007 | 0.009 | 24.9 | 15.9 | 18.6 |
| OCT | Tropics | 0.318 | 0.245 | 0.315 | 0.014 | 0.009 | 0.014 | 21.7 | 14 | 22.7 |
| NOV | Tropics | 0.358 | 0.291 | 0.305 | 0.022 | 0.012 | 0.012 | 33.8 | 19.4 | 19.7 |
| DEC | Tropics | 0.334 | 0.297 | 0.339 | 0.02 | 0.009 | 0.01 | 30.7 | 14.2 | 16.8 |

### 5.1.3.4  Southern midlatitudes (SH)

For the southern hemisphere validation, one needs to keep in mind that there are only two sounding stations available for NRT data delivery in 2010. Southern midlatitude results are therefore less spatially representative than those for the northern hemisphere.

Modelled **stratospheric** ozone concentrations, mostly correspond satisfyingly to the measured profiles (Figure 51). From August till December, monthly relative biases for all model runs increase. The IFS –MOZART run without data assimilation (f7kn) slightly overestimates stratospheric mixing rations (relative bias < 20%) from January till August; towards the second part of the year, the overestimation increases to a maximum of up to 40% in September. The assimilation runs slightly underestimate

the measured mixing ratios between January to June (relative biases around -20%), whereas in the period July to December, the assimilation runs tend to slightly overestimate ozone levels (relative biases around 10%). The ozone hole 2010 is slightly underestimated by both model runs with data assimilation (Figure 61 to Figure 63). Data assimilation improves the results of IFS – MOZART in the stratosphere.

In the **UTLS** region, the results are similar: the IFS-MOZART run f7kn overestimates measured mixing ratios throughout the year except in June. The assimilation runs show an underestimation of measured ozone mixing ratios of up to -40% (f93i) and -30% (f9nd) from January to June and from November to December. In August and September ozone concentrations are slightly overestimated by the models (relative Biases of 30% for run f93i and 20% for run f9nd).

In the **troposphere**, the IFS-TM5 run (f9nd) shows an overestimation of measured O3 concentrations of up to 44% (August) except for the month October, where measured values are underestimated by around -20%. Contrary to this, the IFS-MOZART runs underestimate ozone concentrations throughout the year by up to -20% (f7kn) and -35% (f93i), except for December.

Statistical scores for the stratosphere, UTLS and troposphere region are listed in Table 16 till Table 18.
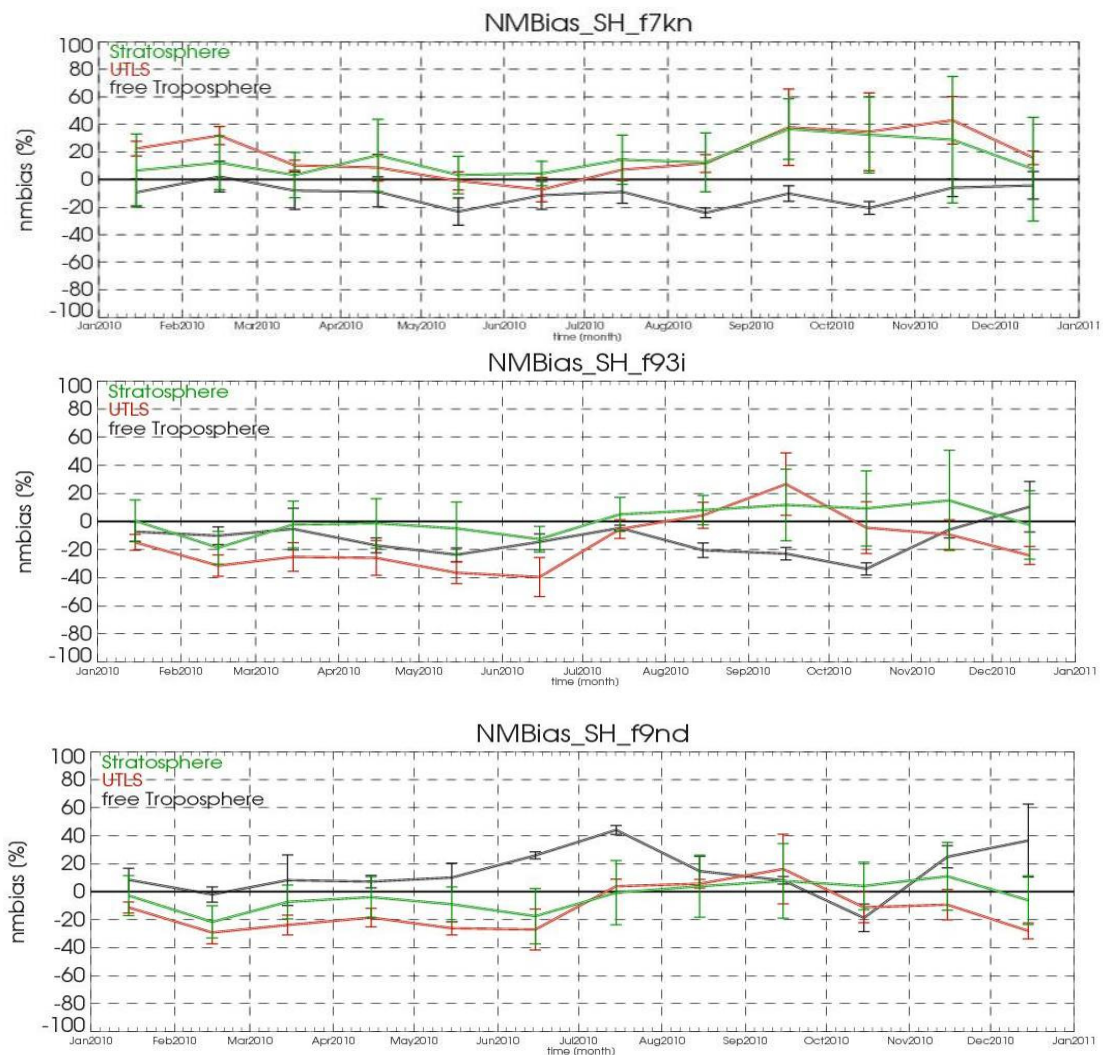


**Figure 60: Monthly averaged relative bias of run f7kn (upper panel), f93i and run f9nd (lower panel) in percent between the southern hemisphere ozone soundings and the forecast runs,**

**Figure 61: Comparison of the mean O3 profiles for August (top) and September (bottom) 2010 in the southern midlatitude region for model run f7kn (left), f93i (middle) and f9nd (right). Modeled results are in black, sonde measurements in green. The UTLS region is displayed separately with a factor.**

**Figure 62: Same as for Figure 61 but now for October (top) and November (bottom) 2010.**

**Figure 63: Same as for Figure 61 but now for December 2010.**

**Table 16: Statistical scores for IFS-MOZART without (f7kn) and with (f93i) data assimilation and IFS-TM5 run (f9nd) for the southern midlatitude stratosphere**

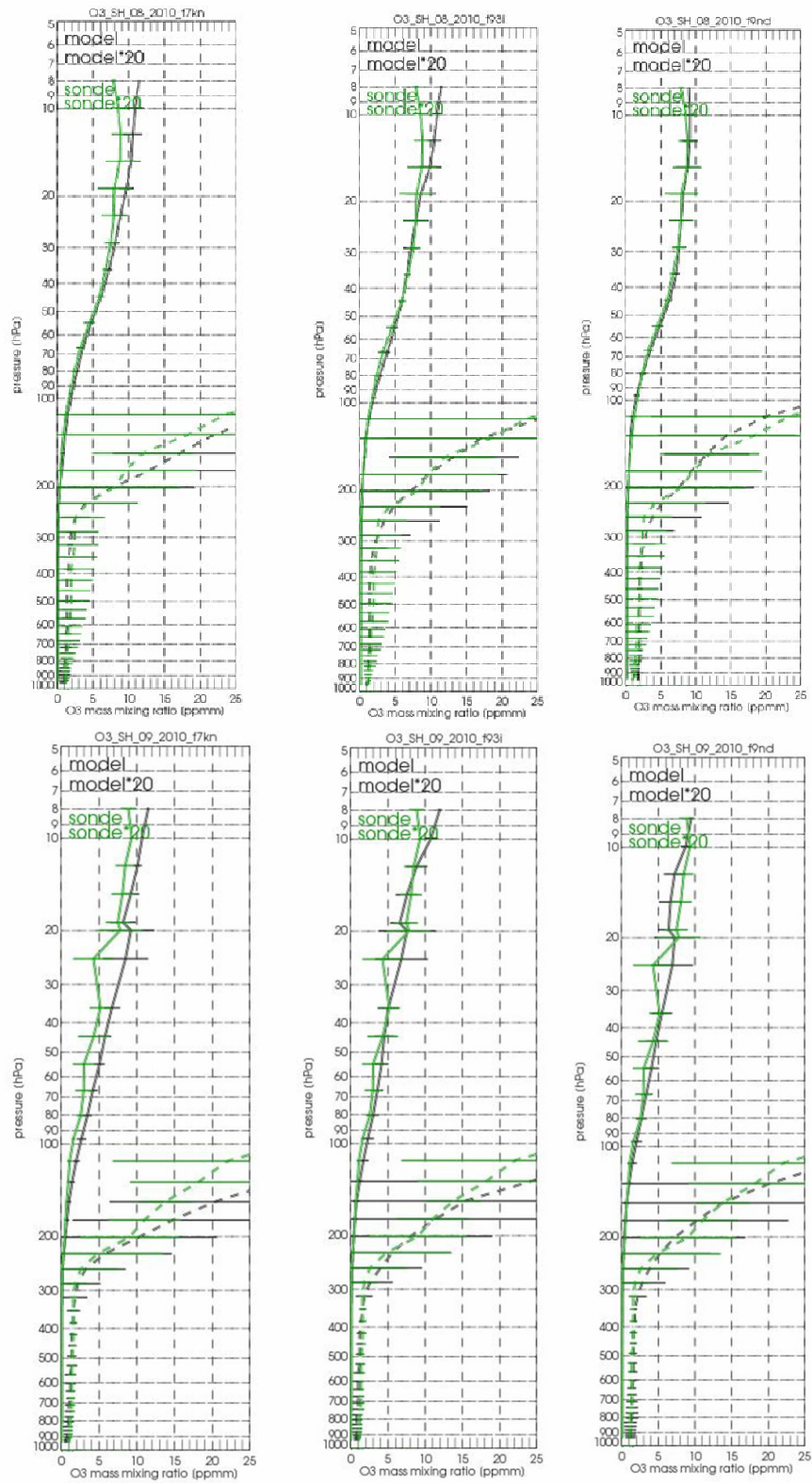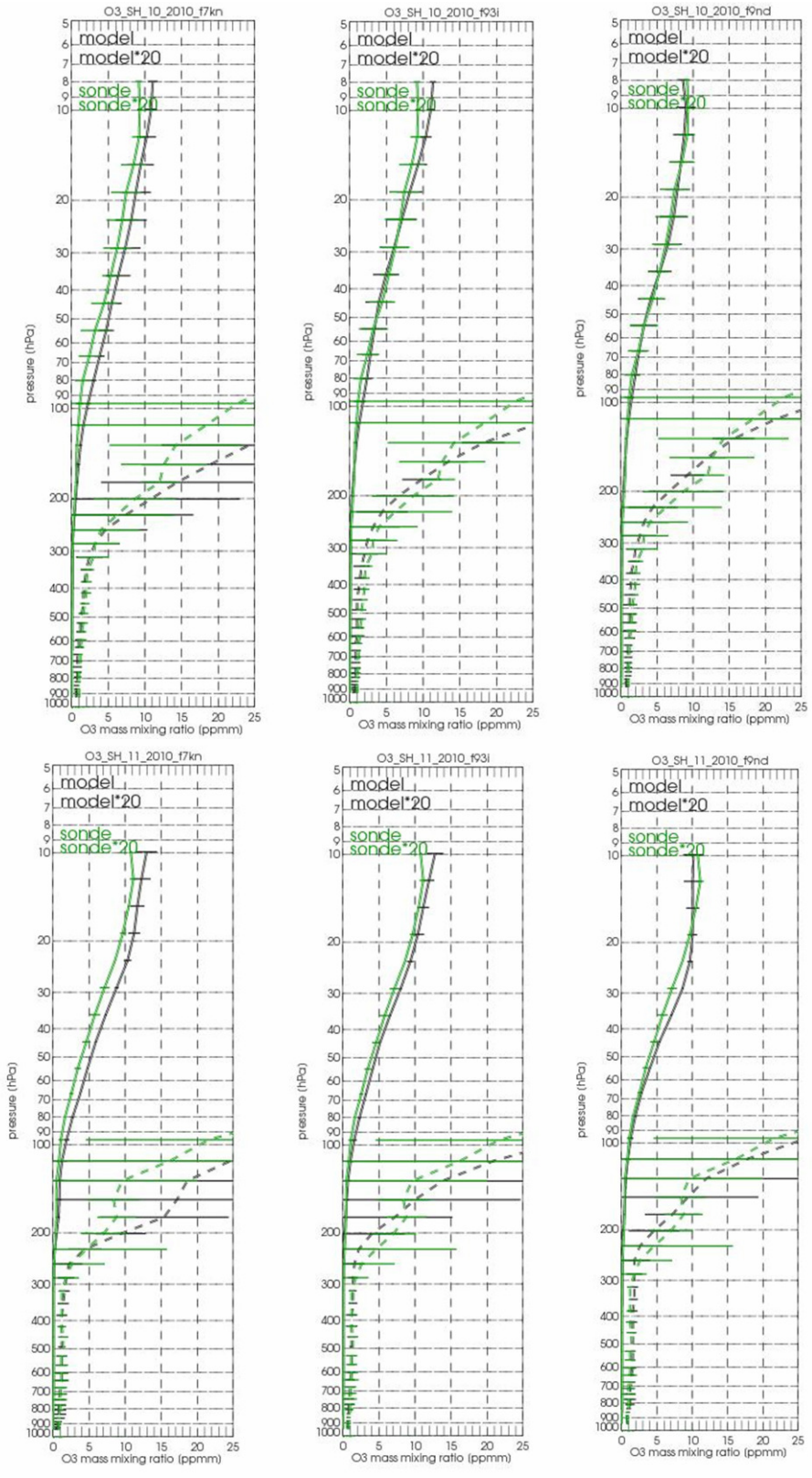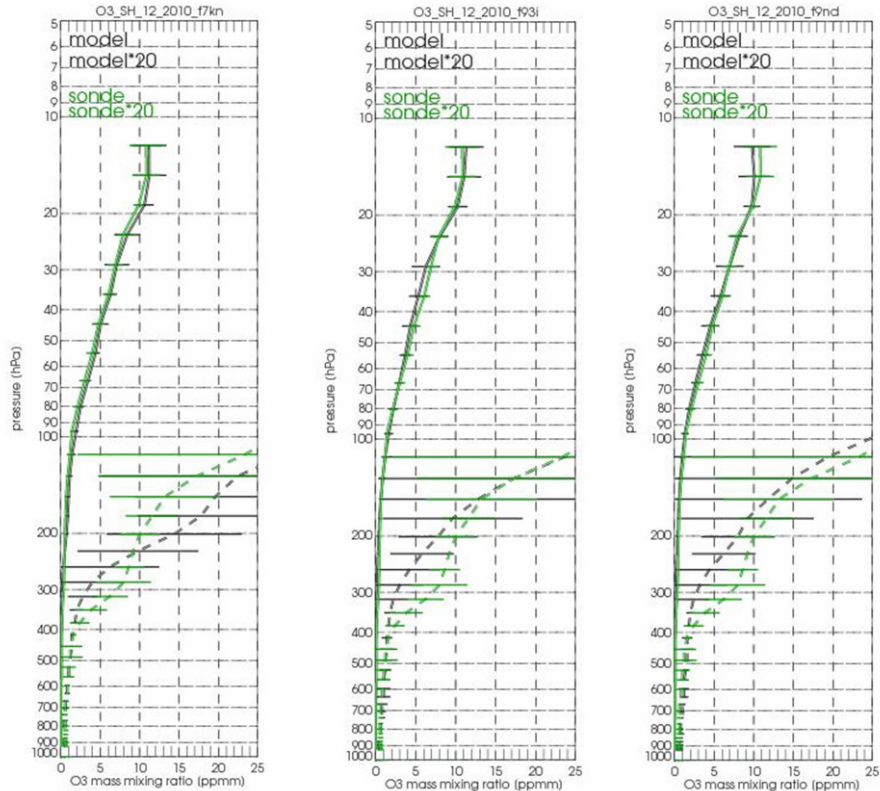| STRATOSPHERE | Region | FGE_f7kn | FGE_f93i | FGE_f9nd | Bias_f7kn [ppmm] | Bias_f93i [ppmm] | Bias_f9nd [ppmm] | RELBias_f7kn [%] | RELBias_f93i [%] | RELBias_f9nd [%] |
|---|---|---|---|---|---|---|---|---|---|---|
| JAN | SH | 0.167 | 0.119 | 0.113 | 0.322 | 0.033 | -0.214 | 6.6 | 0.5 | -2.8 |
| FEB | SH | 0.115 | 0.288 | 0.308 | 0.587 | -0.959 | -1.125 | 12.2 | -18.7 | -21.6 |
| MAR | SH | 0.159 | 0.222 | 0.233 | 0.218 | -0.235 | -0.548 | 3.3 | -2.1 | -7.3 |
| APR | SH | 0.185 | 0.29 | 0.237 | 0.809 | -0.1 | -0.236 | 17.6 | -1.3 | -3.9 |
| MAY | SH | 0.164 | 0.153 | 0.161 | 0.251 | -0.268 | 0.006 | 3.3 | -4.9 | -9 |
| JUN | SH | 0.118 | 0.221 | 0.247 | 0.434 | -0.534 | -0.791 | 4.4 | -12.6 | -17.5 |
| JUL | SH | 0.161 | 0.081 | 0.07 | 0.853 | 0.081 | -0.018 | 14.4 | 5.1 | -0.7 |
| AUG | SH | 0.14 | 0.099 | 0.063 | 0.833 | 0.447 | 0.22 | 12.5 | 8.1 | 3.9 |
| SEP | SH | 0.319 | -0.019 | 0.231 | 1.625 | 0.344 | 0.063 | 36.7 | 11.8 | 7.7 |
| OCT | SH | 0.305 | 0.172 | 0.131 | 1.217 | 0.334 | 0.089 | 32.5 | 9.3 | 4.1 |
| NOV | SH | 0.245 | 0.138 | 0.133 | 1.376 | 0.702 | 0.469 | 28.9 | 15 | 11 |
| DEC | SH | 0.077 | 0.061 | 0.086 | 0.399 | -0.093 | -0.328 | 7.6 | -2.5 | -6.1 |

**Table 17: Statistical scores for IFS-MOZART without (f7kn) and with (f93i) data assimilation and IFS-TM5 run (f9nd) for the southern midlatitude UTLS region**

| UTLS | Region | FGE_f7kn | FGE_f93i | FGE_f9nd | Bias_f7kn [ppmm] | Bias_f93i [ppmm] | Bias_f9nd [ppmm] | RELBias_f7kn [%] | RELBias_f93i [%] | RELBias_f9nd [%] |
|---|---|---|---|---|---|---|---|---|---|---|
| JAN | SH | 0.38 | 0.327 | 0.31 | 0.116 | -0.046 | -0.04 | 22.5 | -14.8 | -11.3 |
| FEB | SH | 0.402 | 0.534 | 0.495 | 0.14 | -0.106 | -0.098 | 31.9 | -31.4 | -29.2 |
| MAR | SH | 0.224 | 0.456 | 0.472 | 0.04 | -0.055 | -0.059 | 10.3 | -25.2 | -23.8 |
| APR | SH | 0.339 | 0.581 | 0.475 | 0.074 | -0.065 | -0.043 | 8.7 | -25.9 | -18.5 |
| MAY | SH | 0.288 | 0.536 | 0.15 | 0.02 | -0.12 | -0.476 | -0.9 | -36.5 | -26.1 |
| JUN | SH | 0.243 | 0.571 | 0.515 | -0.02 | -0.223 | -0.207 | -7.3 | -39.5 | -27 |
| JUL | SH | 0.263 | 0.218 | 0.253 | 0.084 | -0.025 | -0.041 | 7.2 | -5.4 | 3.9 |
| AUG | SH | 0.299 | 0.172 | 0.205 | 0.108 | 0.012 | -0.034 | 11.7 | 4.4 | 5.7 |
| SEP | SH | 0.365 | 0.417 | 0.382 | 0.259 | 0.135 | 0.056 | 37.9 | 26.6 | 16.2 |
| OCT | SH | 0.335 | 0.332 | 0.283 | 0.23 | 0.032 | -0.023 | 34.7 | -4.4 | -11.2 |
| NOV | SH | 0.447 | 0.345 | 0.25 | 0.217 | 0.014 | -0.011 | 43 | -9.3 | -9.3 |
| DEC | SH | 0.362 | 0.355 | 0.37 | 0.135 | -0.109 | -0.152 | 15.8 | -24.2 | -28 |

**Table 18: Statistical scores for IFS-MOZART without (f7kn) and with (f93i) data assimilation and IFS-TM5 run (f9nd) for the southern hemispheric troposphere**

| TROPOSPHERE | Region | FGE_f7kn | FGE_f93i | FGE_f9nd | Bias_f7kn [ppmm] | Bias_f93i [ppmm] | Bias_f9nd [ppmm] | RELBias_ f7kn [%] | RELBias_f93i [%] | RELBias_f9nd [%] |
|---|---|---|---|---|---|---|---|---|---|---|
| JAN | SH | 0.212 | 0.272 | 0.2 | -0.004 | -0.003 | 0.003 | -9.3 | -7.3 | 8.5 |
| FEB | SH | 0.173 | -0.106 | 0.175 | 0.002 | -0.006 | -0.001 | 2.2 | -10.1 | -2 |
| MAR | SH | 0.195 | 0.176 | 0.212 | -0.006 | -0.005 | 0.002 | -8 | -5.3 | 8.2 |
| APR | SH | 0.199 | 0.219 | 0.14 | -0.005 | -0.01 | 0.004 | -8.9 | -17 | 7.2 |
| MAY | SH | 0.281 | 0.266 | 0.338 | -0.014 | -0.015 | -0.092 | -23.2 | -23.6 | 10.1 |
| JUN | SH | 0.173 | 0.178 | 0.22 | -0.007 | -0.009 | 0.016 | -11.4 | -14.5 | 25.9 |
| JUL | SH | 0.155 | 0.158 | 0.362 | -0.006 | -0.003 | 0.362 | -8.9 | -4.6 | 44.1 |
| AUG | SH | 0.293 | 0.211 | 0.392 | -0.022 | -0.019 | 0.012 | -24.1 | -20.4 | 14.7 |
| SEP | SH | 0.133 | 0.276 | 0.121 | -0.007 | -0.016 | 0.006 | -10.1 | -22.9 | 8.1 |
| OCT | SH | 0.238 | 0.426 | 0.244 | -0.015 | -0.026 | -0.015 | -20.6 | -33.7 | -18.7 |
| NOV | SH | 0.088 | 0.094 | 0.231 | -0.004 | -0.003 | 0.015 | -5.9 | -5.8 | 24.9 |
| DEC | SH | 0.247 | 0.229 | 0.346 | -0.004 | 0.002 | 0.014 | -4.2 | 10.5 | 36.5 |

### 5.1.3.5 Antarctica

For the validation in Antarctica, one needs to keep in mind that there are only three sounding stations available for NRT data delivery.

For the entire year, mean modelled mixing ratios of all forecast runs underestimate measured O3 mixing ratios in the **stratosphere**, with maximum values during the ozone hole situation between October and December; the forecast runs with data assimilation obtain higher relative biases (about -40% f7kn, f93i and f9nd around 60%). In 2010, the ozone hole was very weak compared to previous years, due to sudden stratospheric warming in July and August. This has not been simulated entirely correct by the model runs: the stratospheric ozone hole is overestimated in Antarctica in 2010 (Figure 65 to Figure 67).

In the **UTLS** region, measured ozone mixing ratios are underestimated by around -36% (f9nd) to -38% (f93i) throughout the year 2010, with maximum values in October (relative bias of -67%). However, the results vary between the individual stations; see the example for the soundings of Neumayer and Marambio in Figure 68 to Figure 71.

Modelled **tropospheric** ozone levels are underestimated by around -20% by the IFS-MOZART runs. The IFS-TM5 run however, shows a strong overestimation of measured ozone mixing ratios in the months March to September of up to 60% in August.

Statistical scores for the stratosphere, UTLS and troposphere region are listed in *Table 16 to 18.*
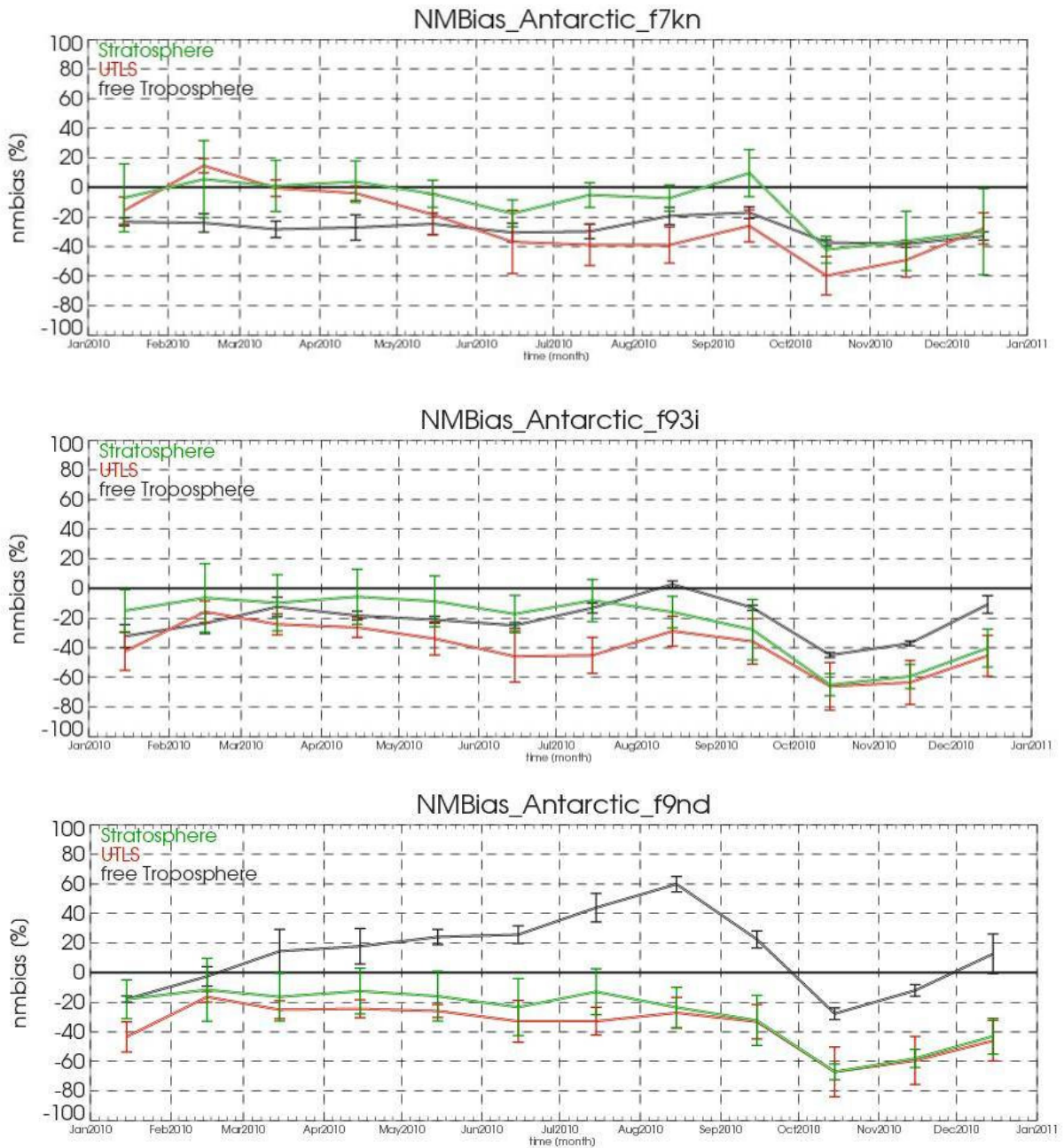
**Figure 64: Monthly averaged relative bias of run f7kn (upper panel), f93i and run f9nd (lower panel) in percent between the antarctic ozone soundings and the forecast runs, January 2010 to December 2010. Colour codes denote the three altitude regions free troposphere in black, the UTLS region in red and the stratosphere in green.**

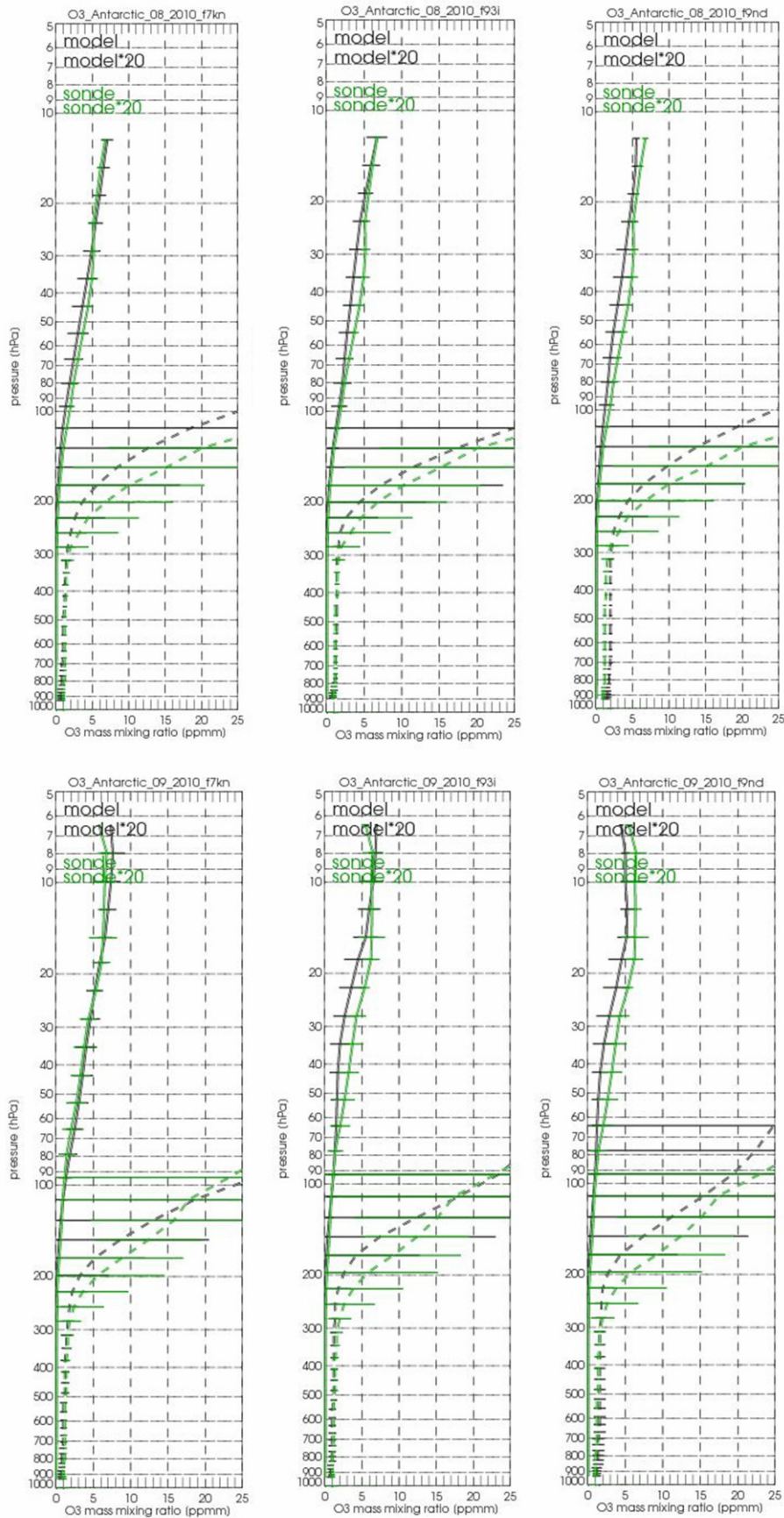**Figure 65:** *Comparison of the mean O3 profiles for August (top) and September (bottom) 2010 in Antarctica for model runs f7kn (left), f93i (middle) and f9nd (right). Modelled results are in black, sonde measurements in green. The UTLS region is displayed separately with a factor.*
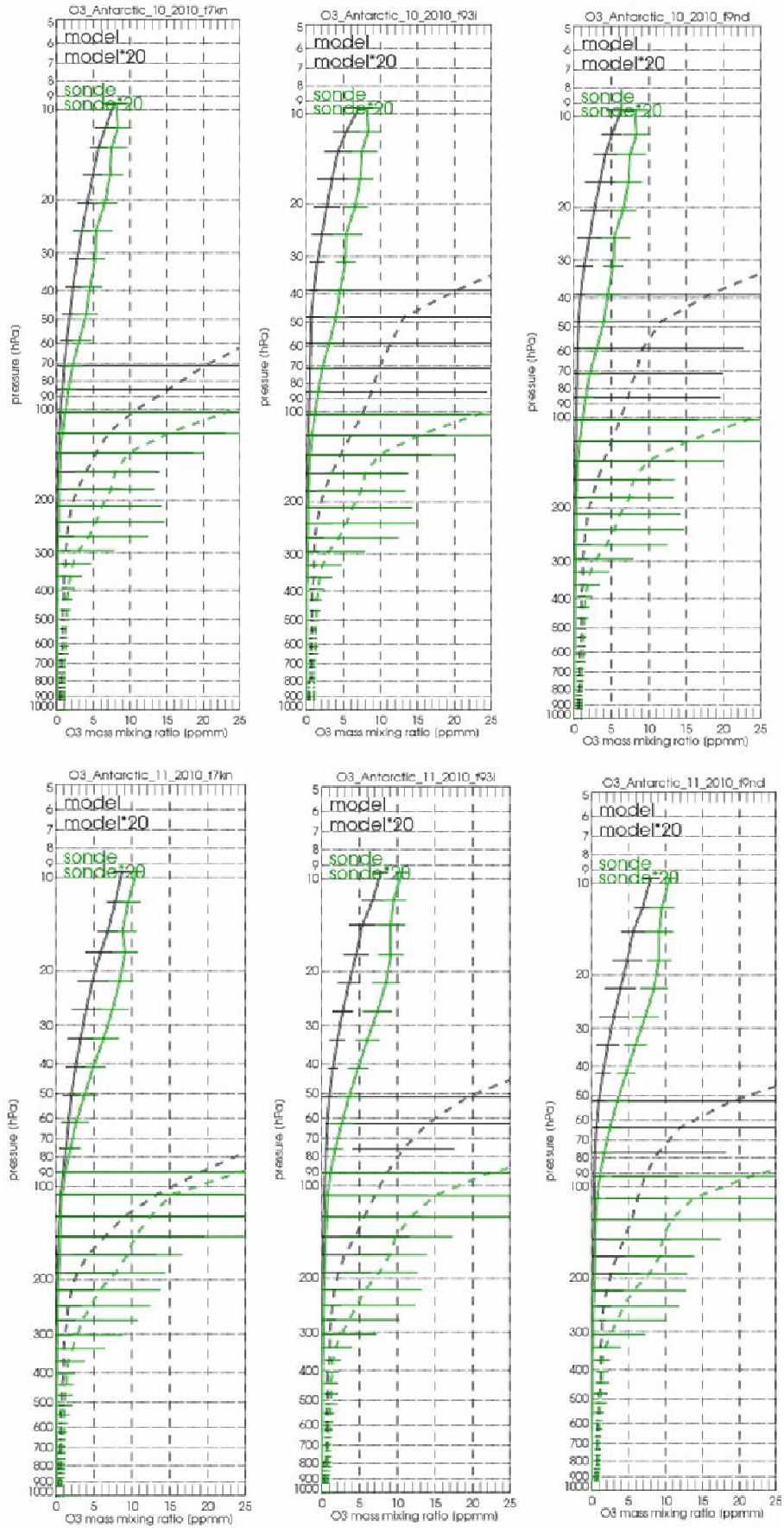
**Figure 66: Same as for Figure 65 but now for October (top) and November (bottom) 2010.**
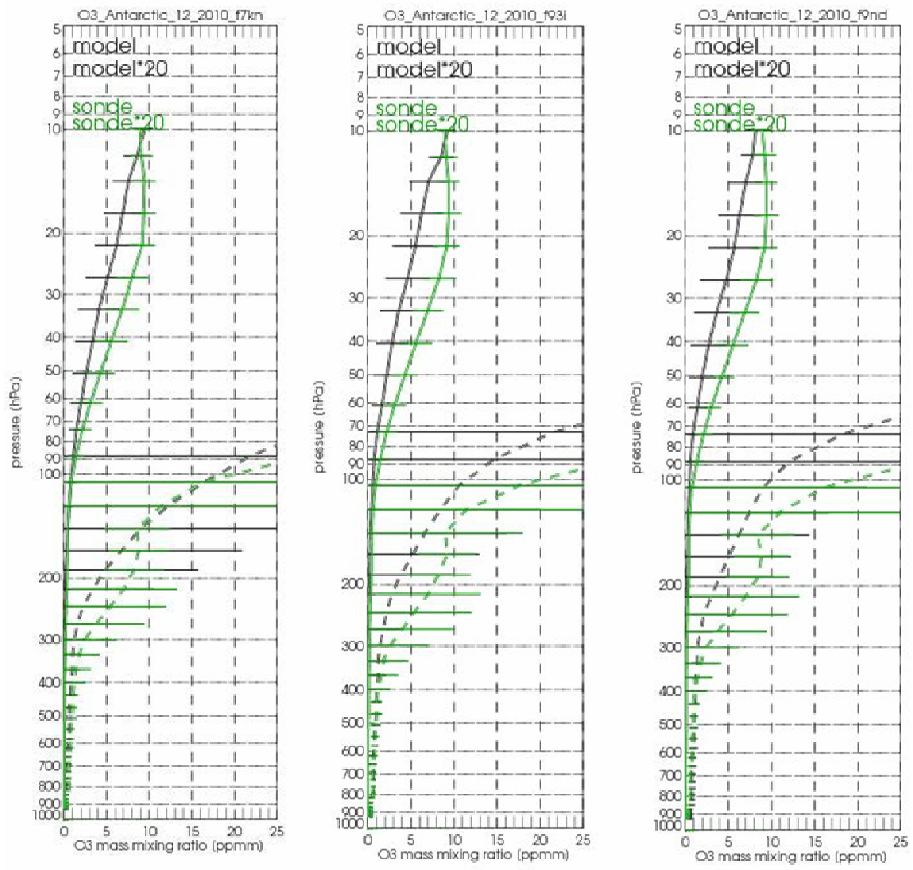
**Figure 67: Same as for Figure 48 but now for December 2010.**

**Figure 68: Comparison of validation results between the two stations Neumayer (top) and Marambio (bottom) at respectively 20 and 19 Sept 2010. Modelled results are in black, sonde measurements in red and green (mean profiles). The UTLS region is displayed separately with a factor.**
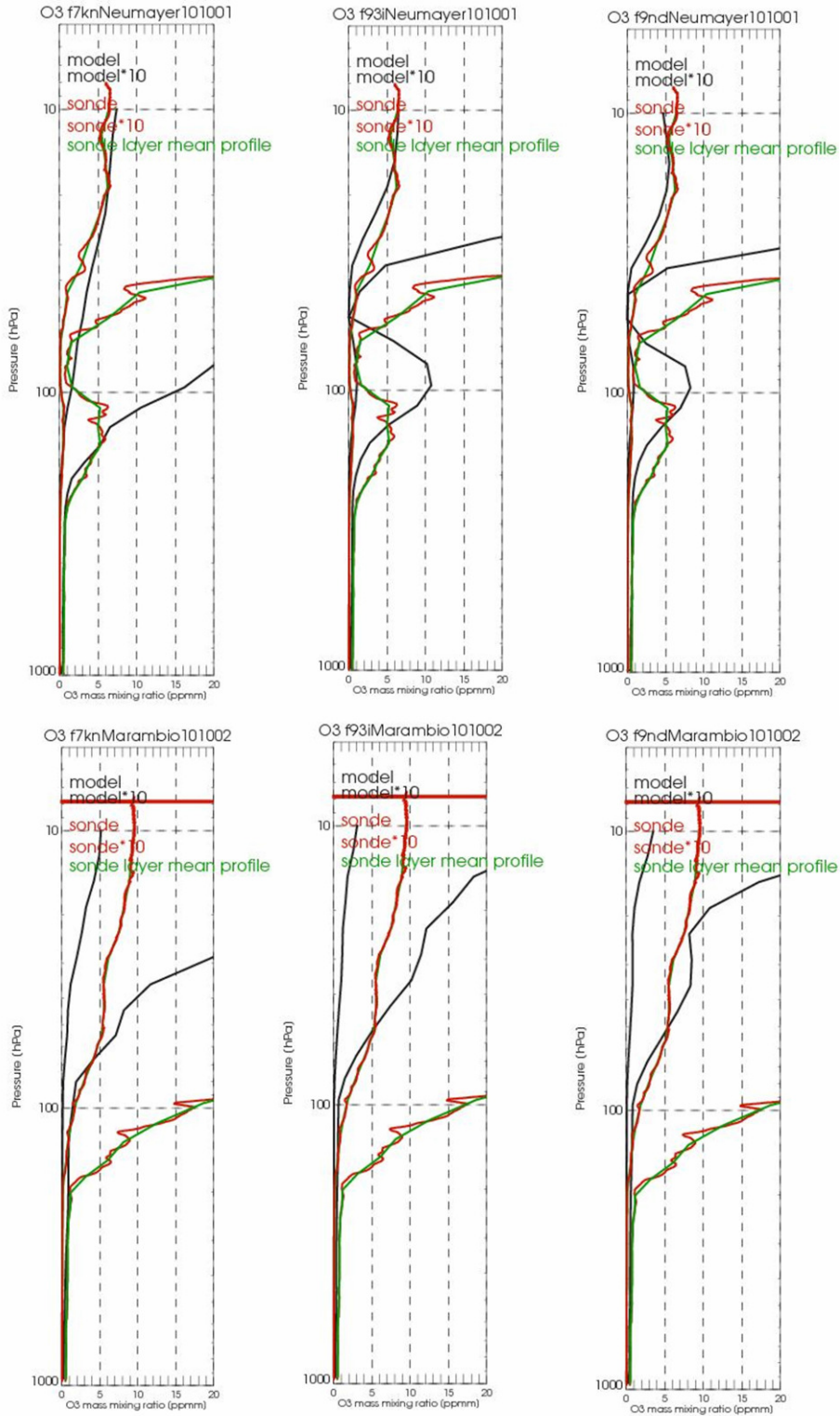
**Figure 69: Comparison of validation results between the two stations Neumayer (top) and Marambio (bottom) at respectively the 1st and 2nd of Oct 2010. Modelled results are in black, sonde measurements in red and green (mean profiles). The UTLS region is displayed separately with a factor.**

**Figure 70: Comparison of validation results between the two stations Neumayer (top) and Marambio (bottom) at respectively 18 and 17 Nov 2010. Modelled results are in black, sonde measurements in red and green (mean profiles). The UTLS region is displayed separately with a factor.**
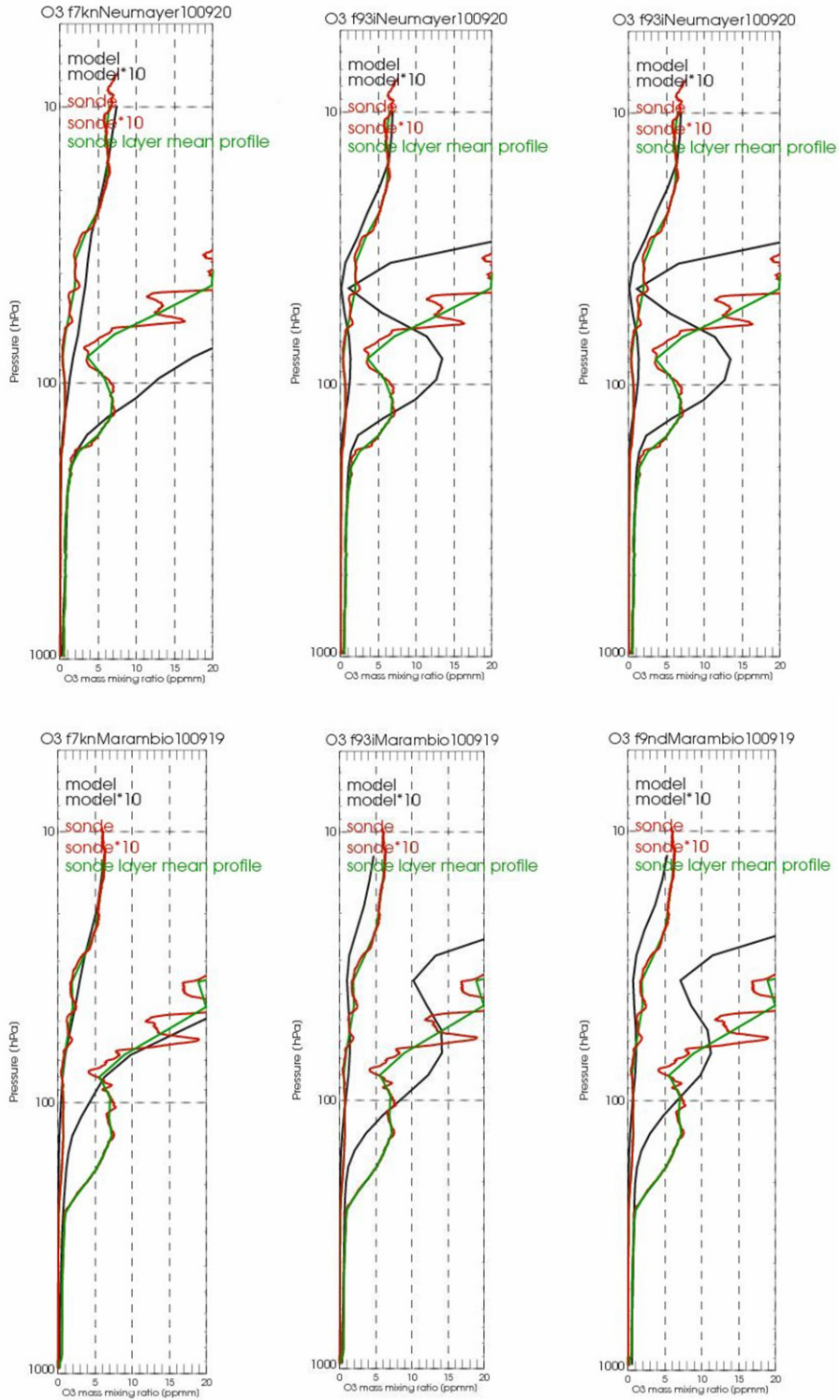
**Figure 71: Comparison of validation results between the two stations Neumayer (top) and Marambio (bottom) at 14 and 15 December 2010. Modelled results are in black, sonde measurements in red and green (mean profiles). The UTLS region is displayed separately with a factor.**
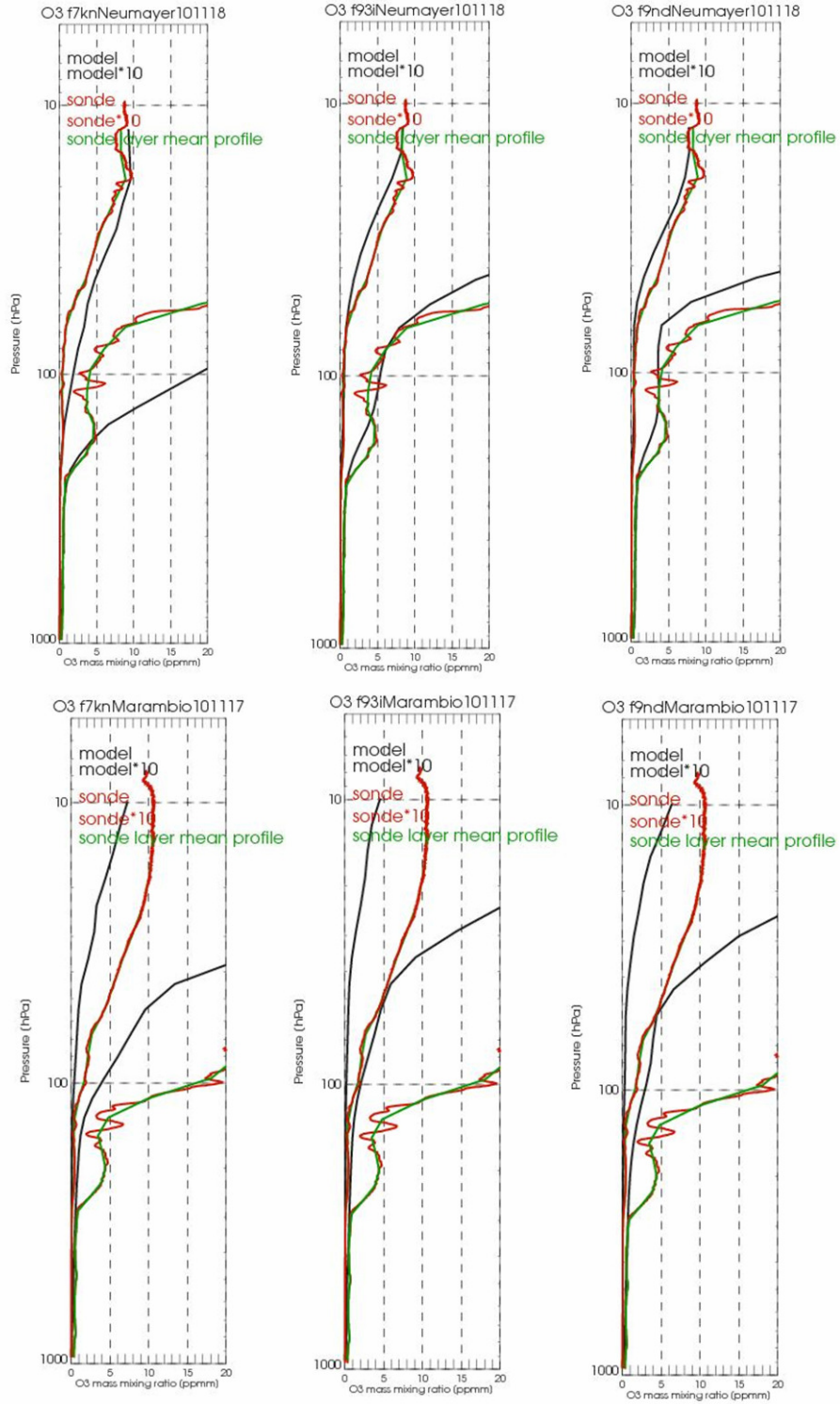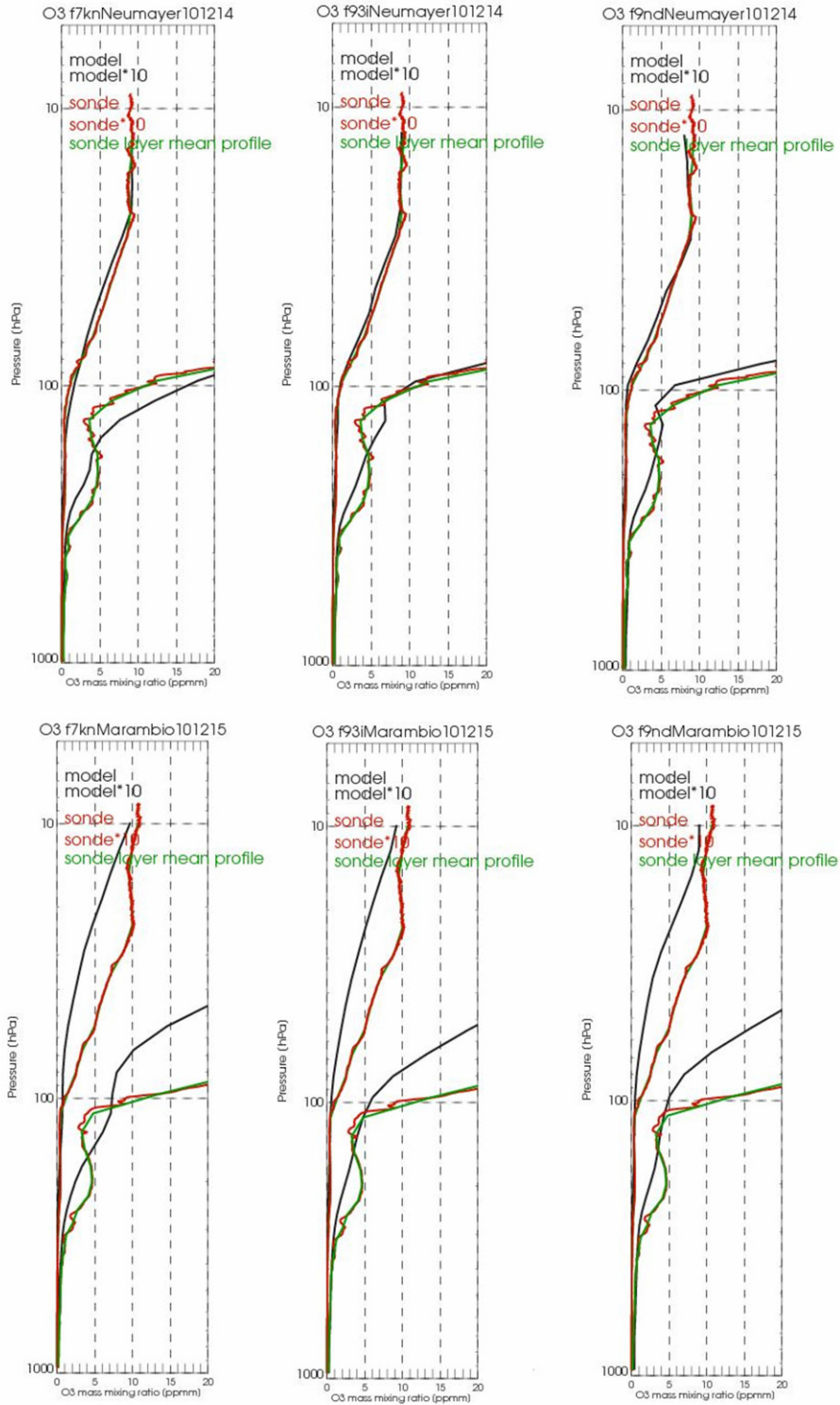
**Table 19: Statistical scores for IFS-MOZART without (f7kn) and with (f93i) data assimilation and IFS-TM5 run (f9nd) for the Antarctic stratosphere**

| STRATOSPHERE | Region | FGE_f7kn | FGE_f93i | FGE_f9nd | Bias_f7kn [ppmm] | Bias_f93i [ppmm] | Bias_f9nd [ppmm] | RELBias_f7kn [%] | RELBias_f93i [%] | RELBias_f9nd [%] |
|---|---|---|---|---|---|---|---|---|---|---|
| JAN | Antarctica | 0.264 | 0.286 | 0.303 | -0.284 | -0.668 | -0.846 | -7.1 | -15 | -17.9 |
| FEB | Antarctica | 0.184 | 0.189 | 0.205 | 0.242 | -0.298 | -0.604 | 5.5 | -6.3 | -11.6 |
| MAR | Antarctica | 0.22 | 0.229 | 0.278 | 0.038 | -0.413 | -0.722 | 1 | -9.7 | -16.3 |
| APR | Antarctica | 0.18 | 0.157 | 0.209 | 0.206 | -0.243 | -0.577 | 3.9 | -5.6 | -12.5 |
| MAY | Antarctica | 0.243 | 0.22 | 0.254 | -0.109 | -0.349 | -0.674 | -4.4 | -8.7 | -15.9 |
| JUN | Antarctica | 0.388 | 0.371 | 0.397 | -0.612 | -0.657 | -0.923 | -17.6 | -17.2 | -23.3 |
| JUL | Antarctica | 0.286 | 0.257 | 0.262 | -0.161 | -0.35 | -0.572 | -5.1 | -8.1 | -12.9 |
| AUG | Antarctica | 0.327 | 0.296 | 0.354 | -0.212 | -0.688 | -1.013 | -7.3 | -15.9 | -23.5 |
| SEP | Antarctica | 0.435 | 0.537 | 0.545 | 0.257 | -1.109 | -1.237 | 9.7 | -27.8 | -32.3 |
| OCT | Antarctica | 0.782 | 1.063 | 1.079 | -1.894 | -3.004 | -3.089 | -42.1 | -64.9 | -67 |
| NOV | Antarctica | 0.707 | 0.816 | 0.818 | -2.081 | -3.37 | -3.177 | -36.2 | -59.3 | -57.9 |
| DEC | Antarctica | 0.513 | 0.591 | 0.629 | -1.767 | -2.26 | -2.343 | -29.9 | -40.2 | -42.9 |

**Table 20: Statistical scores for IFS-MOZART without (f7kn) and with (f93i) data assimilation and IFS-TM5 run (f9nd) for the Antarctic UTLS region**

| UTLS | Region | FGE_f7kn | FGE_f93i | FGE_f9nd | Bias_f7kn [ppmm] | Bias_f93i [ppmm] | Bias_f9nd [ppmm] | RELBias_f7kn [%] | RELBias_f93i [%] | RELBias_f9nd [%] |
|---|---|---|---|---|---|---|---|---|---|---|
| JAN | Antarctica | 0.646 | 0.65 | 0.643 | -0.042 | -0.225 | -0.233 | -15.7 | -42.5 | -43.4 |
| FEB | Antarctica | 0.382 | 0.405 | 0.39 | 0.114 | -0.04 | -0.05 | 14.7 | -15.7 | -16.4 |
| MAR | Antarctica | 0.402 | 0.502 | 0.509 | 0.027 | -0.093 | -0.105 | -0.5 | -24.2 | -25 |
| APR | Antarctica | 0.325 | 0.468 | 0.421 | 0.006 | -0.09 | -0.09 | -3.9 | -26.3 | -24.4 |
| MAY | Antarctica | 0.365 | 0.551 | 0.444 | -0.071 | -0.106 | -0.099 | -18.4 | -33.9 | -25.9 |
| JUN | Antarctica | 0.558 | 0.663 | 0.5 | -0.193 | -0.199 | -0.187 | -36.9 | -45.8 | -32.8 |
| JUL | Antarctica | 0.653 | 0.716 | 0.593 | -0.212 | -0.214 | -0.208 | -38.8 | -45.1 | -32.8 |
| AUG | Antarctica | 0.797 | 0.735 | 0.711 | -0.229 | -0.128 | -0.185 | -38.9 | -28.8 | -27.1 |
| SEP | Antarctica | 0.52 | 0.63 | 0.573 | -0.087 | -0.116 | -0.135 | -26 | -35.7 | -33.2 |
| OCT | Antarctica | 0.951 | 1.071 | 1.013 | -0.263 | -0.299 | -0.314 | -59.7 | -66 | -67 |
| NOV | Antarctica | 0.878 | 0.895 | 0.79 | -0.18 | -0.256 | -0.234 | -49.1 | -63.4 | -59.4 |
| DEC | Antarctica | 0.813 | 0.726 | 0.698 | -0.083 | -0.175 | -0.188 | -27.7 | -45.4 | -46 |

**Table 21: Statistical scores for IFS-MOZART without (f7kn) and with (f93i) data assimilation and IFS-TM5 run (f9nd) for the Antarctic troposphere**

| TROPOSPHERE | Region | FGE_f7kn | FGE_f93i | FGE_f9nd | Bias_f7kn [ppmm] | Bias_f93i [ppmm] | Bias_f9nd [ppmm] | RELBias_f7kn [%] | RELBias_f93i [%] | RELBias_f9nd [%] |
|---|---|---|---|---|---|---|---|---|---|---|
| JAN | Antarctica | 0.322 | 0.431 | 0.246 | -0.01 | -0.013 | -0.008 | -23.3 | -32.2 | -17.9 |
| FEB | Antarctica | 0.32 | 0.3 | 0.141 | -0.01 | -0.01 | -0.002 | -24 | -23.6 | -2.5 |
| MAR | Antarctica | 0.333 | 0.22 | 0.243 | -0.013 | -0.006 | 0.005 | -28.3 | -12.4 | 14.5 |
| APR | Antarctica | 0.327 | 0.2 | 0.227 | -0.013 | -0.009 | 0.008 | -27.1 | -18.3 | 17.8 |
| MAY | Antarctica | 0.301 | 0.235 | 0.222 | -0.013 | -0.011 | 0.013 | -24.7 | -21.1 | 24.1 |
| JUN | Antarctica | 0.373 | 0.287 | 0.234 | -0.018 | -0.015 | 0.015 | -30.5 | -24.9 | 25.7 |
| JUL | Antarctica | 0.35 | 0.142 | 0.377 | -0.018 | -0.008 | 0.027 | -29.8 | -13.2 | 43.9 |
| AUG | Antarctica | 0.22 | 0.09 | 0.461 | -0.012 | 0.002 | 0.037 | -19.3 | 2.8 | 59.8 |
| SEP | Antarctica | -0.17 | 0.182 | 0.254 | -0.011 | -0.008 | 0.014 | -17 | -13 | 22.5 |
| OCT | Antarctica | 0.463 | 0.577 | 0.341 | -0.024 | -0.03 | -0.019 | -37.2 | -44.9 | -27.7 |
| NOV | Antarctica | 0.46 | 0.437 | 0.198 | -0.022 | -0.02 | -0.007 | -38.2 | -37 | -12 |
| DEC | Antarctica | 0.44 | 0.282 | 0.259 | -0.015 | -0.006 | 0.004 | -32.9 | -10.8 | 12.7 |

### 5.1.4 Conclusions

The vertical ozone distribution of the IFS-MOZART with (f93i) and without data assimilation (f7kn) and IFS-TM5 (f9nd) model forecast runs with data assimilation have been evaluated for the year 2010 using ozone soundings of 38 stations.

**In the stratosphere,** there is a good accordance between modelled and measured O3 mixing ratios for the Arctic and northern midlatitude region. Especially in the northern midlatitude region all models obtain biases < 10%. In the Tropics, there is a slight underestimation of measured profiles mostly < 20%, except for the months June and July, where modelled concentrations exceed the measured mixing ratios by over 30%. In the southern midlatitude region, measured ozone profiles are underestimated

by the model runs with data assimilation from January to June (relative bias <20%), whereas from July to December O3 mixing ratios are slightly overestimated (relative biases mostly <10%). IFS-MOZART without data assimilations overestimates measured O3 mixing ratios throughout the year, from January to August <20%, from September to December by around 30%. In Antarctica, all model runs are underestimating measured O3 mixing ratios by about -20% from January to September.

During ozone hole conditions, maximum relative bias values reach up to -70% in October. The Antarctic ozone hole is thus overestimated by all model runs. This is contrary to previous validation results (GEMS-Project), where forecast runs underestimated the Antarctic ozone hole. However, in 2010, the ozone hole was a lot weaker than in previous years due to sudden stratospheric warming occurring in July and August.

For all regions, the IFS-MOZART model with data assimilation tends to show a better performance than the IFS-TM5 run in the stratosphere. Data assimilation improves the validation results except for the Antarctic region where the underestimation of O3 mixing ratios is increased.

**In the UTLS region,** both model runs with data assimilation show a strong and consistent underestimation of measured O3 mixing ratios in all regions, with average discrepancies between -10% (Arctic) to -50% (Tropics). In the northern midlatitude region, arctic and tropics, the IFS-MOZART combination obtains better results, whereas in the southern midlatitude region and Antarctica, the IFS-TM5 model receives better results. The IFS-MOZART model without data assimilation is overestimating measured ozone mixing ratios in the arctic and at the northern and southern midlatitudes (relative biases mostly < 20%). In the Tropics, there is a strong overestimation of measured mixing ratios between January and July whereas between August and December the measured mixing ratios are underestimated by about -40%. In Antarctica, measured ozone mixing ratios are underestimated by about -30%. Data assimilation improves the IFS-MOZART model results only at the southern midlatitudes and the Arctic.

**In the free troposphere,** there is a good accordance between modelled and measured mixing ratios for the arctic and northern hemisphere with relative biases of mostly < 20%. All model forecast runs slightly underestimate ozone mixing ratios in the arctic and northern midlatitude region (relative bias mostly < 20%). At southern midlatitudes and in Antarctica, the IFS-MOZART runs obtain negative relative biases (mostly <20%), whereas the IFS-TM5 run tends to overestimate measured mixing ratios (around 20% at southern midlatitudes, around 30% in Antarctica). In the Tropics all model runs are overestimating measured mixing ratios with relative biases between 20% (f93i) - 40% (f7kn).

IFS-TM5 obtains better results in the Arctic and at northern midlatitudes, whereas IFS-MOZART achieves better results in the Tropics, at southern midlatitudes and in the Antarctic region. Data assimilation improves the results only in the Tropics and in Antarctica, in the other regions the results in the free troposphere are degraded by the assimilation.

## Appendix A: How closely does the BASCOE assimilation of Aura/MLS match the original Aura/MLS observations at the stratospheric North Pole region?

In order to evaluate whether or not the BASCOE analyses are representative for the Aura/MLS observations it assimilates, we show in Figure 73 and Figure 73 the bias and standard deviation of the BASCOE Aura/MLS analysis versus the observations that were assimilated for the North Pole region (lat > 60°N). This proves that for the region 100-10hPa, BASCOE AN for O3, HNO3, H2O and HCl are very close to the observed values (bias < 2%). Assimilation of HOCl and ClO cannot be trusted due to low data quality in this region. Aura/MLS data exhibit an artifact in lower stratospheric ClO (a negative bias present in both daytime and nighttime mixing ratios below 22 hPa) and HOCl (negative averages for p > +/- 10 hPa currently make this product unsuitable for use in this region), as described in http://mls.jpl.nasa.gov/data/v2-2_data_quality_document.pdf.
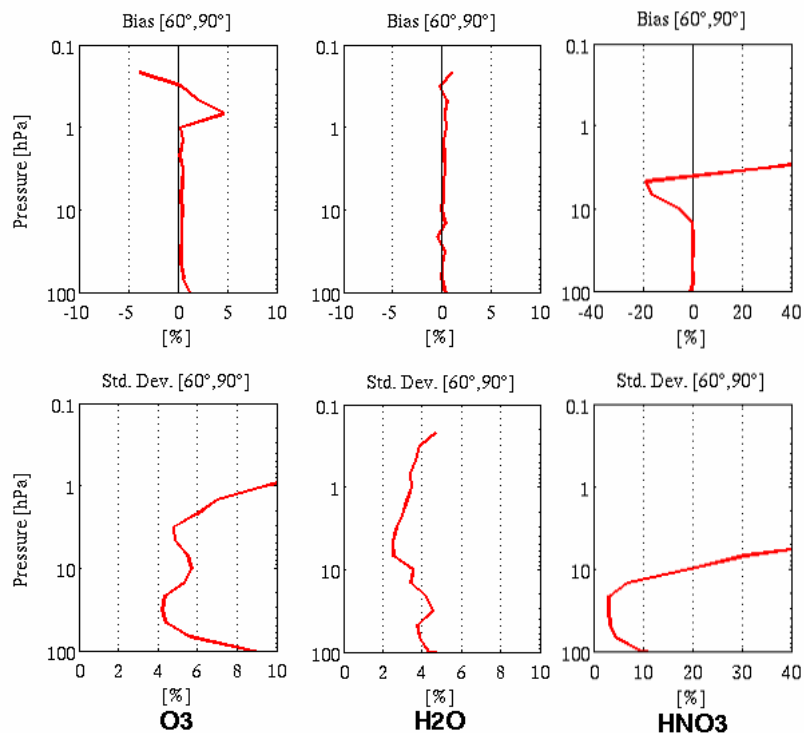


**Figure 72: Bias and standard deviation of the BASCOE Aura/MLS analyses (AMLS_q02.05_NRT with a first guess error of 0.5 and using ECMWF operational fields) compared to the assimilated Aura/MLS profiles for O3, H2O, and HNO3 for 20-30 November 2010.**
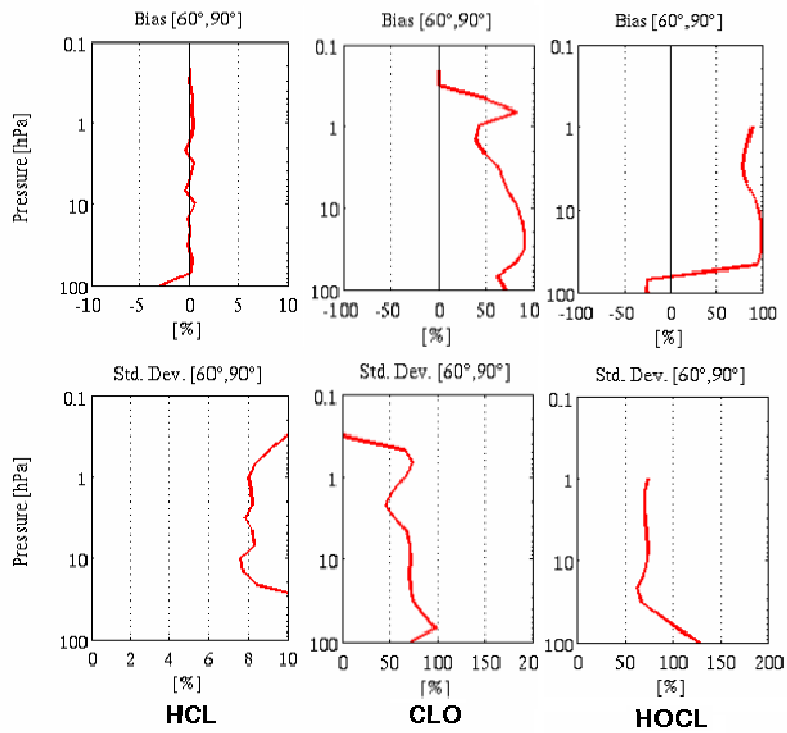
**Figure 73: Same as Figure 72, but for HCl, ClO, and HOCl.**